ABSTRACT

DOPPLER SPREAD ESTIMATION IN MOBILE FADING CHANNELS

by
Hong Zhang

The Doppler spread, or equivalently, the mobile speed, is a measure of the spectral dispersion of a mobile fading channel. Accurate estimation of the mobile speed is important in wireless mobile applications which require such as knowledge of the rate of channel variations. In this dissertation, first the performance of classical crossing- and covariance-based speed estimators is studied. Next, the problem of mobile speed estimation using diversity combining is investigated. Then, a nonparametric estimation technique is proposed that is robust to different channel variations. Finally, cyclostationarity-based speed estimators which can be applied either blindly or with the aid of pilot data, are developed.

A unified framework for the performance analysis of well-known crossing and covariance based speed estimation techniques is presented. This allows a fair analytical comparison among all the methods. Interestingly, it is proved that all these methods are asymptotically equivalent, i.e., for large observation intervals. The extensive performance analysis, supported by Monte Carlo simulations, has revealed that depending on the channel condition and the observation interval, one needs to use a crossing or a covariance based technique to achieve the desired estimation accuracy over a large range of mobile speeds.

Two common diversity schemes, selection combining (SC) and maximal ratio combining (MRC), are considered for Doppler spread estimation. Four new estimators are derived which rely on the inphase zero crossing rate, inphase rate of maxima, phase zero crossing rate, and the instantaneous frequency zero crossing rate of the output of SC. Two estimators, which work based on the level crossing rates of the envelopes at the output of SC and MRC, are also proposed. The performances of all these estimators are investigated in realistic noisy environments with different kinds of scatterings and different numbers of diversity branches.

Then a novel speed estimation technique is proposed that is applicable to both mobile and base stations, based on the characteristics in the power spectrum of mobile fading channels. The analytic performance analysis, verified by Monte Carlo simulations, shows that this low-complexity estimator is not only robust to both Gaussian and non-Gaussian noises, but also insensitive to nonisotropic scattering observed at the mobile. The estimator performs very well in both two- and three-dimensional propagation environments. By taking advantage of resolvable paths in wideband fading channels, the robustness against both nonisotropic scattering and line of sight can be further increased, due to the differences among the Doppler spectra observed at different paths. This technique is also extended to base stations with antenna arrays. By exploiting the spatial information, the proposed space-time estimator exhibits excellent performance over a wide range of noise power, nonisotropic scattering, and the line-of-sight component. This is all verified by simulation. The utility of the new method is further demonstrated by applying it to the measured data.

Finally, to design robust blind and data-aided mobile speed estimators, a proposal is made to exploit the inherent cyclostationarity of linearly modulated signals transmitted through fading channels. Two categories of cyclic-correlation- and cyclic-spectrum-based methods are developed. Extension to space-time speed estimation at the base station in macrocells is also provided. In comparison with the existing methods, the new estimators can be used without any need for pilot tones and are robust to additive stationary noise or interference of any color or distribution. Unlike the conventional multi-antenna based method, the proposed space-time speed estimator does not assume the receiver noise to be spatially white. A suboptimal training sequence is also devised for pilot-symbol assisted methods, to reduce the estimation error. The performance of the proposed estimators are illustrated via extensive Monte Carlo simulations.

DOPPLER SPREAD ESTIMATION IN MOBILE FADING CHANNELS

by
Hong Zhang

A Dissertation
Submitted to the Faculty of
New Jersey Institute of Technology
in Partial Fulfillment of the Requirements for the Degree of
Doctor of Philosophy in Computer Engineering

Department of Electrical and Computer Engineering

January 2007

APPROVAL PAGE

DOPPLER SPREAD ESTIMATION IN MOBILE FADING CHANNELS

Hong Zhang

Dr. Ali Abdi, Dissertation Advisor Date
Assistant Professor, Department of Electrical and Computer Engineering, NJIT

Dr. Yeheskel Bar-Ness, Committee Member Date
Distinguished Professor, Department of Electrical and Computer Engineering, NJIT

Dr. Alexander M. Haimovich, Committee Member Date
Professor, Department of Electrical and Computer Engineering, NJIT

Dr. Hongya Ge, Committee Member Date
Associate Professor, Department of Electrical and Computer Engineering, NJIT

Dr. Dmitry Chizhik, Committee Member Date
Member of Technical Staff, Lucent Technologies

BIOGRAPHICAL SKETCH

Author:	Hong Zhang
Degree:	Doctor of Philosophy
Date:	January 2007

Undergraduate and Graduate Education:

- Doctor of Philosophy in Computer Engineering,
  New Jersey Institute of Technology, Newark, NJ, 2007
- Master of Science in Electrical Engineering,
  Beijing University of Aeronautics and Astronautics, Beijing, China, 1997
- Bachelor of Science in Electrical Engineering,
  Beijing University of Aeronautics and Astronautics, Beijing, China, 1994

Major: Computer Engineering

Patents, Presentations and Publications:

Hong Zhang and Ali Abdi, "Robust mobile velocity estimator for wireless system," United States patent application No. 11/336,301, Jan. 20, 2006.

Hong Zhang and Ali Abdi, "A space-time mobile speed estimator using multiple antennas," United States patent application No. 11/551,658, Oct. 20, 2006.

Hong Zhang and Ali Abdi, "Blind mobile speed estimation in wireless fading channels," United States provisional patent application, Jan. 2006.

Hong Zhang and Ali Abdi, "Pilot symbol assisted mobile speed estimation in wireless fading channels," United States provisional patent application, Jan. 2006.

Hong Zhang and Ali Abdi, "Cyclostationarity-based Doppler spread estimation in mobile fading channels," submitted to *IEEE Trans. Commun.*, Dec. 2006.

Hong Zhang and Ali Abdi, "Nonparametric mobile speed estimation in fading channels: Performance analysis and experimental results," submitted to *IEEE Trans. Wireless Commun.*, Apr. 2006.

Hong Zhang and Ali Abdi, "On the average crossing rates in selection diversity," to appear in *IEEE Trans. Wireless Commun.*.

Ali Abdi, Hong Zhang and Cihan Tepedelenlioglu, "A unified approach to performance analysis of speed estimation techniques in mobile communication," submitted to *IEEE Trans. Commun.*, Nov. 2005.

Hong Zhang, Ali Abdi, and Alexander M. Haimovich, "Reduced-rank multi-antenna cyclic Wiener filtering for interference cancellation," to be published in *IEEE Military Commun. Conf. (MILCOM)*, Washington, DC, 2006.

Hong Zhang and Ali Abdi, "Space time Doppler spread estimation in mobile fading channels," to be published in *IEEE Military Commun. Conf. (MILCOM)*, Washington, DC, 2006.

Hong Zhang and Ali Abdi, "Cyclostationarity-based mobile speed estimation in fading channels: Blind and data-aided approaches," to be published in *IEEE Global Telecommun. Conf. (GLOBECOM)*, San Francisco, CA, 2006.

Hong Zhang and Ali Abdi, "A robust mobile speed estimator in fading channels: Performance analysis and experimental results," in *Proc. IEEE Global Telecommun. Conf. (GLOBECOM)*, St. Louis, MO, 2005, pp. 2567-2573.

Hong Zhang and Ali Abdi, "Mobile speed estimation using diversity combining in fading channels," in *Proc. IEEE Global Telecommun. Conf. (GLOBECOM)*, Dallas, TX, 2004, pp. 3685-3689.

Ali Abdi, Hong Zhang, and Cihan Tepedelenlioglu, "Speed estimation techniques in cellular systems: Unified performance analysis," in *Proc. IEEE Veh. Technol. Conf. (VTC)*, Orlando, FL, 2003, pp. 1522-1526.

To my parents

ACKNOWLEDGMENT

I wish to acknowledge all of the people who have made this dissertation possible. First, I would like to express my sincere gratitude to my advisor, Dr. Ali Abdi, for his encouragement, his assistance in obtaining financial support, his research insight, and his guidance throughout my Ph.D. studies. He led me into the area of digital and wireless communication which has been of great interest to me for many years. He showed me different ways to approach a research problem and the need to be persistent in order to accomplish any goal. The methods of conducting scientific research I learned from him are invaluable and will continue to guide me in the future. In addition to my advisor, special thanks go to Dr. Alexander M. Haimovich who co-advised me along with Dr. Ali Abdi regarding interference cancelation, which was also very useful for my research.

I would also like to thank Dr. Yeheskel Bar-Ness, Dr. Alexander M. Haimovich, Dr. Hongya Ge, and Dr. Dmitry Chizhik for taking time to serve as my committee members. Their insightful and invaluable comments improved the quality of this dissertation significantly.

I'm grateful to many wonderful researchers with whom I had fruitful discussions at the Center for Wireless Communications and Signal Processing Research (CWCSPR). Such interactions greatly expanded my knowledge in many areas. I am grateful, as well, to Ms. Marlene Toeroek for taking care of all the administrative details at CWCSPR and assisting me in so many ways.

I also want to thank Dr. Ronald Kane, Dr. Nirwan Ansari, and Dr. Sotirios G. Ziavras for their support in helping me through difficult times during my Ph.D. studies.

Last, but not least, I thank my parents for giving me life, for educating me, and for providing me unconditional support and encouragement throughout my life.

TABLE OF CONTENTS

TABLE OF CONTENTS
(Continued)

Chapter Page

TABLE OF CONTENTS
(Continued)

Chapter **Page**

LIST OF TABLES

LIST OF FIGURES

LIST OF FIGURES
(Continued)

LIST OF FIGURES
(Continued)

CHAPTER 1

INTRODUCTION

As a result of multipath propagation, in mobile communication systems, the received signal strength varies significantly in time due to constructive and destructive superpositions of the replicas of transmitted signals. In addition, the motion of mobile station (MS) results in the channel is spectrally broadened by Doppler shifts with different frequencies. The Doppler spread, corresponding to the maximum Doppler shift and proportional to the mobile speed, dictates how fast, in time, fading is experienced by the receiver. This knowledge is useful for many mobile communication subsystems.

One important application of speed estimation is adaptive transceiver design. In order to improve performance or reduce complexity, the system parameters need to be adapted to changing channel conditions [1]. This, in turn, necessitates the estimation of Doppler spread. For example, the MS can use Doppler information to regularly adjust the power of the received signal to optimize the dynamic range of AD converters. This is an important power control issue in CDMA based mobile communication systems for the detection process in the base station (BS). Channel estimation algorithms can also benefit from knowledge of the mobile speed, i.e., optimization of the channel tracker step size and adaption of the complexity of the algorithm. In addition, other anti-fading applications including variable coding and interleaving can also take advantage of the Doppler information.

Knowledge of the mobile speed is also greatly beneficial to cellular network control algorithms such as handoff and channel/cell assignment [2]. Handoff algorithms normally use the average strength of the received signal as the parameter by which to determine when the MS should be serviced by another BS. The appropriate choice of a temporal averaging window length for signal strength measure is dependent on the mobile speed. In order to significantly reduce the number of handoffs in an area with both slow- and fast-moving mobiles, the channel/cell assignment technique is used to allocate slow mobiles to microcells and fast ones to macrocells. This also relies upon the mobile speed information as well.

1.1 Problem Statement

Obviously, accurate estimation of the mobile speed, or the Doppler spread f_D, is an important task in wireless mobile systems. There are three major classes of speed estimation techniques: crossing-based methods, covariance-based methods, and maximum likelihood (ML) based methods.[1] Crossing-based approaches [2] [5] rely on counting the number of the received signal's level crossing which is proportional to the mobile speed. Covariance-based algorithms exploit the maximum Doppler spread information which exists in the sample autocovariance of the received signal [6] [7] [8] [9] [10]. However, both crossing-based and covariance-based speed estimators are sensitive to noise, especially for small Doppler spreads [2] [5] [11]. Although the ML-based estimators [12] [13] are optimal or near optimal, they are complex to implement, need knowledge of signal-to-noise-ratio (SNR), and require noise to be Gaussian. Furthermore, the effects of nonisotropic scattering and line-of-sight (LOS) on ML-based estimators are not investigated in [12] and [13]. Wavelet and pattern recognition methods are also used for speed estimation [14] [15], but they are computationally intensive.

Clearly, the goal of this dissertation is to develop an efficient speed estimation algorithm, that is not only robust to noise and interference, but also to nonisotropic scattering and line-of-sight (LOS), with low computational complexity. Unlike conventional methods which assume pilot tones are available, another important issue is blind speed estimation in order to increase system data throughput.

---

[1] Recently, two new methods were proposed based on integrating or differentiating power spectrum density estimate of the received signal [3] [4].

1.2 Organization of Dissertation

The dissertation is organized as follows. The mobile fading channel models including both two- and three-dimensional propagations are discussed in Chapter 2. A unified framework for the performance analysis of covariance- and crossing-based speed estimation techniques is presented in Chapter 3. In Chapter 4, new speed estimators in selection combining (SC) and maximum ratio combining (MRC) systems are derived in closed forms, and their performance is compared via Monte Carlo simulations. A robust nonparametric speed estimation technique, based on the unique observation of the Doppler spectrum, is proposed in Chapter 5. This method can be extended to a BS in macrocells where multiple antennas are available. Theoretical performance analysis for the single antenna based estimator is conducted and confirmed by simulation. Application of this method to measured data collected at the MS demonstrates its usage when compared with the conventional approaches. Chapter 6 deals with both blind and data-aided speed estimation approaches by exploring the cyclostationarity of linearly modulated signals. Finally, Chapter 7 concludes the dissertation and suggests future work.

CHAPTER 2

MOBILE FADING CHANNEL MODELS

This Chapter addresses channel models that will be used to later investigate the problem of Doppler spread estimation. In general, a two-dimensional (2-D) angle-of-arrival (AOA) of the incoming waves from only the azimuthal plane is assumed and widely used when modeling multipath fading channels. Section 2.1 briefly reviews the 2-D AOA channel model first. Section 2.2 discusses a straightforward extension to the three-dimensional (3-D) AOA model where incoming waves come from both azimuthal and elevational planes.

2.1 2-D AOA Channel Model

The lowpass complex envelope $h(t)$ of the narrowband (NB) randomly time-varying channel impulse response process is the superposition of a diffuse component $h^c(t)$ and a specular component (LOS) $h^d(t)$

$$\begin{aligned} h(t) &= h^c(t) + h^d(t) \\ h^c(t) &= \frac{\sigma_h}{\sqrt{K+1}} \lim_{M \to \infty} \frac{1}{\sqrt{M}} \sum_{m=1}^{M} a_m e^{-j(2\pi f_D t \cos\theta_m + \psi_m)} \\ h^d(t) &= \sigma_h \sqrt{\frac{K}{K+1}} e^{-j(2\pi f_D t \cos\alpha_0 + \psi_0)} \end{aligned} \tag{2.1}$$

where

$\sigma_h^2 = E[|h(t)|^2]$: the power of the received signal $h(t)$;

f_D: the maximum Doppler frequency in Hz, equal to $\nu/\lambda = \nu f_c/c$ where ν is the MS speed, λ is the wavelength, f_c is the carrier frequency, and c is the speed of light;

$a_m, m = 1, \ldots, M$: deterministic complex constants normalized to satisfy $\lim_{M\to\infty} \frac{1}{\sqrt{M}} \sum_{m=1}^{M} |a_m|^2 = 1$ so that $\sigma_h^2 = E[|h(t)|^2]$ holds;

$\theta_m, m = 1, \ldots, M$: independent and identically distributed (i.i.d.) angles that the incoming waves make with the mobile direction, with density functions given by $p(\theta)$;

$\psi_m, m = 1, \ldots, M$: i.i.d. phases, uniformly distributed on $[0, 2\pi)$;

K: the Rician factor, which is the ratio of the specular component $h^d(t)$'s power to the diffuse component $h^c(t)$'s power;

α_0: the AOA of LOS component which is a deterministic constant;

ψ_0: the phase of LOS component which is a deterministic constant.

Assuming M is large enough, i.e., $M > 6$, the central limit theorem ensures $h^c(t)$ to be a complex Gaussian process resulting in $|h(t)|$ being Rician distributed. In the absence of the specular component, $K = 0$, $|h(t)|$ is a Rayleigh random process.

The autocorrelation function of $h(t)$ is defined by $r_h(\tau) = E[h(t)h^*(t+\tau)]$ with $*$ as the complex conjugate. Using the assumptions on a_m, θ_m, and ψ_m, with unit-gain isotropic receive antenna , $r_h(\tau)$ can be expressed as

$$r_h(\tau) = \frac{\sigma_h^2}{K+1} \int_0^{2\pi} e^{j2\pi f_D \tau \cos\theta} p(\theta) d\theta + \frac{K\sigma_h^2}{K+1} e^{j2\pi f_D \tau \cos\alpha_0}. \tag{2.2}$$

To incorporate the effects of directional scattering into $r_h(\tau)$, using von Mises PDF $p(\phi) = e^{\kappa\cos(\theta-\alpha)}/(2\pi I_0(\kappa))$ which has been empirically justified to be an accurate model for the AOA distribution, (2.2) can then be written as [16]

$$r_h(\tau) = \frac{\sigma_h^2}{K+1} \frac{I_0\left(\sqrt{\kappa^2 - 4\pi f_D^2 \tau^2 + j4\pi\kappa f_D \tau \cos\alpha}\right)}{I_0(\kappa)} + \frac{K\sigma_h^2}{K+1} e^{j2\pi f_D \tau \cos\alpha_0}, \tag{2.3}$$

where $\alpha \in [0, 2\pi)$ is the mean direction of the azimuth AOA, $\kappa \geq 0$ controls the width of the azimuth AOA, and $I_0(.)$ is the zero-order modified Bessel function of the first kind. Note that for $K = \kappa = 0$, $r_h(\tau) = \sigma_h^2 J_0(2\pi f_D \tau)$, the classic Clarke's model. Consequently, the power spectral density (PSD) of $h(t)$ is given by [16]

$$\Omega_h(f) = \frac{\sigma_h^2}{K+1} \frac{\exp\left(\kappa f/f_D \cos\alpha\right) \cosh\left(\kappa \sin\alpha \sqrt{1-(f/f_D)^2}\right)}{\pi I_0(\kappa)\sqrt{f_D^2 - f^2}} + \frac{K\sigma_h^2}{K+1}\delta(f + f_D \cos\alpha_0), \tag{2.4}$$

where $|f| \leq f_D$, $\delta(.)$ is the Dirac delta function, and $\cosh(.)$ is the hyperbolic cosine. For Clarke's model, (2.4) reduces to the well-known U-shape Doppler spectrum $\Omega_h(f) = \sigma_h^2 \pi^{-1}(f_D^2 - f^2)^{-1/2}$.

2.2 3-D AOA Channel Model

By including the incoming waveforms from the elevational plane, it is easy to extend the 2-D AOA model in (2.1) to a 3-D AOA one. The corresponding autocorrelation function of $h(t)$ in a general 3-D propagation can be shown to be [17]

$$r_h(\tau) = \frac{\sigma_h^2}{K+1} \int_{\phi=0}^{\pi} \int_{\theta=0}^{2\pi} e^{j2\pi f_D \tau \cos\theta \sin\phi} p(\theta) q(\phi) \sin\phi \, d\theta d\phi + \frac{K\sigma_h^2}{K+1} e^{j2\pi f_D \tau \cos\alpha_0 \sin\beta_0}, \tag{2.5}$$

where $q(\phi)\sin\phi$ is the PDF of the AOA in the elevation plane and $\beta_0 \in [0, \pi)$ is the elevation AOA of the LOS component. This dissertation considers the model in which the azimuth and elevation AOA's are uniformly distributed over $[-\pi, \pi)$ and $[-\beta + \pi/2, \beta + \pi/2]$ with $\beta \in [0, \pi/2)$, respectively. In such a channel, (2.5) is expressed as [18]

$$r_h(\tau) = \frac{\sigma_h^2}{K+1} \frac{1}{2\sin\beta} \int_{\theta=\frac{\pi}{2}-\beta}^{\frac{\pi}{2}+\beta} J_0(2\pi f_D \tau \sin\phi) \sin\phi \, d\phi + \frac{K\sigma_h^2}{K+1} e^{j2\pi f_D \tau \cos\alpha_0 \sin\beta_0}. \tag{2.6}$$

The corresponding PSD of $h(t)$ is [18]

$$\Omega_h(f) = \frac{\sigma_h^2}{K+1} \Omega_{h^c}(f) + \frac{K\sigma_h^2}{K+1} \delta(f + f_D \cos\alpha_0 \sin\beta_0), \tag{2.7}$$

where

$$\Omega_{h^c}(f) = \begin{cases} \dfrac{\sin^{-1}\left(\dfrac{\sin\beta}{\cos\beta_f}\right)}{\pi f_D \sin\beta}, & 0 \le |f| < f_D \cos\beta \\ \dfrac{1}{2 f_D \sin\beta}, & f_D \cos\beta \le |f| \le f_D \end{cases}, \tag{2.8}$$

in which $\beta_f = \sin^{-1}(f/f_D)$.

CHAPTER 3

PERFORMANCE ANALYSIS FOR CROSSING- AND COVARIANCE-BASED ESTIMATORS

3.1 Introduction

As mentioned in Chapter 1, there are three major classes of speed estimation techniques in the literature: crossing-based techniques [2, 11], covariance-based methods [6, 8, 10], and maximum likelihood (ML) based approaches [12, 13]. Among these speed estimation solutions, crossing-based and covariance-based methods are of low complexity and therefore some of them have been extensively used today. However, what has been missing is an analytic performance analysis of these two approaches. Such an analysis would help the system designer to choose among different methods without extensive Monte Carlo simulations.[1] In this chapter, four crossing-based and two covariance-based schemes are considered, and a unified theoretical performance analysis framework is presented. In addition, a new crossing-based estimator is proposed which relies upon the number of maxima of the inphase component. Performances of the estimators are studied for finite-length and large observation intervals.

The rest of this chapter is organized as follows. The channel model is discussed in Section 3.2. In Section 3.3 all six estimators are derived and their bias properties are discussed. Section 3.4 presents the unified performance analysis framework, along with exact variance expressions for the inphase-based methods and some asymptotic results. Simulations of the envelope-based techniques, for which theoretical performance analysis is not tractable, are given in Section 3.5 along with a comprehensive performance comparison of all the methods. Section 3.6 concludes the chapter.

---

[1] For the analytical performance analysis for the ML methods, please refer to [13].

3.2 The Channel Model

In a noisy Rician frequency-flat fading channel with two-dimensional propagation of planar waves, the lowpass complex envelope at the mobile station (MS), downlink, can be written as

$$z(t) = h(t) + n(t), \tag{3.1}$$

where the complex Gaussian process $n(t)$ represents the receiver noise, whereas the complex process $h(t)$ includes the random diffuse component and the deterministic line-of-sight (LOS) component. The autocorrelation function of $h(t)$ is given in (2.3). When there is no LOS, it reduces to

$$r_h(\tau) = \sigma_h^2 \frac{I_0\left(\sqrt{\kappa^2 - \omega_D^2\tau^2 + j2\kappa\omega_D\tau\cos\alpha}\right)}{I_0(\kappa)}, \tag{3.2}$$

where $\omega_D = 2\pi f_D$ is the maximum Doppler frequency in rad/sec. For the received signal at the base station (BS), uplink, the same equation as (3.2) holds [19].

As will become clear, the form of autocorrelation function given in (2.2) will be very useful in the asymptotic performance analysis. Especially for a Rayleigh fading channel which in general, is much easier to mathematically tract than a Rician channel, (2.2) simplifies to

$$r_h(\tau) = \sigma_h^2 \int_{-\pi}^{\pi} p(\theta) \exp[-j\omega_D \cos(\theta)\tau] d\theta. \tag{3.3}$$

3.3 Speed Estimation: A Continuous-Time Approach

Section 3.3 adopts the basic propagation mechanism of isotropic scattering with no LOS in a noise-free environment. This entails straightforward derivation and performance analysis of a variety of existing and new speed estimation techniques under the same umbrella. The effect of nonisotropic scattering, LOS, and Gaussian noise will be studied later, either via analytic methods or simulation.

In the absence of noise and LOS, $K = 0$, and assuming $\sigma_h^2 = 1$, unit received power, $z(t) = h(t)$ is obtained for the received signal according to (3.1). Therefore, this section concentrates solely on $h(t)$. In what follows, and with $r_h(\tau) = J_0(\omega_D \tau)$, two classes of estimation methods are considered: crossing-based and covariance-based techniques. Since the vehicle speed v is proportional to the maximum Doppler frequency ω_D, the rest of this chapter focuses on the estimation of ω_D, to simplify the notation. The suggestion is to use either $\xi(t) = \Re\{h(t)\}$, the inphase component, where $\Re\{.\}$ gives the real part, or $\eta(t) = |h(t)|^2$, the envelope-squared. Each one is observed over a time interval of length T. Note that $\xi(t)$ is a zero-mean real Gaussian process with variance $1/2$, whereas $\eta(t)$ has an exponential distribution. In other words, $p(\eta) = \exp(-\eta)$. $|h(t)|^2$ is used rather than $|h(t)|$, the envelope, as the correlation function of envelope-squared in some cases of interest can be expressed in simple closed forms [2], required for analytic studies. For $r_\xi(\tau) = E[\xi(t)\xi(t+\tau)]$ one has $r_\xi(\tau) = (1/2)\Re\{r_h(\tau)\}$. On the other hand, for $r_\eta(\tau) = E[\eta(t)\eta(t+\tau)]$, it is shown that $r_\eta(\tau) = 1 + |r_h(\tau)|^2$ [2]. Hence, with $r_h(\tau) = J_0(\omega_D \tau)$, obtain $r_\xi(\tau) = (1/2)J_0(\omega_D \tau)$ and $r_\eta(\tau) = 1 + J_0^2(\omega_D \tau)$.

Last but not the least, note that rather than working with the sampled version of $h(t)$, i.e., $h[\ell] = h(\ell T_s)$, $\ell = 0, 1, 2, ...$, with T_s as the sampling period, this work deals with the continuous-time process itself. This allows derivation of closed-form results for the variance of the estimators. The effect of sampling, briefly discussed in [20], is negligible as long as T_s is small enough.

3.3.1 Crossing-Based Methods

For a given real random process $y(t)$, define $N_y(y_{th}, T)$ as the number of times that the process crosses the threshold level y_{th}, with positive slope, over the time interval $(0, T]$. Also, let $M_y(T)$ denote the number of maxima of the process $y(t)$ over the time interval $(0, T]$. The number of zero crossing of $\xi(t)$ is given in [2, p. 66] as

$$E[N_\xi(0,T)] = T\omega_D/(2\pi\sqrt{2}). \tag{3.4}$$

According to Appendix A, the number of maxima of $\xi(t)$ can be easily derived from (A.4) as

$$E[M_\xi(T)] = T\omega_D\sqrt{3}/(4\pi). \tag{3.5}$$

On the other hand, for the level crossing and the maxima of $\eta(t)$, obtain the following results from [2, p. 64] and [21, eq. (22)], respectively

$$E[N_\eta(1,T)] = T\omega_D/(e\sqrt{2\pi}), \tag{3.6}$$

$$E[M_\eta(T)] = T\omega_D 3/(4\pi), \tag{3.7}$$

where $e = 2.7813$ is the base of the natural logarithm. Based on (3.4)-(3.7), the following estimators can be considered

$$\hat{\omega}_{D,1} = (2\pi\sqrt{2})N_\xi(0,T)T^{-1}, \tag{3.8}$$

$$\hat{\omega}_{D,2} = (4\pi/\sqrt{3})M_\xi(T)T^{-1}, \tag{3.9}$$

$$\hat{\omega}_{D,3} = (e\sqrt{2\pi})N_\eta(1,T)T^{-1}, \tag{3.10}$$

$$\hat{\omega}_{D,4} = (4\pi/3)M_\eta(T)T^{-1}. \tag{3.11}$$

All four of these estimators are unbiased, i.e., $E[\hat{\omega}_{D,i}] = \omega_D$, $i = 1, ..., 4$. According to the literature survey of [22] and among these four crossing-based estimators, $\hat{\omega}_{D,2}$ which employs the number of maxima of the inphase component appears to be new.

3.3.2 Covariance-Based Methods

Covariance matching method Based on the covariance function definitions $c_\xi(\tau) = r_\xi(\tau) - \{E[\xi(t)]\}^2$ and $c_\eta(\tau) = r_\eta(\tau) - \{E[\eta(t)]\}^2$, along with $r_\xi(\tau) = (1/2)J_0(\omega_D\tau)$, $r_\eta(\tau) = 1 + J_0^2(\omega_D\tau)$, $E[\xi(t)] = 0$, and $E[\eta(t)] = 1$, obtain

$$c_\xi(\tau) = (1/2)J_0(\omega_D\tau), \tag{3.12}$$

$$c_\eta(\tau) = J_0^2(\omega_D\tau). \tag{3.13}$$

According to Taylor expansion, $J_0(\omega_D\tau) = 1 - (\omega_D^2/4)\tau^2 + O(\tau^4)$, as $\tau \longrightarrow 0$, where $f_1(t) = O(f_2(t))$ as $t \longrightarrow 0$ means that $f_1(t)/f_2(t)$ is bounded in a neighborhood around zero. Therefore

$$c_\xi(\tau) = (1/2) - (\omega_D^2/8)\tau^2 + O(\tau^4), \text{ as } \tau \longrightarrow 0, \tag{3.14}$$

$$c_\eta(\tau) = 1 - (\omega_D^2/2)\tau^2 + O(\tau^4), \text{ as } \tau \longrightarrow 0. \tag{3.15}$$

The quadratic form of the covariance functions in (3.14) and (3.15) for small τ, i.e., $c_y(\tau) \approx a - b\omega_D^2\tau^2$, where $a = 1/2, 1$ and $b = 1/8, 1/2$ for $y(t) = \xi(t), \eta(t)$, respectively, leads to estimating ω_D^2 by fitting a quadratic equation $a - b\omega_D^2\tau^2$ to the sample covariance function, $\hat{c}_y(\tau)$, via a minimum mean squared error (MMSE) procedure, i.e.

$$\min_{\omega_D^2} E\left\{\int_0^{T_0} [\hat{c}_y(\tau) - a + b\omega_D^2\tau^2]^2 d\tau\right\}, \tag{3.16}$$

where T_0 is sufficiently small. By setting the derivative (with respect to ω_D^2) of the expectation in (3.16) to zero, the MMSE estimate of ω_D^2 can be shown to be

$$\widehat{\omega_{D,5}^2} = \frac{5a}{3bT_0^2} - \frac{5}{bT_0^5}\int_0^{T_0} \tau^2 \hat{c}_y(\tau) d\tau. \tag{3.17}$$

The natural choice for estimating ω_D from (3.17) is

$$\hat{\omega}_{D,5} = \sqrt{\widehat{\omega^2_{D,5}}}. \tag{3.18}$$

Obviously this is a biased estimator for ω_D. To calculate the bias approximately, assume the variance of the estimator is small enough. This allows a first-order Taylor expansion for $\sqrt{\widehat{\omega^2_{D,5}}}$ around $E[\widehat{\omega^2_{D,5}}]$, which implies that $E[\hat{\omega}_{D,5}] \approx \sqrt{E[\widehat{\omega^2_{D,5}}]}$. This argument is the same as the one used in [20]. With this unbiased estimator

$$\hat{c}_y(\tau) = \frac{1}{T}\int_0^T \left(y(t) - \overline{y(t)}\right)\left(y(t+\tau) - \overline{y(t)}\right) dt, \tag{3.19}$$

where $\overline{y(t)} = T^{-1}\int_0^T y(t)dt$, thus obtain

$$E[\widehat{\omega^2_{D,5}}] = \frac{5a}{3bT_0^2} - \frac{5}{bT_0^5}\int_0^{T_0} \tau^2 c_y(\tau)d\tau. \tag{3.20}$$

Based on $c_y(\tau) = a - b\omega_D^2\tau^2 + O(\tau^4)$, as $\tau \longrightarrow 0$, with a and b defined after (3.14) and (3.15), eq. (3.20) can be written as

$$E[\widehat{\omega^2_{D,5}}] = \omega_D^2 + O(T_0^2), \text{ as } T_0 \longrightarrow 0. \tag{3.21}$$

Since $\sqrt{1+t} = 1 + O(t)$, as $t \longrightarrow 0$, the following result for the bias of $\hat{\omega}_{D,5}$, appears valid for both $\xi(t)$ and $\eta(t)$

$$E[\hat{\omega}_{D,5}] \approx \omega_D + O(T_0^2), \text{ as } T_0 \longrightarrow 0. \tag{3.22}$$

Clearly this approximate-asymptotic result, derived analytically, provides an insight into the bias behavior of $\hat{\omega}_{D,5}$ with respect to T_0. The approximation $E[\hat{\omega}_{D,5}] \approx \sqrt{E[\widehat{\omega^2_{D,5}}]}$, with $E[\widehat{\omega^2_{D,5}}]$ given by (3.20), is useful for any T_0. More conclusions can be made only via Monte Carlo simulation. Also, note that for a good-quality estimate of $c_y(\tau)$, T in (3.19) should be much larger than T_0.

The idea of least-squares fitting of a parabola to the sample covariance function at small lags was first proposed in [8], in a discrete-time setting. However, explicit form of the estimator, such as the one given in (3.17), the bias analysis discussed in the previous paragraphs and summarized in (3.20) and (3.22), and the variance analysis, discussed in the next section, are not addressed in [8]. In the context of spectral moment estimation, closely related to the maximum Doppler estimation problem, utilization of the quadratic form of a correlation function at a *single* small lag, different from the MMSE formulation in (3.16), is discussed in [23] (see also [24] and [25]). Moreover, the bias/variance analysis of [23] is different from the one in this chapter and does not apply to the basic correlation function of interest in wireless communications, i.e., $J_0(\omega_D \tau)$, which is not absolutely integrable. This important issue will be discussed later.

Integration method For an arbitrary real process $y(t)$, it is known that $r_{\dot{y}}(\tau) = -r''_y(\tau)$ [7], where dot and prime denote differentiation with respect to the time t and the delay τ, respectively. According to (3.12) and (3.13)

$$E[\dot{\xi}^2(t)] = r_{\dot{\xi}}(0) = \omega_D^2/4, \tag{3.23}$$

$$E[\dot{\eta}^2(t)] = r_{\dot{\eta}}(0) = \omega_D^2. \tag{3.24}$$

Now, based on these two identities, consider the following estimator for ω_D^2

$$\widehat{\omega_{D,6}^2} = d\frac{1}{T}\int_0^T \dot{y}^2(t)dt, \tag{3.25}$$

where $d = 4, 1$ for $y(t) = \xi(t), \eta(t)$, respectively. Note that unlike $\widehat{\omega_{D,5}^2}$ in (3.17), $\widehat{\omega_{D,6}^2}$ is an unbiased estimator for ω_D^2. However,

$$\hat{\omega}_{D,6} = \sqrt{\widehat{\omega_{D,6}^2}} \tag{3.26}$$

is clearly a biased estimator for ω_D. To make a fair comparison between $\hat{\omega}_{D,5}$ in (3.18) and $\hat{\omega}_{D,6}$, the same first-order Taylor expansion approximation is used, yielding

$$E[\hat{\omega}_{D,6}] \approx \omega_D. \tag{3.27}$$

Eq. (3.25) was first proposed and substantially analyzed in [20], in order to estimate the spectral moment of a real Gaussian process. However, the envelope-squared non-Gaussian process is not considered in [20]. Furthermore, some of the conclusions made in [20] do not apply to the non-absolutely integrable correlation $J_0(\omega_D\tau)$. In addition, application of (3.25) to the envelope was first proposed in [26], without any statistical analysis. On the other hand, the estimators proposed in [6] and [27] can be considered as the discrete-time equivalent of (3.25), where integration is replaced by summation and $\dot{y}(t)$ is approximated by the first-order difference $[y((\ell+1)T_s) - y(\ell T_s)]/T_s$, with $\ell = 0, 1, ...$, and T_s as the sampling period.

3.4 Analytic Performance Analysis

In this section, closed-form expressions are provided for the variance of the inphase-based estimators discussed in the previous section. This has been possible due to the Gaussianity of $\xi(t)$. For the non-Gaussian envelope-squared process $\eta(t)$, it is difficult, if not impossible, to derive closed-form results, and Monte Carlo simulation is the only resort. Throughout this section, an arbitrary PDF for the AOA in (3.3) is considered, making the results of this section applicable to any possible $r_h(\tau)$, and consequently, $r_\xi(\tau)$.

In what follows, closed-form expressions are derived for the variance of $\xi(t)$-based estimators $\hat{\omega}_{D,1}$, $\hat{\omega}_{D,2}$, $\hat{\omega}_{D,5}$, and $\hat{\omega}_{D,6}$. It is then shown that as the observation time T increases, the variances of all these estimators converge to zero at the same rate of $\ln(T)/T$, where $\ln(.)$ is the natural logarithm. This novel result shows the asymptotic equivalence of these four estimators.

3.4.1 Crossing-Based Methods

For a zero-mean, unit-variance, and real Gaussian $\zeta(t)$, the following result is given in [20] for the variance of $(2\pi/T)N_\zeta(0,T)$, the normalized number of zero upcrossings of $\zeta(t)$ over $(0,T]$

$$
\begin{aligned}
Var[\frac{2\pi}{T}N_\zeta(0,T)] &= \frac{2\pi\gamma}{T} + \frac{2}{T}\int_0^T \left(1-\frac{\tau}{T}\right) \\
&\times \left[\frac{\sigma_\zeta^2(\tau)}{\sqrt{1-r_\zeta^2(\tau)}}\left\{\sqrt{1-\rho_\zeta^2(\tau)}\right.\right. \\
&\left.\left.+\rho_\zeta(\tau)\cos^{-1}(-\rho_\zeta(\tau))\right\} - \gamma^2\right] d\tau, \qquad (3.28)
\end{aligned}
$$

where $r_\zeta(\tau) = E[\zeta(t)\zeta(t+\tau)]$ and

$$
\begin{aligned}
\gamma^2 &= -r_\zeta''(0), \\
\sigma_\zeta^2(\tau) &= \gamma^2 - r_\zeta'^2(\tau)/[1-r_\zeta^2(\tau)], \\
\rho_\zeta(\tau) &= -r_\zeta''^2(\tau) - r_\zeta(\tau)r_\zeta'^2(\tau)/[1-r_\zeta^2(\tau)]. \qquad (3.29)
\end{aligned}
$$

With $\zeta(t) = \sqrt{2}\xi(t)$, the variance of $\hat{\omega}_{D,1}$ in (3.8) can be easily expressed in terms of (3.28). To calculate the variance of $\hat{\omega}_{D,2}$ in (3.9) using (3.28), note that each maximum of $\xi(t)$ corresponds to a zero downcrossing of the derivative $\dot{\xi}(t)$. Since the number of zero upcrossings and downcrossings are the same, conclude that $M_\xi(T) = N_{\dot{\xi}}(0,T)$. This, along with $\zeta(t) = (2/\omega_D)\dot{\xi}(t)$ and $r_{\dot{\xi}}(\tau) = -r_\xi''(\tau)$, gives the variance of $\hat{\omega}_{D,2}$ in closed form.

By extending the asymptotic analysis of [20] to these estimators, and by using the asymptotic form of $r_h(\tau)$ [28]

$$
\begin{aligned}
r_h(\tau) &= \left(\frac{\omega_D\tau}{2\pi}\right)^{-1/2}[p(0)e^{j(\omega_D\tau-\pi/4)} \\
&+ p(\pi)e^{-j(\omega_D\tau-\pi/4)}] + O(\tau^{-1}), \text{ as } \tau \to \infty, \qquad (3.30)
\end{aligned}
$$

it has been proved in Appendix B that

$$Var[\hat{\omega}_{D,1}], Var[\hat{\omega}_{D,2}] = O(T^{-1}\ln T), \text{ as } T \to \infty. \tag{3.31}$$

This interesting new result shows that for large observation intervals, the variance of both estimators converges to zero at the same rate.

3.4.2 Covariance-Based Methods

Covariance matching method Based on the fourth-order moment of zero-mean and jointly Gaussian variables [29], and using the definition of the covariance estimator given in (3.19), it can be shown that

$$\begin{aligned} E[\hat{c}_\xi(\tau_1)\hat{c}_\xi(\tau_2)] &= c_\xi(\tau_1)c_\xi(\tau_2) + \frac{1}{T}\int_{-T}^{T}\left(1-\frac{|\tau|}{T}\right) \\ &\times [c_\xi(\tau)c_\xi(\tau+\tau_2-\tau_1) + c_\xi(\tau+\tau_2)c_\xi(\tau-\tau_1)]d\tau. \end{aligned} \tag{3.32}$$

For $\tau_1 = \tau_2$, (3.32) simplifies to eq. (5.69) given in [30, p. 194]. Using (3.20), it is straightforward to calculate the variance of $\widehat{\omega^2_{D,5}}$, defined in (3.17)

$$\begin{aligned} Var[\widehat{\omega^2_{D,5}}] = \left(\frac{5}{bT_0^5}\right)^2 \int_0^{T_0}\int_0^{T_0} &\tau_1^2\tau_2^2\{E[\hat{c}_\xi(\tau_1)\hat{c}_\xi(\tau_2)] \\ &- c_\xi(\tau_1)c_\xi(\tau_2)\}d\tau_1 d\tau_2. \end{aligned} \tag{3.33}$$

As before, consider the first-order Taylor expansion [20] for $\sqrt{\widehat{\omega^2_{D,5}}}$ around $E[\widehat{\omega^2_{D,5}}] = \omega^2_D$, which implies that

$$Var[\hat{\omega}_{D,5}] \approx Var[\widehat{\omega^2_{D,5}}]/(4E[\widehat{\omega^2_{D,5}}]), \tag{3.34}$$

with the numerator and denominator given in (3.33) and (3.20), respectively.

If T_0 is small enough, it can be assumed that $\hat{\omega}_{D,5}$ is approximately unbiased, as shown in (3.22), and therefore $Var[\hat{\omega}_{D,5}]$ in (3.34) is enough to assess the performance. However, if the bias is not negligible, one needs to look at the estimation error $E[(\hat{\omega}_{D,5} -$

$\omega_D)^2] = Var[\hat{\omega}_{D,5}] + (E[\hat{\omega}_{D,5}] - \omega_D)^2$. With $T = 1$ sec. and uniform PDF for the AOA, i.e., $c_\xi(\tau)$ given by (3.12), the estimation error of $\hat{\omega}_{D,5}/(2\pi)$ is plotted in Fig. 1 versus T_0. COV in the legend box is the abbreviation for covariance and the subscript T stands for theoretical. Note that for each f_D, there is a single $T_{0,opt}$ which yields the smallest estimation error. For $T_0 < T_{0,opt}$, the estimation error could be very large, especially for small f_D s. On the other hand, for each f_D, there is a neighborhood around $T_{0,opt}$, over which the estimation error remains almost constant. As f_D increases, this neighborhood becomes smaller.

At this point, it seems difficult to study the asymptotic performance of $\hat{\omega}_{D,5}$, due to the complicated form of the estimator's bias, variance, and the parameter T_0 involved. However, the indirect argument of [28, p. 2204, the paragraph right before the Conclusions], which takes advantage of the asymptotic properties of moment-based estimators, without deriving the variance expressions explicitly, might be applicable, which yields $Var[\hat{\omega}_{D,5}] \approx O(T^{-1}\ln T)$, as $T \to \infty$.

Integration method Based on [20, eq. (2.1)], the variance of $\widehat{\omega_{D,6}^2}$ in (3.25) can be written as

$$Var[\widehat{\omega_{D,6}^2}] = \frac{64}{T}\int_0^T \left(1 - \frac{\tau}{T}\right) r_\xi''^2(\tau)d\tau. \tag{3.35}$$

Again, consider the first-order Taylor expansion [20] for $\sqrt{\widehat{\omega_{D,6}^2}}$ around $E[\widehat{\omega_{D,6}^2}] = \omega_D^2$, i.e., $Var[\hat{\omega}_{D,6}] \approx Var[\widehat{\omega_{D,6}^2}]/(4E[\widehat{\omega_{D,6}^2}])$. Therefore

$$Var[\hat{\omega}_{D,6}] \approx \frac{16}{\omega_D^2 T}\int_0^T \left(1 - \frac{\tau}{T}\right) r_\xi''^2(\tau)d\tau. \tag{3.36}$$

There are two integrals on the right-hand side of (3.36). Based on the asymptotic form of $r_\xi''^2$ in (B.10), Appendix B, and by integrating τ^{-1}, the first integral yields $O(\ln T), T \to \infty$. Using a similar argument, the second integral can be easily shown to be $O(T), T \to \infty$. Therefore $TVar[\hat{\omega}_{D,6}] \approx O(\ln T) + T^{-1}O(T) = O(\ln T)$, as $T \to \infty$.

Thus the asymptotic variance of $\hat{\omega}_{D,6}$ can be written as

$$Var[\hat{\omega}_{D,6}] \approx O(T^{-1}\ln T), \text{ as } T \to \infty. \tag{3.37}$$

Interestingly, the Holtzman-Sampath estimator given in eq. (10) of [28] is the discrete-time equivalent of $\hat{\omega}_{D,6}$ in (3.26). The asymptotic result in (3.37) agrees with the asymptotic variance given in the last two lines of Sec. 4 of [28], p. 2204, obtained by a different approach and in a discrete-time setting.

3.5 Simulation Results and Performance Comparison

This section considers four inphase-based and four envelope-based estimators and compares their performance in terms of the estimation error which is defined as the root mean square error (RMSE), given by

$$\left(E[(\hat{\omega}_{D,i} - \omega_D)^2]\right)^{\frac{1}{2}} = \left(Var[\hat{\omega}_{D,i}] + (E[\hat{\omega}_{D,i}] - \omega_D)^2\right)^{\frac{1}{2}}, \tag{3.38}$$

where $i = 1, 2, ..., 8$, and the second term in the right side stands for the bias. Rayleigh fading channel is first used to investigate the estimation error of all these estimators. For the inphase-based methods the closed-form expressions (3.28), (3.33) and (3.36) have been employed to calculate the variance, whereas the bias is computed using (A.3), (A.4), (A.5) and (A.6) in Appendix A. The estimation errors of the envelope-based techniques for Rayleigh channel are obtained via Monte Carlo simulation. On the other hand, for Rician fading, the estimation errors of both the inphase-based and envelope-based estimators are evaluated through Monte Carlo simulations. Using the spectral method [31], 100 independent realizations of complex Gaussian processes are generated, with $N = 10000$ complex samples per realization, which is equivalent to $T = 1$ sec. The simulated autocorrelations are given in (3.2) and (2.3) for Rayleigh and Rician fading, respectively. The spectral method is also used for generating the lowpass complex Gaussian bandlimited noise, with a flat power spectrum over the fixed receiver bandwidth of $B_{rx} = 101$ Hz. In simulations, the estimation error of eight estimators $\hat{f}_D = \hat{\omega}_D/(2\pi)$ is given. The abbreviations LCR, ROM, INT, COV, and ZCR in legend boxes refer to the level crossing rate, rate of maxima, integration, covariance, and zero crossing rate, respectively. In addition, the subscripts S and T stand for simulated and theoretical, respectively.

Note that in the covariance matching method, using either the inphase component or the envelope, T_0 needs to be specified. Since $T_{0,opt}$ varies over a large range, as f_D changes, in the sequel, unless specified otherwise, $T_0 = 0.005$ and 0.06 sec. are chosen, from Fig. 3.1, for $31 \leq f_D \leq 81$ and $1 \leq f_D < 31$ Hz, respectively. This means that a rough prior knowledge of the speed is available, when using the covariance matching method. Also note that choosing the appropriate T_0 for the envelope-based covariance matching, from the inphase-based curves of Fig. 3.1, is convenient but not optimum. Clearly, there is no need to predetermine any parameter for the other six methods.

First the performance analysis for the four inphase-based estimators is validated via Monte-Carlo simulation. As shown in Fig. 3.2, where noise-free isotropic scattering is considered, the derived theoretical estimation error expressions are in good agreement with simulation. Note that for the covariance matching method appropriate $T_{0,opt}$ is chosen from Fig. 3.1 for each f_D, to only compare the simulation and theory.

Based on Fig. 3.3, where isotropic scattering occurs without noise, InphaseROM and EnvelopeROM demonstrate the best performance, whereas InphaseCOV and EnvelopeCOV are the worst. When including the effect of nonisotropic scattering without noise, depicted in Fig. 3.4, InphaseROM is the best and Envelope{LCR, INT, COV} are the worst for $f_D \geq 10$ Hz, whereas InphaseCOV shows large errors when $f_D < 10$ Hz. The effect of the nonisotropic scattering parameter κ is shown in Fig. 3.5, where $\alpha = 0^\circ$ and $f_D = 21$. Note that Inphase{ROM, COV} are robust against κ. Fig. 3.6 illustrates the estimation error versus the mean AOA α, for $\kappa = 3.3$ [16] and $f_D = 21$ Hz. Once again, InphaseROM demonstrates a robust performance. Note that the optimal $T_0 = 0.02$ sec. is chosen from Fig. 3.1, for $f_D = 21$ Hz, and used in both Fig. 3.5 and Fig. 3.6.

Fig. 3.7 and Fig. 3.8 demonstrate the effect of the LOS parameters K and α_0 in a noise-free isotropic fading channel with $f_D = 21$ Hz, respectively. As seen in Fig. 3.7, ROM-based and COV-based methods are fairly insensitive to the Rice factor K, with ROM-based methods showing much smaller errors. In terms of the robustness to the LOS AOA ϕ_0 in Fig. 3.8, COV-based estimators are less sensitive, whereas the InphaseZCR estimation error changes significantly.

With isotropic scattering and a finite SNR of 10 dB, Fig. 3.9 shows the impact of noise. For large Dopplers, all the techniques do reasonably well in the presence of noise. For medium and large Dopplers, $f_D \geq 20$ Hz, InphaseZCR seems the best choice. On the other hand, when f_D is small, InphaseCOV and EnvelopeCOV perform better than the other techniques. This is due to the proper choice of the parameter T_0 for small speeds.

Finally, the effect of the estimation time window T is investigated. Fig. 3.10 shows the estimation error with respect to T for a noiseless isotropic Rayleigh fading channel with $f_D = 21$ Hz. Clearly, all the crossing-based techniques degrade for very short observation intervals, say, $T < 25$ msec. This is also observed in [8] as the channel does not experience many crossings in a short time interval. Overall, for $T > 50$ msec, all eight estimators are approximately insensitive to the choice of T.

3.6 Conclusion

In this chapter a variety of crossing-based and covariance-based speed estimation techniques have been studied in a unified framework. Such a framework has helped to assess the performance of all the estimators, analytically, under the same umbrella when the inphase component is used. As a by-product of this approach, it has been demonstrated, mathematically that for large observation intervals, the performance of all these estimators is the same. Closed-form expressions for the bias and variance of the inphase-based estimators were also presented and verified via simulation. It has been observed that the rate of maxima of the inphase component and also the envelope provide the best performance

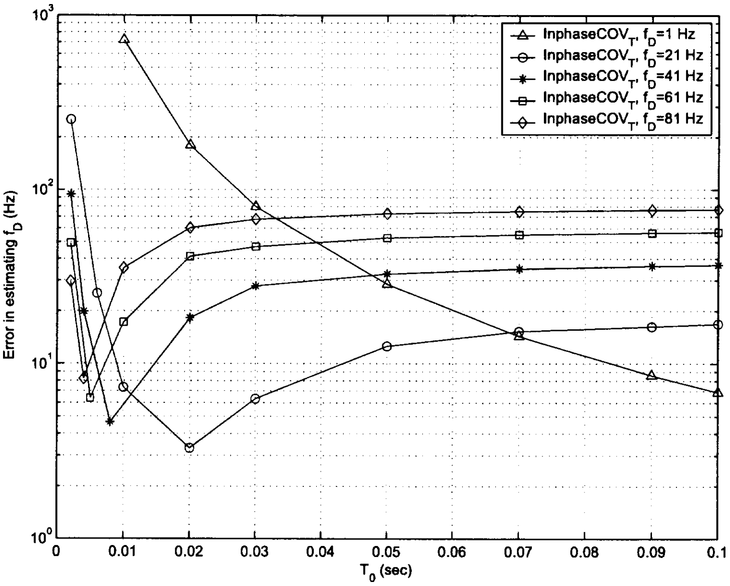

Figure 3.1 Estimation error of the covariance matching method using the inphase component, versus the parameter T_0, assuming isotropic scattering.

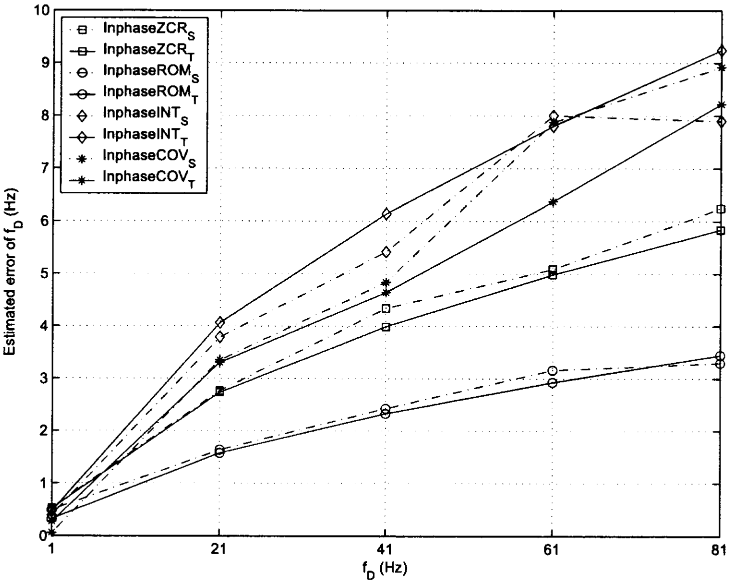

Figure 3.2 Comparison of simulated and theoretical estimation errors for four inphase-based estimators, versus the maximum Doppler frequency (no noise, isotropic scattering).

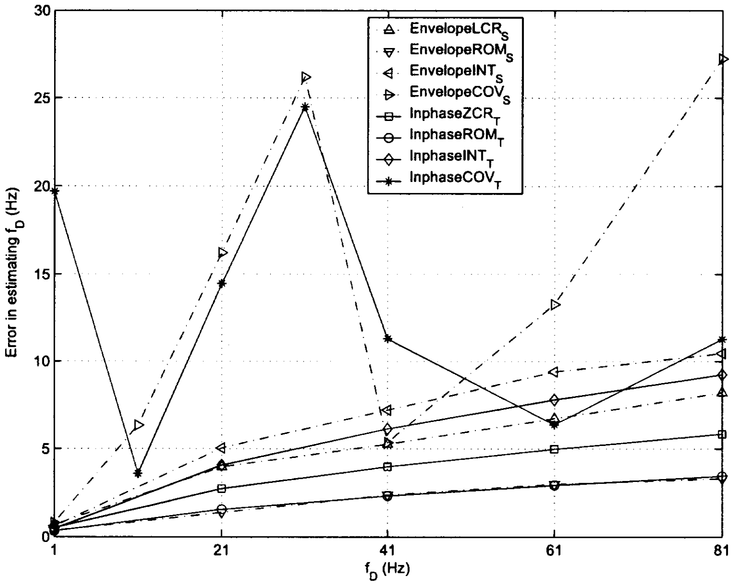

Figure 3.3 Estimation errors of eight estimators versus the maximum Doppler frequency (no noise, isotropic scattering).

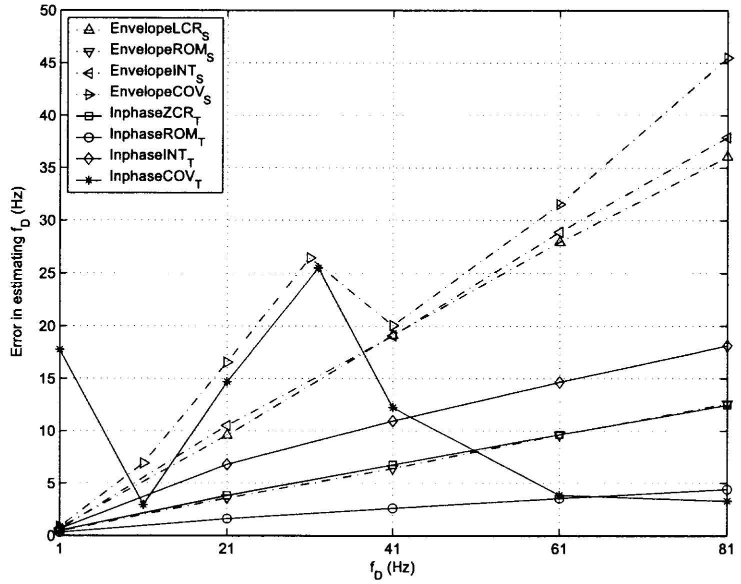

Figure 3.4 Estimation errors of eight estimators versus the maximum Doppler frequency (no noise, nonisotropic scattering).

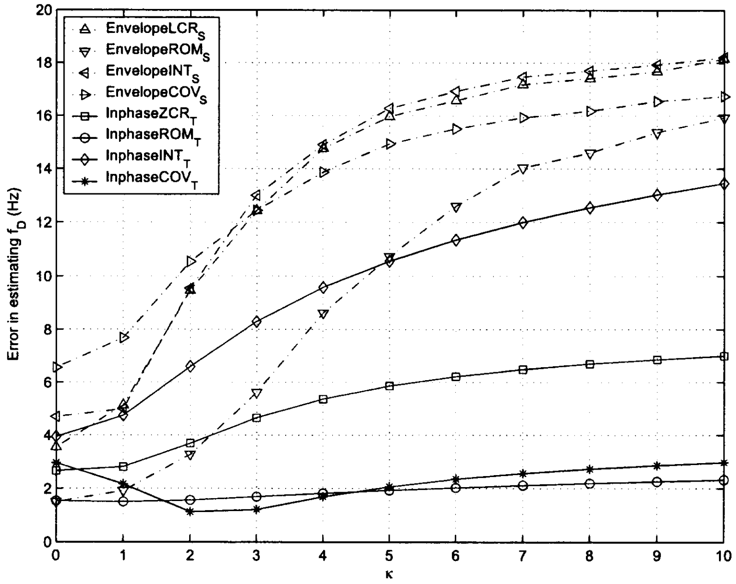

Figure 3.5 Estimation errors of eight estimators versus κ, $f_D = 21$ Hz, $\alpha = 0°$ (no noise, nonisotropic scattering).

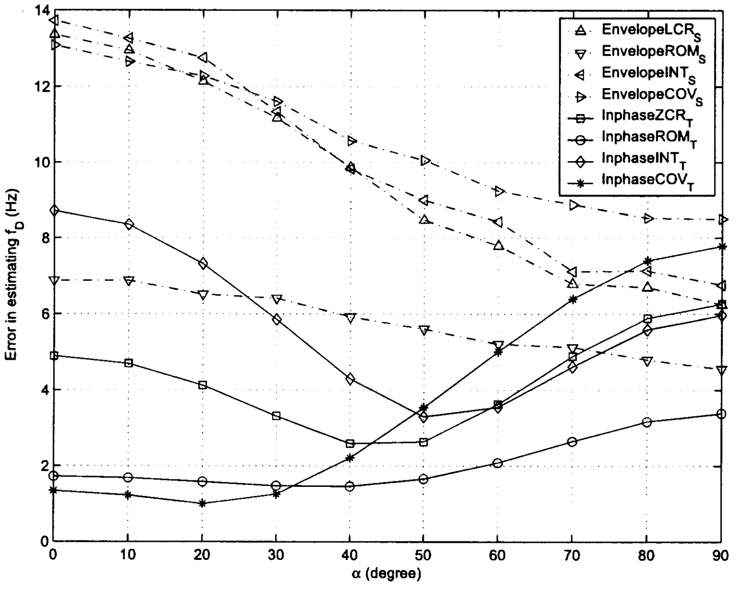

Figure 3.6 Estimation errors of eight estimators versus α, $f_D = 21$ Hz, $\kappa = 3.3$ (no noise, nonisotropic scattering).

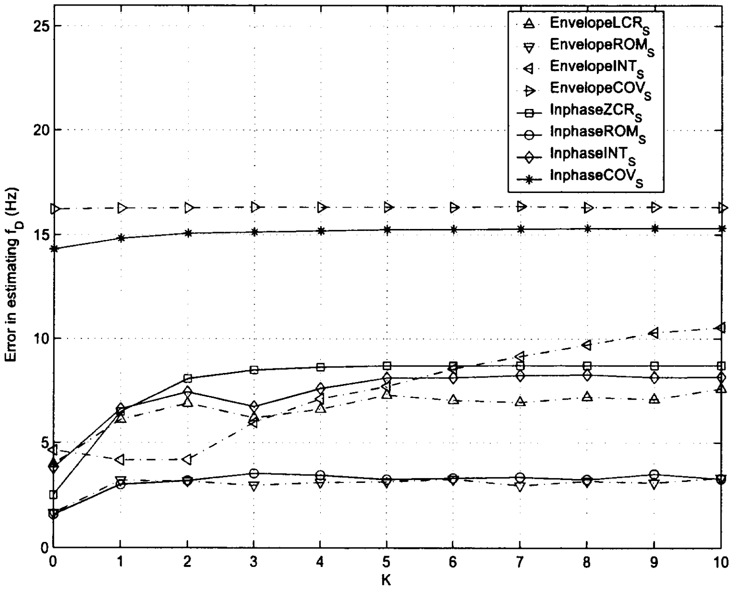

Figure 3.7 Estimation errors of eight estimators versus K, f_D = 21 Hz, α_0 = 0° (no noise, isotropic scattering).

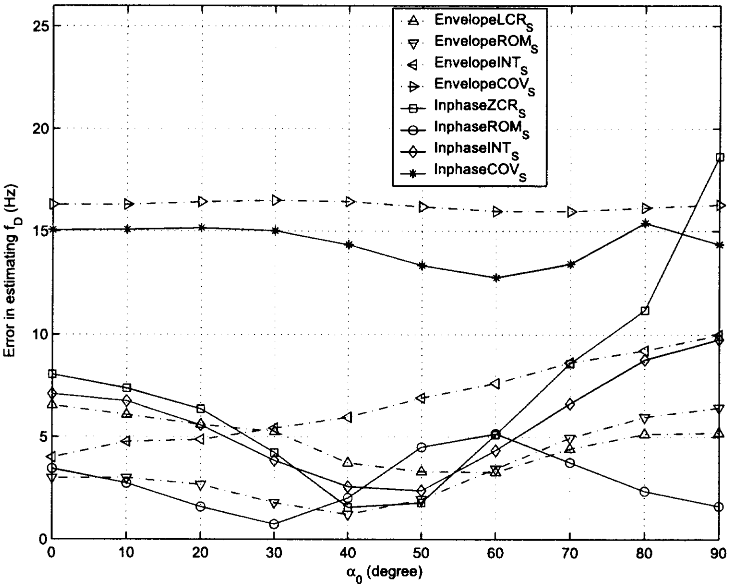

Figure 3.8 Estimation errors of eight estimators versus α_0, f_D = 21 Hz, K = 2 (no noise, isotropic scattering).

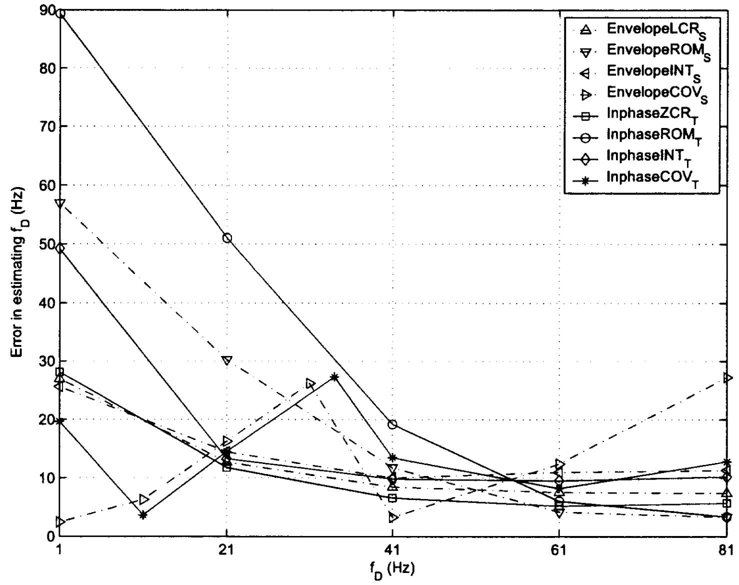

Figure 3.9 Estimation errors of eight estimators versus the maximum Doppler frequency (SNR=10 dB, isotropic scattering).

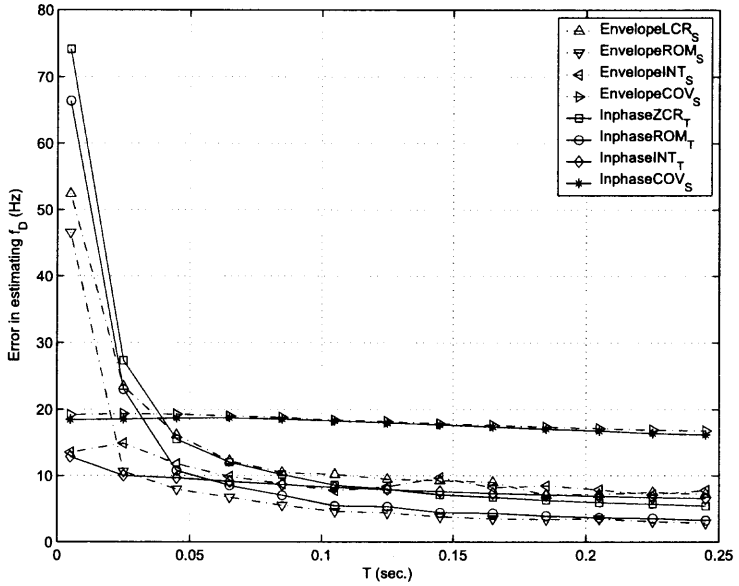

Figure 3.10 Estimation errors of eight estimators versus T, $f_D = 21$ Hz, $K = 0$ (no noise, isotropic scattering).

when noise is negligible. The proposed rate of maxima of the inphase component also remains to be the best with respect to the nonisotropic scattering parameter and Ricean factor. When noise is not negligible and speed is high, most of the methods show a good performance. In particular, for medium and high speeds, the zero crossing rate of the inphase component is the best choice. However, for small speeds, the covariance matching technique seems to be capable of providing an accurate estimate when noise is present, provided that the parameter T_0 is chosen properly. For very small observation intervals, covariance-based estimators demonstrate a better performance.

CHAPTER 4

DOPPLER SPREAD ESTIMATION USING DIVERSITY COMBINING

4.1 Introduction

As shown in Chapter 3, the main disadvantage of the traditional crossing- and covariance-based speed estimators is that they are sensitive to noise, especially for small Dopplers. Diversity combining techniques are often used to combat the effect of fading. This results in increase of the signal to noise ratio (SNR) of the combined signal when compared with the non-diversity signal. On the other hand, it is well known that the average crossing rate represents the fading rate and effectively quantifies the impact of the diversity combiner on channel fluctuations. This leads to use of diversity combining to estimate the Doppler spread.

Among the diversity combining techniques, selection combining (SC) is one of the simplest diversity methods, and maximal ratio combining (MRC) is the optimal one [2]. In this Chapter, the problem of mobile speed estimation using these two common diversity schemes is considered. Four new estimators are derived which rely on the inphase zero crossing rate, inphase rate of maxima, phase zero crossing rate, and the instantaneous frequency zero crossing rate of the output of SC. Monte Carlo simulation results are provided to verify the four new theoretical expressions as well. Two estimators are also proposed, which work based on the level crossing rates of the envelopes at the output of SC and MRC. The performances of all these estimators are investigated in realistic noisy environments with different kinds of scatterings and different numbers of diversity branches.

Chapter 4 is organized as follows. The signal model is discussed in Section 4.2; six diversity-based estimators are derived in Section 4.3. Section 4.4 presents the performance comparison through extensive Monte Carlo and Section 4.5 concludes this Chapter.

4.2 Signal and Channel Models

Consider a noisy Rayleigh frequency-flat fading channel and a combiner with L branches. The received lowpass complex envelope at the i-th branch is

$$z_i(t) = h_i(t) + v_i(t) \ , \ \ i = 1, 2, ..., L, \tag{4.1}$$

where the independent zero-mean complex Gaussian processes $h_i(t)$ and $v_i(t)$ represent the channel gain (assuming a pilot has been transmitted) and the additive noise, respectively. In the Cartesian coordinates one has

$$z_i(t) = x_i(t) + jy_i(t), \tag{4.2}$$

where $j^2 = -1$, and $x_i(t)$ and $y_i(t)$ are the inphase and quadrature components, respectively. Using the polar representation obtain

$$z_i(t) = \rho_i(t) \exp\left\{-j\varphi_i(t)\right\}, \tag{4.3}$$

where $\rho_i(t)$ and $\varphi_i(t)$ are the envelope and phase of $z_i(t)$, defined by

$$\rho_i(t) = \sqrt{x_i^2(t) + y_i^2(t)}, \ \ \tan\varphi_i(t) = y_i(t)/x_i(t). \tag{4.4}$$

The autocorrelation function of $z_i(t)$ is defined by $r_{z_i(t)} = E[z_i(t)z_i^*(t+\tau)]$ with $*$ as the complex conjugate. One also needs the n-th spectral moment of $z_i(t)$, $b_{i,n}$, $n = 0, 1, 2, ...,$ given by [32]

$$b_{i,n} = (2\pi)^n \int_{-\infty}^{\infty} f^n S_{z_i}(f) df = \left. \frac{d^n r_{z_i}(\tau)}{j^n d\tau^n} \right|_{\tau=0}, \tag{4.5}$$

in which $S_{z_i}(f)$ is the power spectral density of $z_i(t)$.

The results derived in the following section hold for a large class of correlation functions whose power spectra are even symmetric with respect to the center frequency. When doing the simulations in Section 4.4, this flexible, empirically-verified correlation in

(2.3) is used. This is a natural extension of Clarke's model (also known as Jake's model)

$$r_{h_i}(\tau) = \sigma_{h_i}^2 \frac{I_0\left(\sqrt{\kappa_i^2 - 4\pi f_D^2 \tau^2 + j4\pi\kappa_i f_D \tau \cos\alpha_i}\right)}{I_0(\kappa_i)}, \tag{4.6}$$

where obviously $\sigma_{h_i}^2 = b_{i,0}$.

Let $z(t)$, $x(t)$, $y(t)$, $\rho(t)$, and $\varphi(t)$ denote the complex envelope, inphase part, quadrature part, envelope, and the phase at the output of the SC, respectively. Then, based on the definition of an L-branch SC [2]

$$\gamma(t) = \gamma_i(t) \text{ if } \rho_i(t) = \max(\{\rho_k(t)\}_{k=1}^{L}), \tag{4.7}$$

where $\gamma(t) \in \{z(t), x(t), y(t), \varphi(t)\}$ represents random process at the SC output and $\gamma_i(t) \in \{z_i(t), x_i(t), y_i(t), \varphi_i(t)\}$ corresponds to the i-th branch. On the other hand, under the assumption of a perfectly known channel, the envelope of the output of an MRC can be written as [2]

$$\rho(t) = \left(\sum_{k=1}^{L} \rho_k^2(t)\right)^{1/2}. \tag{4.8}$$

4.3 Diversity Based Estimators

The advantage of SC is that it does not require channel estimate, whereas implementation of MRC needs perfect estimate and/or tracking of the channel. In the following section, four SC-based estimators and one MRC-based estimator are derived.

Conventionally, there are two classes of speed estimation methods: crossing-based and covariance-based techniques [5]. This dissertation concentrates on the former category. Given a stationary real random process, $\chi(t)$, $N_\chi(\chi_{th}, T)$ represents the number of times that the process crosses the threshold level χ_{th} with positive (or negative) slope over the time interval T. Also let $M_\chi(T)$ denote the number of maxima of the process $\chi(t)$, over the time interval T. Based on [29], the expected values of $N_\chi(\chi_{th}, T)$ and $M_\chi(T)$ can be calculated according to

$$E[N_{\chi}(\chi_{th},T)] = T\int_0^{\infty} \dot{\chi} p_{\chi\dot{\chi}}(\chi_{th},\dot{\chi})d\dot{\chi}, \tag{4.9}$$

and

$$E[M_{\chi}(T)] = T\int_0^{\infty} \ddot{\chi} p_{\dot{\chi}\ddot{\chi}}(0,\ddot{\chi})d\ddot{\chi}, \tag{4.10}$$

where $p_{\chi\dot{\chi}}(\chi,\dot{\chi})$ is the joint probability density function (PDF) of $\chi(t)$ and $\dot{\chi}(t)$, $p_{\dot{\chi}\ddot{\chi}}(\dot{\chi},\ddot{\chi})$ is the joint PDF of $\dot{\chi}(t)$ and $\ddot{\chi}(t)$, and dot denotes differentiation with respect to t. In order to calculate the average crossing rates of interest in diversity combiners using the above equations, independent and identically distributed (i.i.d.) branches are assumed. When branches are not i.i.d., one needs to use another approach [33].

In what follows, first closed form expressions for four crossing rates in SC diversity systems are provided: inphase zero crossing rate (IZCR) $E[N_x(0,T)]/T$, inphase rate of maxima (IROM) $E[M_x(T)]/T$, the phase zero crossing rate (PZCR) $E[N_\theta(0,T)]/T$, and the instantaneous frequency zero crossing rate (FZCR) $E[N_{\dot{\theta}}(0,T)]/T$. These results are believed to be new. The average envelope level crossing rate (ELCR) in SC and MRC are also considered, and given in [34] and [35], respectively. Based on these six crossing rates, six new diversity-based speed estimators are proposed. They are derived under the no noise assumption with isotropic scattering, i.e., $r_{h_i}(\tau) = b_{i,0}J_0(2\pi f_D\tau)$. The effect of noise and nonisotropic scattering will be discussed in Section 4.4.

4.3.1 IZCR Speed Estimator with SC

The covariance matrix of the three dimensional Gaussian random vector $\mathbf{V}_{IZCR} = [x_i \; y_i \; \dot{x}_i]^{\mathsf{T}}$, with $(.)^{\mathsf{T}}$ as the transpose, at the i-th branch, is given by [32]

$$\mathbf{A}_{IZCR} = \begin{bmatrix} b_0 & 0 & 0 \\ 0 & b_0 & 0 \\ 0 & 0 & b_2 \end{bmatrix}, \tag{4.11}$$

where the subscript i of $b_{i,n}$ is dropped, due to the identically distributed branches. Clearly, the PDF of V_{IZCR} can be written as

$$p_{\mathrm{V}_{IZCR}}(x_i, y_i, \dot{x}_i) = \frac{\exp\left\{-\frac{1}{2}\left(\frac{x_i^2+y_i^2}{b_0}+\frac{\dot{x}_i^2}{b_2}\right)\right\}}{(2\pi)^{3/2}b_0 b_2^{1/2}}. \tag{4.12}$$

Another random vector of interest is $\mathrm{W}_{IZCR} = [\rho_i \; x_i \; \dot{x}_i]^{\mathrm{T}}$, whose PDF can be determined from the PDF of V_{IZCR} in (4.12) as

$$p_{\mathrm{W}_{IZCR}}(\rho_i, x_i, \dot{x}_i) = \sum \frac{p_{\mathrm{V}_{IZCR}}(x_i, y_i, \dot{x}_i)}{|J_{IZCR}(x_i, y_i, \dot{x}_i)|}, \tag{4.13}$$

where $J_{IZCR}(x_i, y_i, \dot{x}_i) = -y_i/\sqrt{x_i^2+y_i^2}$ is the Jacobian [29] of the transformation V_{IZCR} $\rightarrow$ W_{IZCR}. Based on (4.4), one then obtains the PDF of W_{IZCR}

$$p_{\mathrm{W}_{IZCR}}(\rho_i, x_i, \dot{x}_i) = \frac{\rho_i \exp\left\{-\frac{1}{2}\left(\frac{\rho_i^2}{b_0}+\frac{\dot{x}_i^2}{b_2}\right)\right\}}{\sqrt{2\pi b_2}\pi b_0\sqrt{\rho_i^2 - x_i^2}}. \tag{4.14}$$

According to (C.8) in the Appendix C, the joint PDF of $x(t)$ and $\dot{x}(t)$ at the output of the L-branch SC can be shown to be

$$\begin{aligned} p_{x\dot{x}}(x, \dot{x}) =& \frac{L}{\sqrt{2\pi b_2}\pi b_0}\exp\left\{-\frac{\dot{x}^2}{2b_2}\right\} \\ &\times \sum_{k=0}^{L-1}\binom{L-1}{k}(-1)^k \int_{|x|}^{\infty}\frac{\rho_1 \exp\left\{-\frac{(k+1)r_1^2}{2b_0}\right\}}{\sqrt{\rho_1^2 - x^2}}d\rho_1, \end{aligned} \tag{4.15}$$

where $\binom{m}{n} = m!/[(m-n)!n!]$. Equation (4.15) can be simplified to

$$p_{x\dot{x}}(x, \dot{x}) = \frac{1}{\sqrt{2\pi b_2}}\exp\left(-\frac{\dot{x}^2}{2b_2}\right)\frac{L}{\sqrt{2\pi b_0}}\sum_{k=0}^{L-1}\binom{L-1}{k}\frac{(-1)^k\exp\left(-\frac{k+1}{2b_0}x^2\right)}{\sqrt{k+1}}. \tag{4.16}$$

It is interesting to note that the inphase component of the SC complex envelope and its derivative at any time instant t, are independent. Also, the distribution of $\dot{x}(t)$ does not depend on L , and is still Gaussian. By substituting (4.16) into (4.9) with $x_{th} = 0$, one obtains the average zero crossing rate of the SC inphase component as

$$\frac{E[N_x(0,T)]}{T} = \frac{L}{2\pi}\sqrt{\frac{b_2}{b_0}}\sum_{k=0}^{L-1}\binom{L-1}{k}\frac{(-1)^k}{\sqrt{k+1}}. \tag{4.17}$$

On the other hand, based on (4.5), the following spectral moments are obtained for the Clarke's model with correlation function $r_h(\tau) = b_0 J_0(2\pi f_D \tau)$

$$\begin{aligned} b_2 &= 2\pi^2 b_0 f_D^2, \\ b_4 &= 6\pi^4 b_0 f_D^4. \end{aligned} \tag{4.18}$$

This reduces (4.17) to

$$\frac{E[N_x(0,T)]}{T} = f_D \frac{\sqrt{2}L}{2}\sum_{k=0}^{L-1}\binom{L-1}{k}\frac{(-1)^k}{\sqrt{k+1}}. \tag{4.19}$$

Consequently, the IZCR estimator of the L-branch SC system is introduced as

$$\hat{f}_D = \frac{\sqrt{2}\hat{N}_x(0,T)}{TL\sum_{k=0}^{L-1}\binom{L-1}{k}\frac{(-1)^k}{\sqrt{k+1}}}. \tag{4.20}$$

With $L = 1$, (4.20) reduces to the well-known inphase zero crossing speed estimator [2].

4.3.2 IROM Speed Estimator with SC

As with the IZCR estimator, define two random vectors $\mathbf{V}_{IROM} = [x_i\ \ddot{x}_i\ y_i\ \dot{x}_i]^\mathsf{T}$ and $\mathbf{W}_{IROM} = [\rho_i\ \dot{x}_i\ \ddot{x}_i\ \varphi_i]^\mathsf{T}$. The covariance matrix of the Gaussian vector $\mathbf{V}_{IROM}$ is [32]

$$\mathbf{A}_{IROM} = \begin{bmatrix} b_0 & -b_2 & 0 & 0 \\ -b_2 & b_4 & 0 & 0 \\ 0 & 0 & b_0 & 0 \\ 0 & 0 & 0 & b_2 \end{bmatrix}. \tag{4.21}$$

Then the PDF of $\mathbf{V}_{IROM}$ can be written as

$$p_{\mathbf{V}_{IROM}}(x_i, \ddot{x}_i, y_i, \dot{x}_i) = \frac{\exp\left(-\frac{1}{2}\mathbf{V}_{IROM}^\mathsf{T}\mathbf{A}_{IROM}^{-1}\mathbf{V}_{IROM}\right)}{4\pi^2\sqrt{\det(\mathbf{A}_{IROM})}}, \tag{4.22}$$

where $\det(.)$ is the determinant. The Jacobian of the transformation $\mathbf{V}_{IROM} \rightarrow \mathbf{W}_{IROM}$ is $J_{IROM}(x_i, \ddot{x}_i, y_i, \dot{x}_i) = \sqrt{x_i^2 + y_i^2} = \rho_i$. Therefore, obtain the PDF of $\mathbf{W}_{IROM}$ as

$$
\begin{aligned}
p_{\mathbf{W}_{IROM}}(\rho_i, \dot{x}_i, \ddot{x}_i, \varphi_i) =& \frac{r_i}{4\pi^2\sqrt{\det(\mathbf{A}_{IROM})}} \exp\left\{-\frac{(b_0 b_2 b_4 \rho_i^2 - b_0 b_2^2 \dot{x}_i^2 + b_0^2 b_4 \dot{x}_i^2)}{2\det(\mathbf{A}_{IROM})}\right\} \\
& \times \exp\left\{\frac{b_2^3 \rho_i^2 \sin^2\varphi_i - b_0^2 b_2 \ddot{x}_i^2 - 2b_0 b_2^2 \rho_i \ddot{x}_i \cos\varphi_i}{2\det(\mathbf{A}_{IROM})}\right\}. \qquad (4.23)
\end{aligned}
$$

Based on (C.8) in the Appendix C, the joint PDF of $\dot{x}(t)$ and $\ddot{x}(t)$ at the output of the L-branch SC can be expressed as

$$
\begin{aligned}
p_{\dot{x}\ddot{x}}(\dot{x}, \ddot{x}) =& L \sum_{k=0}^{L-1} \binom{L-1}{k} (-1)^k \int_0^\infty \int_0^{2\pi} p_{\mathbf{W}_{IROM}}(\rho_1, \dot{x}, \ddot{x}, \varphi_1) \exp\left(-\frac{k\rho_1^2}{2b_0}\right) d\varphi_1 d\rho_1 \\
=& \frac{1}{\sqrt{2\pi b_2}} \exp\left(-\frac{\dot{x}^2}{2b_2}\right) \frac{L}{\pi\sqrt{2\pi b_0 B}} \exp\left(-\frac{b_0}{2B}\ddot{x}^2\right) \sum_{k=0}^{L-1} \binom{L-1}{k} (-1)^k \\
& \times \int_0^{2\pi} \int_0^\infty \exp\left\{-\frac{b_2 \ddot{x} \cos\varphi_1}{B}\rho_1 - \left(\frac{k+1}{2b_0} + \frac{b_2^2 \cos^2\varphi_1}{2b_0 B}\right)\rho_1^2\right\} \rho_1 d\rho_1 d\varphi_1, \\
& \qquad (4.24)
\end{aligned}
$$

where $B = b_0 b_4 - b_2^2$. Note that at any given time t, random variables $\dot{x}$ and $\ddot{x}$ are independent, and $\dot{x}$ is Gaussian, as observed in (4.16), with zero mean and variance b_2. After substituting (4.24) into (4.10) and following the derivation given in Appendix D, finally obtain the average rate of maxima of the SC inphase component

$$
\begin{aligned}
\frac{E[M_x(T)]}{T} =& \frac{L}{2\pi} \sum_{k=0}^{L-1} \binom{L-1}{k} (-1)^k \left\{ \frac{B}{\sqrt{(k+1)^2 b_0 b_2 B + (k+1) b_0 b_2^3}} + \frac{b_2^{1/2}}{b_0^{1/2}(k+1)^{3/2}} \right. \\
& \left. - \frac{4B^{3/2}}{3\pi b_0^{1/2} b_2^{5/2}} \int_0^{\frac{\pi}{2}} \frac{{}_2F_1\left(\frac{3}{2}, 2; \frac{5}{2}; -\frac{(k+1)B}{b_2^2\cos^2\alpha}\right)}{\cos^2\alpha} d\alpha \right\}, \qquad (4.25)
\end{aligned}
$$

where ${}_2F_1(.,.;.;.)$ is the hypergeometric function [36]. Using (4.18), inphase rate of maxima for Clarke's model can be shown as

$$\frac{E[M_x(T)]}{T} = f_D \frac{L}{2\pi} \sum_{k=0}^{L-1} \binom{L-1}{k} (-1)^k \Bigg\{ \frac{\pi}{(k^2+4k+3)^{1/2}} + \frac{\sqrt{2}\pi}{(k+1)^{3/2}} - \frac{2}{3} \int_0^{\frac{\pi}{2}} \frac{{}_2F_1\left(\frac{3}{2}, 2; \frac{5}{2}; -\frac{k+1}{2}\cos^2\alpha\right)}{\cos^2\alpha} d\alpha \Bigg\}. \tag{4.26}$$

Now the IROM estimator can be introduced as

$$\hat{f}_D = \hat{M}_x(T) \Bigg\{ \frac{TL}{2\pi} \sum_{k=0}^{L-1} \binom{L-1}{k} (-1)^k \Bigg(\frac{\pi}{(k^2+4k+3)^{1/2}} + \frac{\sqrt{2}\pi}{(k+1)^{3/2}} - \frac{2}{3} \int_0^{\frac{\pi}{2}} \frac{{}_2F_1\left(\frac{3}{2}, 2; \frac{5}{2}; -\frac{k+1}{2}\cos^2\alpha\right)}{\cos^2\alpha} d\alpha \Bigg) \Bigg\}^{-1}. \tag{4.27}$$

For $L = 1$, (4.27) reduces to the estimator proposed in [5].

4.3.3 PZCR Speed Estimator with SC

The joint PDF of the vector $\mathbf{W}_{PZCR} = [\rho_i \ \varphi_i \ \dot{\varphi}_i]^T$ is given in [37]

$$p_{\mathbf{W}_{PZCR}}(r_i, \varphi_i, \dot{\varphi}_i) = \frac{r_i^2 \exp\left\{ -\frac{1}{2b_0} \left(\rho_i^2 + \frac{b_0}{b_2} \rho_i^2 \dot{\varphi}_i^2 \right) \right\}}{(2\pi)^{3/2} (b_0^2 b_2)^{1/2}}. \tag{4.28}$$

Substitution of (4.28) into (C.8) from the Appendix C leads to

$$p_{\varphi\dot{\varphi}}(\varphi, \dot{\varphi}) = \frac{L}{4\pi} \sqrt{\frac{b_0}{b_2}} \sum_{k=0}^{L-1} \binom{L-1}{k} \frac{(-1)^k}{\left(k + 1 + \frac{b_0}{b_2} \dot{\varphi}^2 \right)^{3/2}}. \tag{4.29}$$

Interestingly, φ and $\dot{\varphi}$ are independent; φ is uniformly distributed over $(-\pi, \pi]$, and the PDF of $\dot{\varphi}$ is consistent with the result given in [38]. By substituting (4.29) into (4.9),[1] one

---

[1] Since (4.29) does not depend on φ, (4.30) is valid for any $\dot{\varphi}_{th}$. To simplify the notation, $\dot{\varphi}_{th} = 0$ is chosen in (4.30).

obtains the average zero crossing rate of the SC phase

$$\frac{E[N_{\varphi}(0,T)]}{T}=\frac{L}{4\pi}\sqrt{\frac{b_2}{b_0}}\sum_{k=0}^{L-1}\binom{L-1}{k}\frac{(-1)^k}{\sqrt{k+1}}.^{2} \tag{4.30}$$

Note that for $L = 1$ and the no-noise isotropic scattering scenario, (4.30) simplifies to $\sqrt{2}f_D/4$, which is consistent with the result that can be derived from [37]. Similarly, for Clarke's model, (4.3) is a linear function of f_D

$$\frac{E[N_{\varphi}(0,T)]}{T}=f_D\frac{\sqrt{2}L}{4}\sum_{k=0}^{L-1}\binom{L-1}{k}\frac{(-1)^k}{\sqrt{k+1}}, \tag{4.31}$$

which results in the PZCR speed estimator

$$\hat{f}_D=\frac{2\sqrt{2}\hat{N}_{\varphi}(0,T)}{TL\sum\limits_{k=0}^{L-1}\binom{L-1}{k}\frac{(-1)^k}{\sqrt{k+1}}}. \tag{4.32}$$

4.3.4 FZCR Speed Estimator with SC

Define the random vector $\mathbf{W}_{FZCR}=[\rho_i\ \varphi_i\ \dot{\varphi}_i\ \ddot{\varphi}_i]^{\mathsf{T}}$, whose PDF is given by [37]

$$\begin{aligned}p_{\mathbf{W}_{FZCR}}(\rho_i,\varphi_i,\dot{\varphi}_i,\ddot{\varphi}_i)=&\frac{\rho_i^3}{(2\pi)^2(b_0b_2B+4b_0^2b_2^2\dot{\varphi}_i^2)^{\frac{1}{2}}}\\&\times\exp\left\{-\frac{\rho_i^2}{2b_0}\left(1+\frac{b_0}{b_2}\dot{\varphi}_i^2+\frac{b_0^2\ddot{\varphi}_i^2}{B+4b_0b_2\dot{\varphi}_i^2}\right)\right\}.\end{aligned} \tag{4.33}$$

As before, by substituting (4.33) into (C.8) and some simplifications, obtain the joint PDF of $\dot{\varphi}(t)$ and $\ddot{\varphi}(t)$ at the output of the L-branch SC

$$\begin{aligned}p_{\dot{\varphi}\ddot{\varphi}}(\dot{\varphi},\ddot{\varphi})=&\frac{L}{4\pi\,(b_0b_2B+4b_0^2b_2^2\dot{\varphi}^2)^{\frac{1}{2}}}\sum_{k=0}^{L-1}\binom{L-1}{k}(-1)^k\\&\times\left\{\frac{1}{2b_0}\left(k+1+\frac{b_0}{b_2}\dot{\varphi}^2+\frac{b_0^2\ddot{\varphi}^2}{B+4b_0b_2\dot{\varphi}^2}\right)\right\}^{-2}.^{3}\end{aligned} \tag{4.34}$$

---

[2] For $\varphi = 0$ and π, one has $y=\rho\sin\varphi=0$. Therefore, $E[N_y(0,T)] = E[N_{\varphi}(0,T)] + E[N_{\varphi}(\pi,T)]$, as $\rho > 0$. On the other hand, since (4.29) does not depend on φ, $E[N_{\varphi}(0,T)] = E[N_{\varphi}(\pi,T)]$. Therefore $E[N_{\varphi}(0,T)] = E[N_y(0,T)]/2$, which agrees with the fact that (4.30) is half of (4.17).

After substituting (4.34) into (4.9) with $\dot{\varphi}_{th} = 0$, obtain the average zero crossing rate of the SC instantaneous frequency

$$\frac{E[N_{\dot{\varphi}}(0,T)]}{T} = \frac{1}{2\pi}\sqrt{\frac{b_4}{b_2} - \frac{b_2}{b_0}}, \tag{4.35}$$

which interestingly, does not depend on L. For the noise-free and isotropic scattering case, (4.35) reduces to $f_D/2$, which for a single branch, can be derived from [37]. Using (4.18), (4.35) simplifies to

$$\frac{E[N_{\dot{\varphi}}(0,T)]}{T} = \frac{1}{2} f_D. \tag{4.36}$$

This leads to the FZCR estimator

$$\hat{f}_D = \frac{2\hat{N}_{\dot{\varphi}}(0,T)}{T}. \tag{4.37}$$

The above equation agrees with the non-diversity estimator discussed in [39].

4.3.5 ELCR Estimators with SC and MRC

Without loss of generality, let $E[|h_i(t)|^2] = 1$. For isotropic scattering, the envelope average level crossing rate of SC diversity is known to be [34]

$$\frac{E[N_\rho(1,T)]}{T} = \sqrt{2\pi} f_D L \sum_{k=0}^{L-1} \binom{L-1}{k} (-1)^k e^{-(k+1)} \tag{4.38}$$

and of course the corresponding estimator is

$$\hat{f}_D = \frac{\hat{N}_\rho(1,T)}{\sqrt{2\pi} T L \sum_{k=0}^{L-1} \binom{L-1}{k} (-1)^k e^{-(k+1)}}. \tag{4.39}$$

---

[3] By integrating (4.34) with respect to $\dot{\varphi}$, the PDF of $\dot{\varphi}$ can be obtained, which agrees with the expression given in [38].

On the other hand, in [35], the envelope average level crossing rate of MRC diversity is derived as

$$\frac{E[N_\rho(1,T)]}{T} = f_D \frac{\sqrt{2\pi}}{e\Gamma(L)}, \tag{4.40}$$

where $\Gamma(.)$ is the gamma function [36]. Therefore, the associated estimator is

$$\hat{f}_D = \frac{e\Gamma(L)\hat{N}_\rho(1,T)}{\sqrt{2\pi}T}. \tag{4.41}$$

To the best of our knowledge, although (4.38) and (4.40) have been derived previously, their performance as speed estimators has not been studied.

4.4 Simulation Results

In this section, first the four new crossing rate expressions are validated; then the performance of six speed estimators are investigated. To verify the new closed-form crossing rates, Monte Carlo simulations using the spectral method [31] have been conducted. 100 independent realizations of L i.i.d. zero-mean complex Gaussian processes have been generated, with 10000 complex samples per realization, over $T = 1$ second. The simulated autocorrelation function at each branch is $b_0 J_0(2\pi f_D \tau)/2$ with $b_0 = 1$. As illustrated in Fig. 4.1, there is perfect agreement between the theoretical and simulation results. Note that the crossing rates are normalized by f_D in Fig. 4.1. As shown by IROM and FZCR in Fig. 4.1, some crossing rates of the combined signal do not necessarily decrease,[4] as the diversity order increases. Furthermore, for a given Doppler, IROM, IZCR, and PZCR can be utilized to measure the fluctuation rate of the combined signal versus the number of branches, whereas FZCR cannot.

Since the combined output signals of diversity systems are no longer Gaussian, it is very difficult to do analytic performance analysis such as those carried out in [5]. Therefore, this section relies on Monte Carlo simulation to compare the estimation error of six

---

[4] The ELCR goes to zero as $L \rightarrow \infty$ [34].

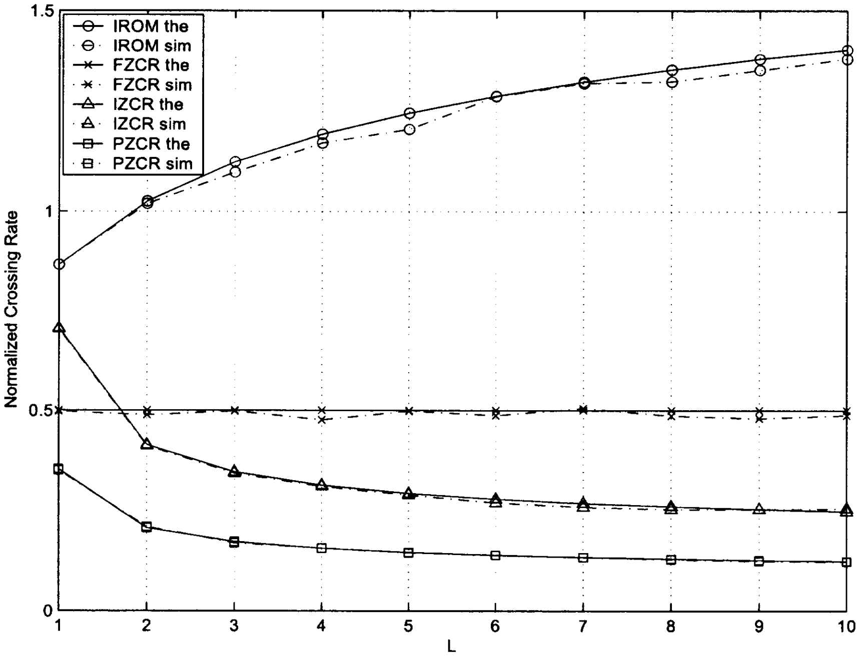

Figure 4.1 Normalized average zero crossing rates versus the number of branches L.

techniques: two inphase-based estimators in (4.20) and (4.27), two phase-based estimators in (4.32) and (4.37) and two envelope-based in (4.39) and (4.41). The estimation error is defined by

$$\left\{E[(\hat{f}_D - f_D)^2]\right\}^{\frac{1}{2}} = \left\{Var[\hat{f}_D] + (E[\hat{f}_D] - f_D)^2\right\}^{\frac{1}{2}} \tag{4.42}$$

where the first term is the variance and the second stands for the bias. All six estimators are derived for isotropic scattering in noise-free environments, and, obviously, under such conditions, are unbiased, i.e., $E[\hat{f}_D] = f_D$. In the sequel, the effect of nonisotropic scattering and Gaussian noise will also be examined in order to study the effect of diversity combining in more realistic environments. In each simulation, 100 independent realizations of L zero-mean complex Gaussian processes are generated, with 10000 complex samples per realization, over $T = 1$ second. The spectral method is also used for generating the complex Gaussian bandlimited noise with a flat power spectrum over the fixed receiver bandwidth of $B_{rx} = 101$ Hz, assuming that the largest possible Doppler frequency f_D is

101 Hz. When applicable, the signal-noise-ratio (SNR) at each branch is 10dB; and each branch experiences the same nonisotropic scattering with $\kappa = 2.1$, $\alpha = 10.8^\circ$ observed in field trials [16].

The estimation error for the IZCR estimator in (4.20) for three different cases: noise-free isotropic scattering, isotropic scattering with noise, and noise-free nonisotropic scattering are shown in Fig. 4.2, versus f_D. It is demonstrated that the IZCR estimator without SC diversity has the best performance in all situations. Fig. 4.3 shows that there is no performance improvement via SC diversity in the three different propagation environments when using the IROM estimator. The PZCR estimator with SC does not provide better performance than one with non-diversity signal, as demonstrated in Fig. 4.4. From Fig. 4.5, note that the FZCR estimator does not gain any enhancement from the SC diversity in all three cases mentioned above.

Fig. 4.6 illustrates that both the MRC-based and SC-based ELCR estimators provide the best performance with $L = 2$. However, the SC-based estimator is preferred as it does not need any channel estimate. The improvement offered by a two-branch estimator does not seem to be significant. To take full advantage of multiple observations in a diversity receiver, apparently it is helpful to look at more complex techniques such as the maximum likelihood estimators.

4.5 Conclusion

In this Chapter, the possibility of mobile speed estimation in cellular systems using diversity combining techniques has been investigated. Several new estimators were derived for selection combining and maximal ratio combining diversity methods. The impact of noise and nonisotropic scattering were extensively investigated, as well as the number of diversity branches. It has been observed that two-branch diversity combiners provide performance enhancement. To achieve higher estimation accuracy, it is helpful to use the more complex methods introduced in the following Chapters.

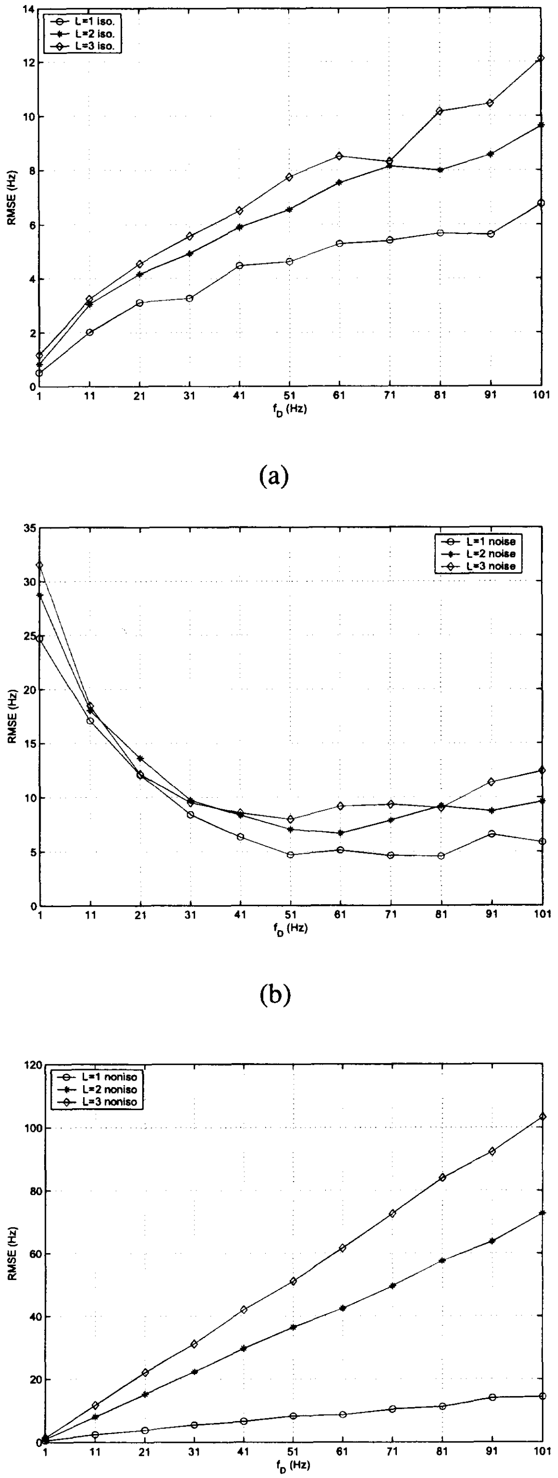

(a)

(b)

(c)

Figure 4.2 Performance of IZCR speed estimator with SC diversity: (a) isotropic scattering, no noise; (b) effect of noise (SNR = 10 dB); (c) nonisotropic scattering ($\kappa = 2.1$, $\alpha = 10.8°$).

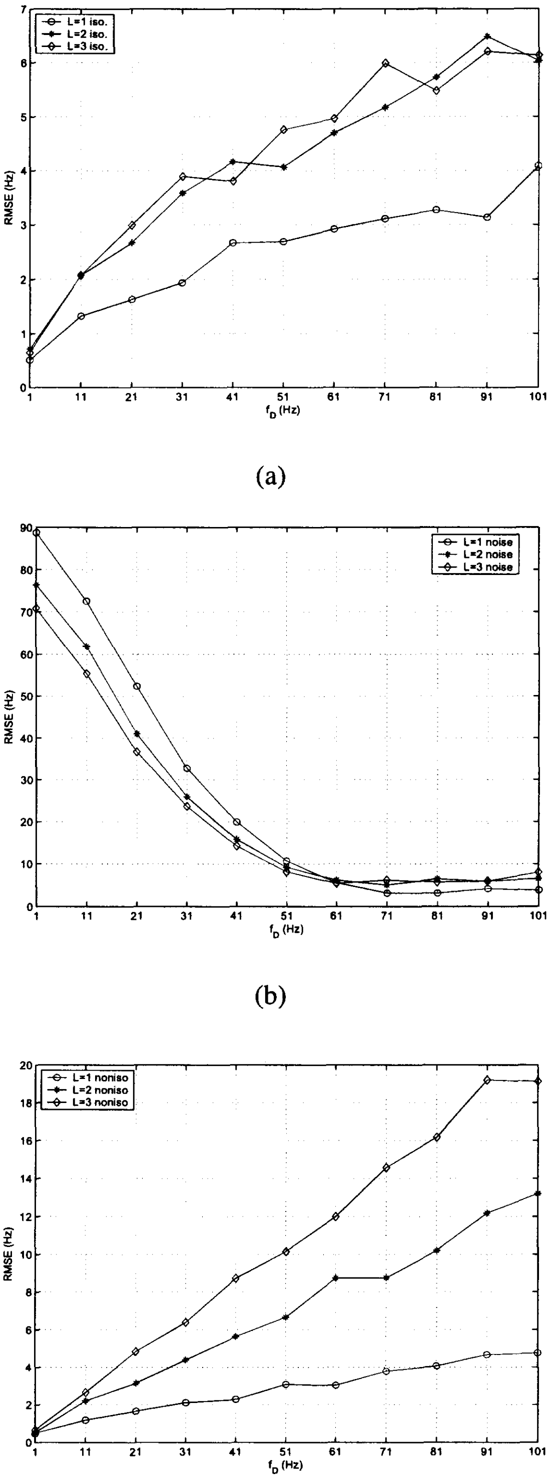

(a)

(b)

(c)

Figure 4.3 Performance of IROM speed estimator with SC diversity: (a) isotropic scattering, no noise; (b) effect of noise (SNR = 10 dB); (c) nonisotropic scattering ($\kappa = 2.1$, $\alpha = 10.8°$).

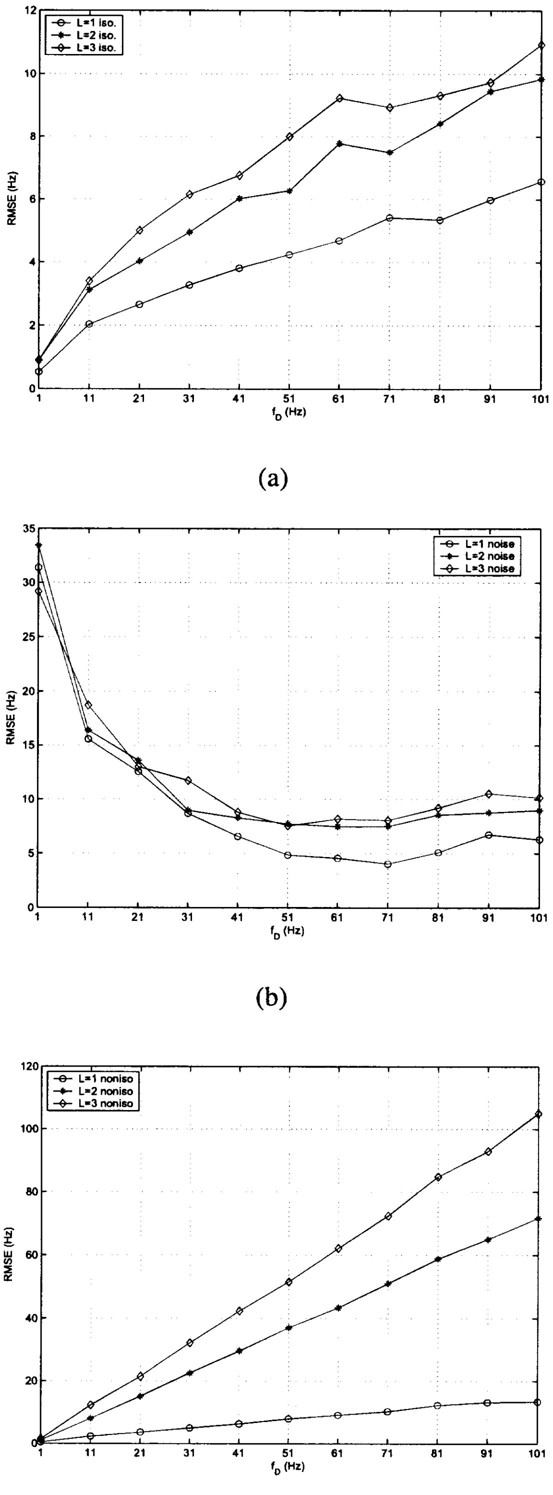

(a)

(b)

(c)

Figure 4.4 Performance of PZCR speed estimator with SC diversity: (a) isotropic scattering, no noise; (b) effect of noise (SNR = 10 dB); (c) nonisotropic scattering ($\kappa = 2.1$, $\alpha = 10.8°$).

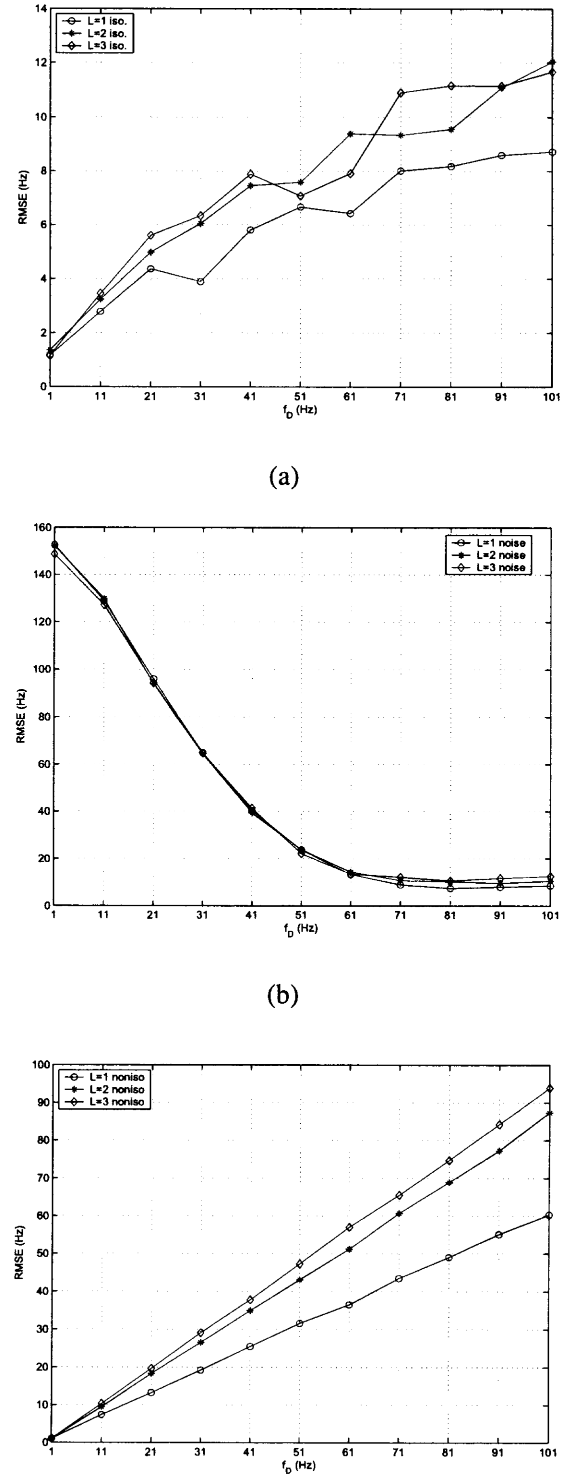

(a)

(b)

(c)

Figure 4.5 Performance of FZCR speed estimator with SC diversity: (a) isotropic scattering, no noise; (b) effect of noise (SNR = 10 dB); (c) nonisotropic scattering ($\kappa = 2.1$, $\alpha = 10.8°$).

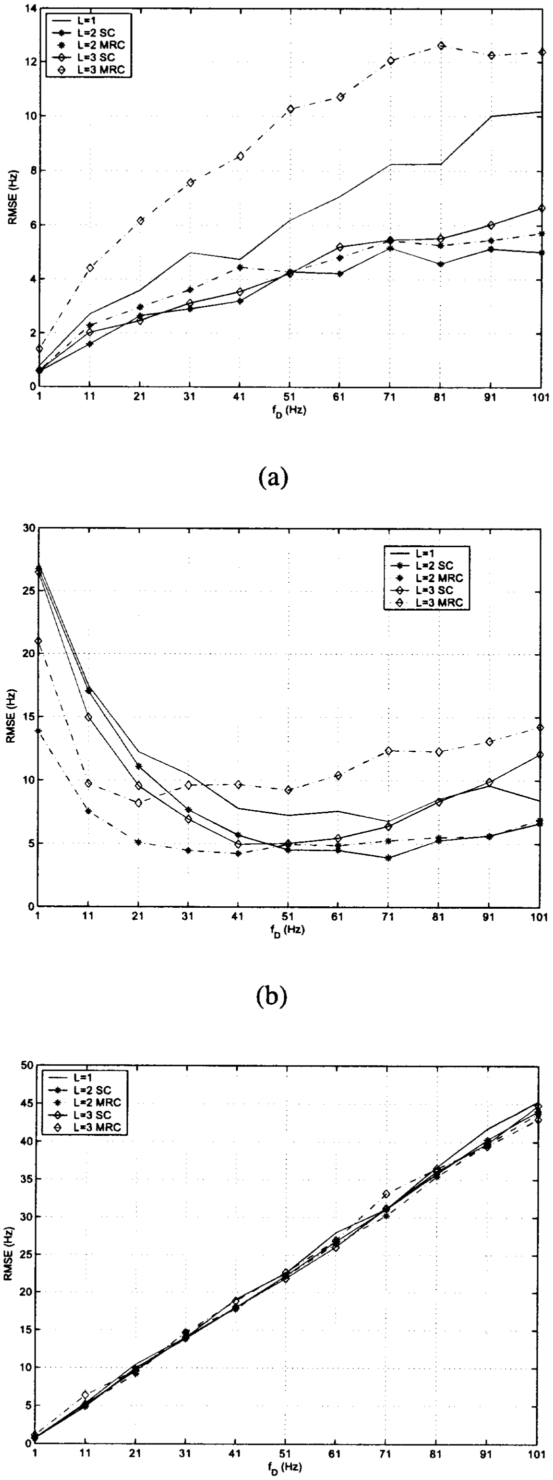

(a)

(b)

(c)

Figure 4.6 Performance of ELCR speed estimators with SC and MRC diversity: (a) isotropic scattering, no noise; (b) effect of noise (SNR=10 dB); (c) nonisotropic scattering ($\kappa = 2.1, \alpha = 10.8°$).

CHAPTER 5

NONPARAMETRIC DOPPLER SPREAD ESTIMATION

5.1 Introduction

In this chapter, a novel, low complex technique is proposed. It is robust against noise, both Gaussian and impulsive non-Gaussian, and insensitive to nonisotropic scattering and LOS. The impact of three dimensional (3-D) propagation, more likely happening in urban environments [18], is investigated as well. Two single-antenna-based speed estimators are proposed for the mobile station (MS). They rely on the new technique and are applicable to both narrowband and wideband channels. Using the antenna array at the base station (BS), a space-time estimator is also developed. Mathematical performance analysis of the single-antenna estimators is presented and confirmed via Monte Carlo simulation.

The organization of this chapter is as follows. Signal, channel, and noise models are discussed in Section 5.2. The novel speed estimation technique and the associated single-antenna solutions are presented in Section 5.3. Extension to multiple antennas is given in Section 5.4. Section 5.5 includes mathematical performance analysis of single-antenna estimators. Section 5.6 provides numerical results obtained via extensive Monte Carlo simulations. Comparison with measured data is carried out in Section 5.7, and Section 5.8 concludes this Chapter.

5.2 Signal, Channel and Noise Models

The received lowpass complex envelope in a noisy Rician frequency-flat fading channel, in response to an unmodulated carrier, is

$$z(t) = h(t) + v(t), \tag{5.1}$$

where $v(t)$ represents the noise and $h(t)$ includes the random diffuse component $h^c(t)$ and the deterministic LOS component $h^d(t)$.

In wireless mobile systems, the complex noise process $v(t)$ in (5.1) is the superposition of two components: the receiver thermal noise $n_g(t)$ and the man-made noise $n_{imp}(t)$ [40]. The receiver noise is commonly modeled as a white Gaussian process. The man-made noise generated by electrical equipments such as vehicle ignition system, neon signs, has an impulsive non-Gaussian characteristic. This is quite different from Gaussian noise and appears in the frequency spectrum up to 7 GHz [40]. Middleton's Class-A model is used where the probability density functions (PDF) of the non-Gaussian noise $v(t)$, with zero-mean and variance σ_v^2, can be written as [41] [42]

$$p_v(v) = e^{-A} \sum_{k=0}^{\infty} \frac{A^k}{k! \pi \sigma_k^2} \exp\left(-\frac{|v|^2}{\sigma_k^2}\right), \tag{5.2}$$

where $\sigma_k^2 = \sigma_v^2((k/A) + \Gamma)/(1 + \Gamma)$, with Γ denoting the power ratio of $n_g(t)$ over $n_{imp}(t)$, and parameter A is called the impulsive index. Small values of A indicate a highly impulsive noise whereas large A corresponds to a near-Gaussian one.

5.3 The New Speed Estimation Algorithm

By looking at the basic fading spectrum for 2-D isotropic scattering, which is proportional to $(f_D^2 - f^2)^{-1/2}$ [2], it is easy to observe the two singularities at $f = \pm f_D$. These peaks at the maximum Doppler frequency remain to exist, even with nonisotropic scattering, LOS, and 3-D propagation, irrespective of the PDF of noise. Therefore, to estimate f_D, to estimate the spectrum of the received signal in (5.1), and then find the largest frequency at which the spectrum has a maximum. There are many methods of estimating the PSD of a random signal [43]. The periodogram-based nonparametric spectrum estimation technique has been chosen due to its simplicity. It has also been observed that more complex nonparametric PSD estimators provide the same performance as the periodogram when applied to the speed estimation problem. In this section, two f_D estimators are proposed for frequency-flat and frequency-selective channels, respectively.

5.3.1 The Speed Estimator in Narrowband Channels

Consider the N-sample discrete-time version of received continuous -time signal $z(t)$ with duration T, $\{z[n] = x[n] + jy[n]\}_{n=0}^{N-1}$, with x and y as the real and imaginary parts, respectively, and define the PSD of $\{z[n]\}_{n=0}^{N-1}$ as $S_z(\mu)$. In the absence of aliasing, $S_z(\mu)$ is the scaled version of the PSD of the continuous signal $z(t)$, $\Omega_z(f)$, given by [43]

$$S_z(\mu) = f_s \Omega_z(\mu f_s),\ |\mu| \leq 1/2, \tag{5.3}$$

where $f_s = N/T$ is the sampling frequency of $z(t)$. $S_z(\mu)$ can be estimated directly from the data using the periodogram defined as

$$\hat{S}_z(\mu_k) = \frac{1}{N}\left|\sum_{n=0}^{N-1} z[n]e^{-j2\pi\mu_k n}\right|^2,\ \mu_k = \frac{k}{N}, k = 1 - \frac{N}{2}, ..., \frac{N}{2}, \tag{5.4}$$

where N is even. Note that (5.4) can be efficiently computed via fast Fourier transform (FFT). The novel estimator is then given by

$$\hat{f}_D = f_s \times \left|\arg \max_{\mu_k} \hat{S}_z(\mu_k)\right|. \tag{5.5}$$

5.3.2 The Speed Estimator in Wideband Channels

Consider an I-tap wideband channel $H(\tau, t)$, with $h_i(t)$ being the i-th channel gain corresponding to the propagation path with the excess delay τ_i

$$H(\tau, t) = \sum_{i=1}^{I} h_i(t)\delta(\tau - \tau_i). \tag{5.6}$$

Wideband channel measurements conducted at the MS exhibit a variety of different Doppler spectrum shapes at different propagation paths [44]. As will later become clear, this special feature is particularly useful in decreasing the estimation error due to some strong nonisotropic scattering and/or LOS which may occur. Based on (5.5), the speed estimator in frequency selective channels can be written as

$$\hat{f}_D = \max\left\{\hat{f}_D^i\right\}_{i=1}^{I}, \tag{5.7}$$

where $\hat{f}_D^i = f_s \times \left|\arg\max_{\mu_k} \hat{S}_{z_i}(\mu_k)\right|$.

5.4 The Space-Time Speed Estimation Algorithm

This section extends the new algorithm to a system with multiple receive antennas in narrowband channels. Consider a uniform linear antenna array at the elevated BS of a marcocell composed of L omnidirectional unit-gain elements, and with element spacing d. The BS experiences no local scattering, whereas the single antenna MS is surrounded by local scatters. When MS transmits an unmodulated carrier, with the received signals at the l-th element $z_l(t) = h_l(t) + v_l(t), l = 1, 2, ..., L$, the space-time crosscorrelation function between $z_a(t)$ and $z_b(t)$, defined by $r_z((b-a)\Delta, \tau) = E[z_a(t) z_b^*(t+\tau)]$ with $\Delta = d/\lambda$, can be written as

$$r_z((b-a)\Delta, \tau) = r_h((b-a)\Delta, \tau) + r_v(\tau)\delta_{a-b}, \tag{5.8}$$

where $r_v(\tau) = E[v_l(t) v_l^*(t+\tau)], l = 1, 2, ..., L$, is the autocorrelation function of the noise component at each branch, δ_c is the Kronecker delta function, 1 for $c = 0$ and 0 otherwise, and $r_h((b-a)\Delta, \tau) = E[h_a(t) h_b^*(t+\tau)]$, when considering 2-D scattering, given by [19]

$$\begin{aligned} r_h((b-a)\Delta, \tau) =& \frac{\sigma_h^2}{K+1} \frac{I_0\left(\sqrt{\kappa^2 - \zeta^2 - \varrho^2 - 2\zeta\varrho + j2\kappa(\zeta+\varrho)\cos\alpha}\right)}{I_0(\kappa)} \\ &+ \frac{K\sigma_h^2}{K+1} \exp\left(j(\zeta+\varrho)\cos\alpha_0\right), \end{aligned} \tag{5.9}$$

where $\zeta = 2\pi f_D \tau$, and $\varrho = 2\pi(a-b)\Delta$ with $1 \le a \le b \le L$. Note that in (5.9), reasonable assumption of equal receive power σ_h^2 and Rician factor K at each antenna are made. The noise components are independent at different elements, with the same power σ_v^2.

According to the experiments conducted at different locations and frequencies [45] [46] [47] [48], the angle spread at the BS is generally small for macrocells in urban, suburban, and rural areas. It is most often less than 30°, which corresponds to $\kappa \geq 14.6$, and in some cases very small, say, less than 10°, which translates into $\kappa \geq 131.3$ [19] [49]. In such heavily nonisotropic scattering environments, the PDF of the diffuse AOA at the BS can be accurately approximated by a Gaussian PDF with mean α and variance $1/\kappa$ [19]. Due to the small angle spread at the BS, it is reasonable to assume $\alpha_0 = \alpha$ [50].

When the channel experiences such heavily nonisotropic scattering, the performance of the proposed estimator degrades. In fact, as proved in Appendix E, the Doppler spectrum $\Omega_h(f)$ of the heavily nonisotropic Rayleigh fading channel has only one strong peak, approximately at $f = f_D \cos\alpha$, while the peaks at $f = \pm f_D$ virtually disappear. However, for each branch $z_l(t)$, one can still use the same technique as (5.5). This provides an accurate estimate of $f_D \cos\alpha$

$$\hat{f}^l_{D,\alpha} = f_s \times \left| \arg\max_{\mu_k} \hat{S}_{z_l}(\mu_k) \right| . \tag{5.10}$$

On the other hand, by setting $\tau = 0$ in (5.8), together with the Gaussian approximation for AOA, the spatial cross correlation function $r_z((b-a)\Delta, 0) = E[z_a(t) z_b^*(t)]$, $1 \leq a \leq b \leq L$, can be accurately approximated by [19]

$$\begin{aligned} r_z((b-a)\Delta,0) &= r_h((b-a)\Delta,0) \\ &\approx \left\{ \frac{\sigma_h^2}{K+1} \exp\left(-\frac{\varrho^2 \sin^2\alpha}{2\kappa} \right) + \frac{K\sigma_h^2}{K+1} \right\} \exp\{ j\varrho\cos\alpha \} , \end{aligned} \tag{5.11}$$

where $r_z(\cdot,0) = r_h(\cdot,0)$, $1 \leq a < b \leq L$, due to the spatial independence of noise components at different branches. Now, estimate $\cos\alpha$ via

$$\widehat{\cos\alpha} \approx \frac{\measuredangle \hat{r}_z(\Delta,0)}{-2\pi\Delta}, \tag{5.12}$$

where $\measuredangle$ denotes the phase of a complex number and $\hat{r}_z(\Delta, 0)$ is the estimate of $r_z(\Delta, 0) = E[z_a(t)z^*_{a+1}(t)], \forall\, a \in [1, L-1]$, given by

$$\hat{r}_z(\Delta, 0) = \frac{1}{L-1}\sum_{l=1}^{L-1} \hat{r}^l_z(\Delta, 0). \tag{5.13}$$

In eq. (5.13), $\hat{r}^l_z(\Delta, 0) = N^{-1}\sum_{n=0}^{N-1} z_l(n)z^*_{l+1}(n)$, $l \in [1, L-1]$, is the l-th adjacent-antenna-pair estimate of $r_z(\Delta, 0)$. Now it is necessary to justify the one-lag phase estimation in (5.12). Note that the estimator given in (5.12) is equivalent to the one-lag Pulse-Pair (PP) frequency estimation [51, eq. (6)] in the presence of Doppler spread. The spatial cross-correlation function (5.11) used here takes the same form as the channel autocorrelation function utilized in [51]. Therefore, the performance analysis conducted for PP frequency estimation in [51] can be applied to (5.12) as well. Although there is an optimum lag to minimize the variance of the PP estimation of $\cos\alpha$, it has been shown [51, Fig.1] that at high SNR, the one-lag and optimum-lag PP estimations are comparable and their performances are close to the CRLB. Clearly, according to (5.11), There is infinite SNR when estimating $\cos\alpha$ using (5.12).

Finally, f_D can be estimated via

$$\hat{f}_D = \frac{\hat{f}_{D,\alpha}}{\widehat{\cos\alpha}}, \tag{5.14}$$

where $\hat{f}_{D,\alpha} = L^{-1}\sum_{l=1}^{L} \hat{f}^l_{D,\alpha}$, and $\hat{f}^l_{D,\alpha}$ and $\widehat{\cos\alpha}$ are given in (5.10) and (5.12), respectively.

5.5 Analytic Performance Assessment

The performance of the estimator can be measured by using the root mean squared error (RMSE) criterion

$$\left\{E[(\hat{f}_D - f_D)^2]\right\}^{\frac{1}{2}} = \left\{Var[\hat{f}_D] + (E[\hat{f}_D] - f_D)^2\right\}^{\frac{1}{2}}, \tag{5.15}$$

where the first term in the right-hand side of (5.15) is the variance, and the second stands for the bias of the estimator. In this section, first the key result is derived for the speed estimator in (5.5) for narrowband channels, and then extended to estimator in (5.7) for wideband channels.

Proposition 1 *For a zero-mean proper complex Gaussian random process* $z(t)$*, the elements of the sequence* $\{\hat{S}_z(\mu_k)\}_{k=1-N/2}^{N/2}$ *are asymptotically independent as* $N \to \infty$*, with an exponential PDF*

$$p_{\hat{S}_z(\mu_k)}(s) = \frac{1}{\bar{S}_z(\mu_k)} \exp\left\{-\frac{s}{\bar{S}_z(\mu_k)}\right\}, \; s > 0, \tag{5.16}$$

where $\bar{S}_z(\mu_k)$ *is the mean of* $\hat{S}_z(\mu_k)$*, given by (F.3) in Appendix F.*

Proof: See Appendix F. ■

In the absence of both LOS and impulsive noise, $z(t)$ in (5.1) is a zero-mean proper complex Gaussian random process [52]. Now define $\hat{f}_{\max} = f_s \times \arg \max_{\mu_k} \hat{S}_z(\mu_k)$ so that $\hat{f}_D = \left|\hat{f}_{\max}\right|$. Obviously $\hat{f}_{\max}$ is a discrete random variable, taking N values from the set $\{f_s\mu_k\}_{k=1-N/2}^{N/2}$. Let $\mathscr{E}_i$ denote the event where μ_i is the discrete frequency at which $\hat{S}_z(\cdot)$ achieves its maximum. Then the probability mass function (PMF) of $\hat{f}_{\max}$ can be obtained as

$$\begin{aligned} p_{\hat{f}_{\max}}(f_i) &= \text{Prob}(\hat{f}_{\max} = f_i) = \text{Prob}(\mathscr{E}_i) = \text{Prob}\left\{\hat{S}_z(\mu_i) = \max\left(\{\hat{S}_z(\mu_k)\}_{k=1-N/2}^{N/2}\right)\right\} \\ &= \int_0^{\infty} \text{Prob}\underbrace{\left\{\hat{S}_z(\mu_{1-N/2}) < s, ..., \hat{S}_z(\mu_{N/2}) < s\right\}}_{N-1 \text{ terms}} p_{\hat{S}_z(\mu_i)}(s)ds, \end{aligned} \tag{5.17}$$

where $f_i = f_s \times \mu_i = i/T$, $1 - N/2 \leq i \leq N/2$. Since $\{\hat{S}_z(\mu_k)\}_{k=1-N/2}^{N/2}$ includes independent random variables when N is large, (5.17) simplifies to

$$p_{\hat{f}_{\max}}(f_i) = \int_0^{\infty} \prod_{l=1-N/2, l\neq i}^{N/2} P_{\hat{S}_z(\mu_l)}(s) p_{\hat{S}_z(\mu_i)}(s)ds, \tag{5.18}$$

where $P_{\hat{S}_z(\mu_k)}(s)$ is the cumulative distribution function (CDF) of $\hat{S}_z(\mu_k)$, given by

$$P_{\hat{S}_z(\mu_k)}(s) = 1 - \exp\left\{-\frac{s}{\bar{S}_z(\mu_k)}\right\},\ s > 0. \tag{5.19}$$

After substituting (5.16) and (5.19) into (5.18), obtain

$$p_{\hat{f}_{\max}}(f_i) = \int_0^\infty \prod_{l=1-N/2}^{N/2} \left(1 - \exp\left\{-\frac{\bar{S}_z(\mu_i)}{\bar{S}_z(\mu_l)} s\right\}\right) \frac{\exp\{-s\}}{1-\exp\{-s\}} ds. \tag{5.20}$$

Finally find that

$$p_{\hat{f}_D}(f_i) = p_{\hat{f}_{\max}}(f_i) + p_{\hat{f}_{\max}}(f_{1-i}),\ i = 0, 1, ..., \frac{N}{2}. \tag{5.21}$$

Note that if $N \to \infty$, for a fixed T, then $\overline{S}_z(\mu_i) \to S_z(\mu_i) = f_s \Omega_z(\mu_i f_s)$ [43]. In this case, (5.20) can be written in terms of the PSD of the continuous-time signal $z(t)$ as

$$p_{\hat{f}_{\max}}(f_i) = \int_0^\infty \prod_{l=1-N/2}^{N/2} \left(1 - \exp\left\{-\frac{\Omega_z(f_i)}{\Omega_z(f_l)} s\right\}\right) \frac{\exp\{-s\}}{1-\exp\{-s\}} ds. \tag{5.22}$$

Based on (5.22) and (5.21), it can be shown that with large N, as T increases, $p_{\hat{f}_D}(f_i)$ becomes more spiky around the true Doppler f_D, and the estimation error decreases accordingly. Needless to say, the performance of the new estimator can be numerically calculated by substituting (5.20) and (5.21) into (5.15). Monte Carlo simulation results presented in the next section further confirm the accuracy of the analysis here.

Now the PDF of the speed estimator in (5.7) for wideband channels needs to be derived. Since $z_i(t)$'s of different propagation paths can be reasonably modeled as independent processes, the corresponding speed estimates $\hat{f}_D^i$ in (5.7) are independent as well. Therefore, similarly to the derivation of eq. (5.18), it can be shown that

$$p_{\hat{f}_D}(f_l) = \sum_{i=1}^{I} \prod_{q=1, q\neq i}^{I} P_{\hat{f}_D^q}(f_l) p_{\hat{f}_D^i}(f_l), l = 0, 1, ..., N/2, \tag{5.23}$$

where $P_{\hat{f}_D^q}(f_l)$ is the CDF of $\hat{f}_D^q$ and can be readily evaluated using (5.20) and (5.21).

5.6 Numerical and Monte Carlo Simulation Results

In this section, the performance of the single-antenna speed estimators in (5.5) and (5.7) is investigated; and the theoretical performance analysis is validated by Monte Carlo simulations. Then the performance of the array-based estimator in (5.14) is simulated. In each simulation, except when mentioned otherwise, 500 independent realizations of Q zero-mean complex Gaussian processes are generated using the spectral method [31], with $N = 256$ complex samples per realization, over $T = 1$ second, where $Q = 1, I, L$, to simulate narrowband and wideband channels for the single-antenna estimators, and the space-time channel for the array-based estimator, respectively. Also the antenna spacing of $\Delta = 1/2$ is chosen for the array-based estimator. If not explicitly stated, the noise is Gaussian with a 10 dB signal-noise-ratio (SNR) defined by σ_h^2/σ_v^2, where σ_v^2 is the power of the band limited noise with a flat spectrum. The receiver bandwidth B_{rx} is fixed at 101 Hz, assuming that the largest possible maximum Doppler frequency f_D is 101 Hz.

5.6.1 Speed Estimator in a Narrowband Channel

Now, Monte Carlo simulation is used to validate the theoretical performance evaluation results in a general scattering environment with 2-D nonisotropic AOA and Gaussian noise in a Rayleigh channel with a single antenna

$$r_z(\tau) = \sigma_h^2 \frac{I_0\left(\sqrt{\kappa^2 - 4\pi f_D^2 \tau^2 + j4\pi\kappa f_D \tau \cos\alpha}\right)}{I_0(\kappa)} + \sigma_v^2 \frac{\sin(2\pi B_{rx}\tau)}{2\pi B_{rx}\tau}. \tag{5.24}$$

Then the effect of LOS, non-Gaussian impulsive noise, and 3-D propagation on the performance are examined via Monte Carlo simulation.

In Fig. 5.1, simulations are shown for isotropic scattering, $\kappa = 0$, which closely match the theoretical results. Note that, as expected, the estimation error drops as the observation time T increases. The accuracy of the estimator for the 10 dB SNR is remarkable when compared with other methods [5] [11]. The estimation error versus the nonisotropic scattering parameter κ with different α's is shown in Fig. 5.2, where the true Doppler

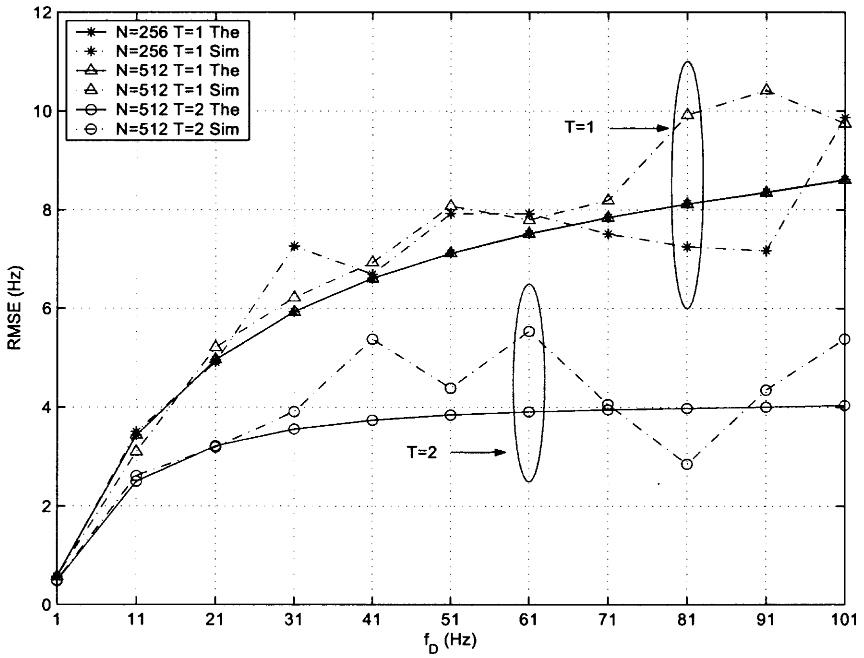

Figure 5.1 Performance over a Rayleigh fading channel, isotropic scattering (SNR = 10 dB).

is 41 Hz. Again, the simulation and theory match perfectly. Note that $0 \leq \kappa \leq 3.3$ and $0^\circ \leq \alpha \leq 36^\circ$ represent typical scatterings observed at the mobile, obtained from experimental data collected at a variety of propagation environments [16]. The estimation error with respect to different SNRs, for $f_D = 41$ Hz, is shown in Fig. 5.3. As seen, the new speed estimation technique provides a good performance, even for SNRs as low as 5 dB.

Fig. 5.4 illustrates the estimation error versus f_D when the mobile experiences LOS in Rician fading. Observe that the performance degrades to some extent as α_0 increases. On the other hand, the LOS component is able to improve the estimator's performance where α_0 is small. This is due to the impulse generated by LOS at $f = f_D \cos \alpha_0$. It will be seen in the next subsection that this dependency on LOS can be easily removed in wideband channels. To look at the effect of the impulsive noise, $(\Gamma = 0.01, A = 0.1)$ and $(\Gamma = 0.01, A = 10)$ are considered, which indicate that the channel noise is highly impulsive and near-Gaussian, respectively [53]. As shown in Fig. 5.5, the new estimator

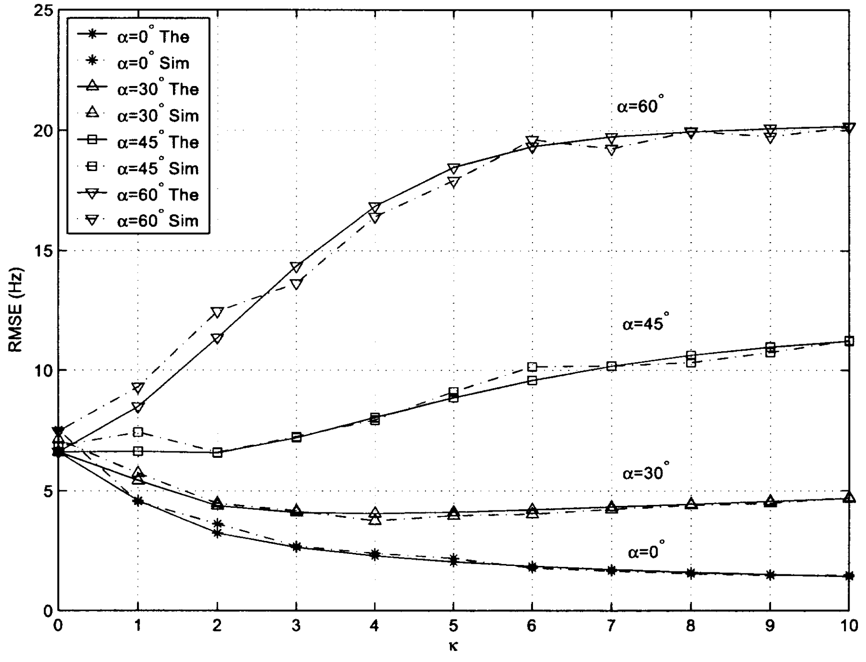

Figure 5.2 Effect of κ and α in a Rayleigh fading channel ($f_D = 41$ Hz, SNR=10 dB).

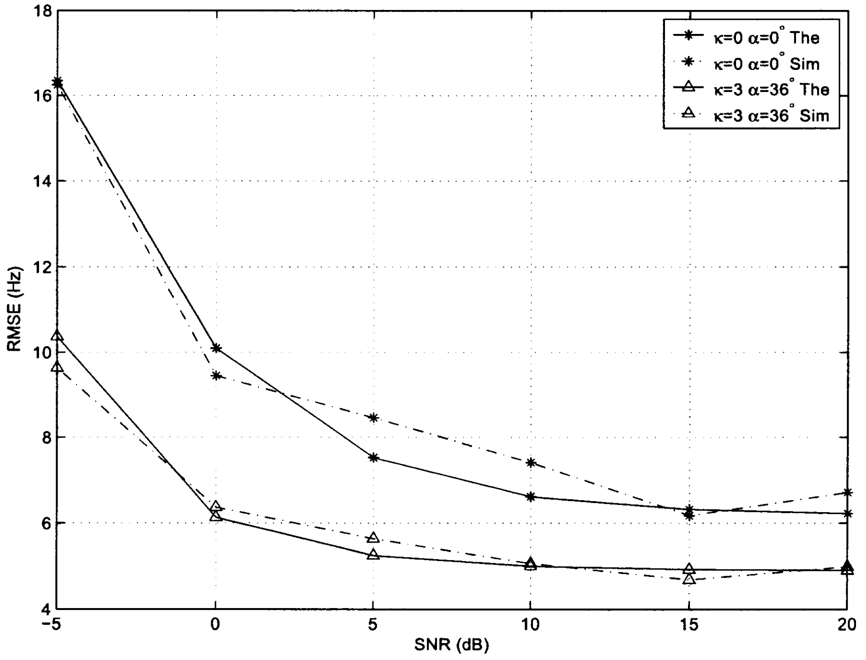

Figure 5.3 Effect of SNR in a noisy Rayleigh fading channel ($f_D = 41$ Hz).

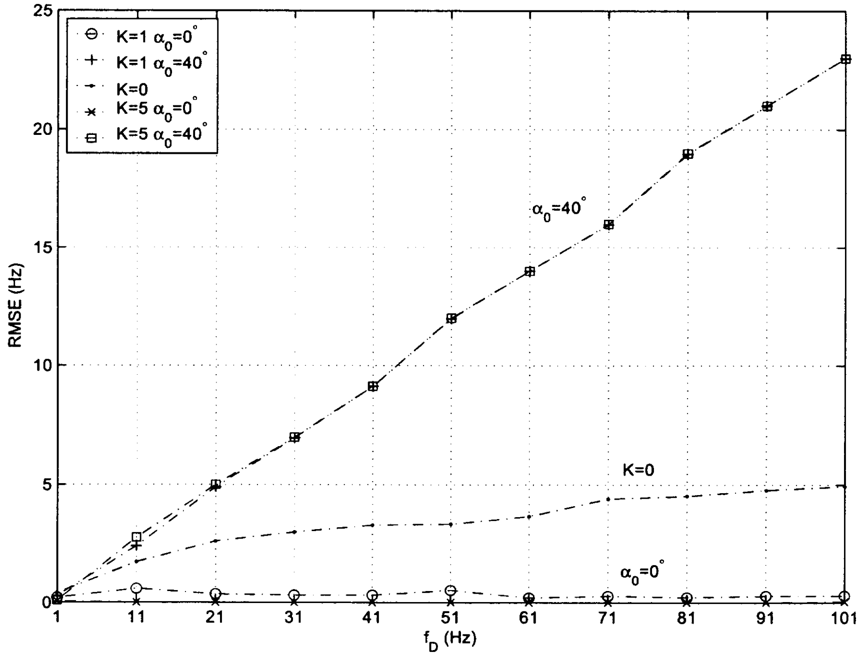

Figure 5.4 Performance over a noisy Rician fading channel (SNR=10 dB, $\kappa = 2.1$, $\alpha = 10.8°$).

is insensitive to the PDF of noise, as expected. The impact of 3-D scattering on speed estimation is shown in Fig. 5.6. Again note that the new method is still able to provide accurate Doppler estimation over a wide range of mobile speeds.

5.6.2 Speed Estimator in a Wideband Channel

As shown in Figs 5.2 and 5.4, the performance of the proposed narrowband estimator degrades in nonisotropic scattering environments as $\alpha \to 90°$ or in the presence of LOS as $\alpha_0 \to 90°$. This is due to the spike generated at $f = f_D \cos \alpha$ and $f_D \cos \alpha_0$, respectively. However, according to the experiments conducted at the MS [44], the Doppler spectra observed at different propagation paths of the wideband channel have different shapes. In fact, only the first or second paths may include LOS or a specular component. Furthermore, the spectra of longer paths are closer to U-shape Clarke's spectrum, with clear peaks at $\pm f_D$. These observations serve as strong motivations for using (5.7). With I denoting the total number of paths, the total signal power is $\sigma_h^2 = \sum_{i=1}^{I} \sigma_{h_i}^2$, where $\sigma_{h_i}^2$ is the received

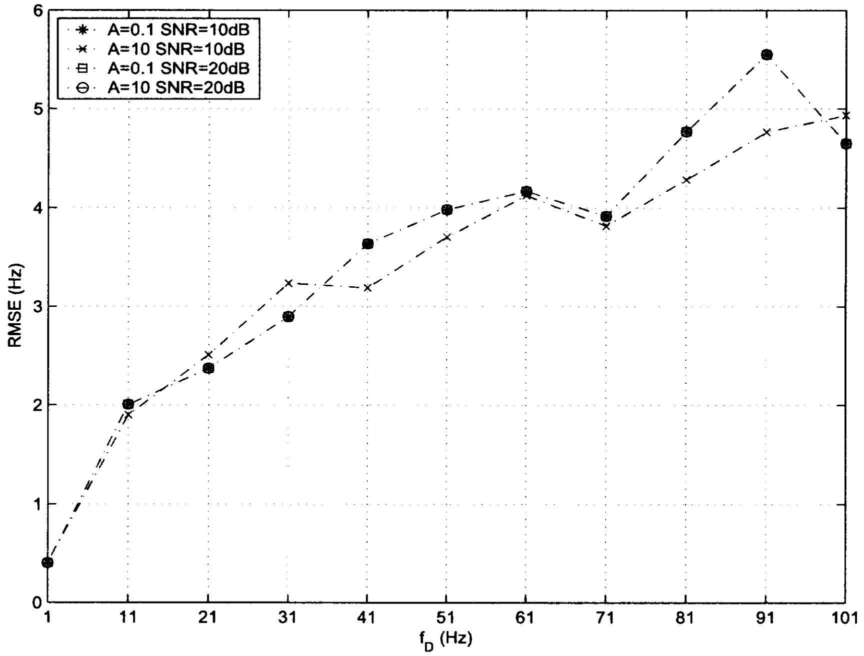

Figure 5.5 Performance over a Rayleigh fading channel with impulsive-noise ($\kappa = 2.1$, $\alpha = 10.8°$).

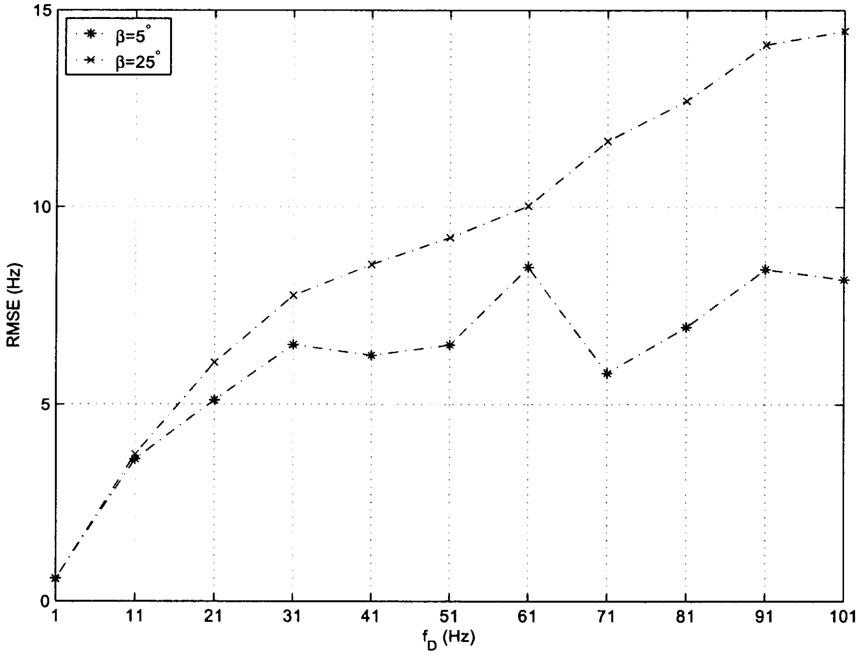

Figure 5.6 Performance over a noisy Rayleigh fading channel with three-dimensional scattering (SNR=10 dB).

signal power via the ith path. Take the number of available paths as $I = 5$ and consider the exponential power delay profile such that $\sigma^2_{h_i} = \sigma^2_{h_1} \exp\{-\eta(\tau_i - \tau_1)\}$ [54], where $\tau_i = i/5$ μs, $1 \leq i \leq 5$.

In simulating (5.7), only the first three paths were picked up as SNR in the last two paths is small. The statistics of the first three paths for scenario 1 are given by $(K = 5, \alpha_0 = 60°, \kappa = 3, \alpha = 36°)$, $(K = 0, \kappa = 3, \alpha = 36°)$, and $(K = 0, \kappa = 2.1, \alpha = 10.8°)$, respectively. In scenario 2, $(K = 0, \kappa = 10, \alpha = 60°)$, $(K = 0, \kappa = 3, \alpha = 36°)$, and $(K = 0, \kappa = 2.1, \alpha = 10.8°)$. Clearly, in scenario 1, there is an LOS in the first path, with mildly nonisotropic scattering in all the paths. In scenario 2 there is no LOS, but strong nonisotropic scattering in the first path and mild scattering in the second and third. Although the path SNR decreases by the path delay, a sufficiently accurate Doppler estimate, as shown in Fig. 5.7, can still be obtained due to the robustness of the nonparametric technique to noise already demonstrated in Fig. 5.3. Note that the total SNR here is still 10 dB. Obviously, by taking advantage of multiple paths, the negative impacts of LOS and strong nonisotropic scattering are avoided. Fig. 5.8 illustrates the effect of η on the performance for scenario 2, at $f_D = 41$ Hz. When η is large, the first path, which is heavily nonisotropic, becomes the dominant path. This is why the performance degrades. Again, in Fig. 5.7 and Fig. 5.8, the analytic results match the simulations.

5.6.3 The Space-Time Speed Estimator with Multiple Antennas

The space-time crosscorrelation of a fading channel with multiple antennas used in the subsequent simulations is

$$r_z((b-a)\Delta, \tau) = r_h((b-a)\Delta, \tau) + \sigma_v^2 \frac{\sin(2\pi B_{rx}\tau)}{2\pi B_{rx}\tau} \delta_{a-b}, \tag{5.25}$$

where $r_h((b-a)\Delta, \tau)$ is given in (5.9). As shown in Fig. 5.2, heavily nonisotropic scattering, normally experienced by BS in marcocells, could degrade the performance if the single-antenna estimator in (5.5) is applied directly. Fig. 5.9 illustrates the performance

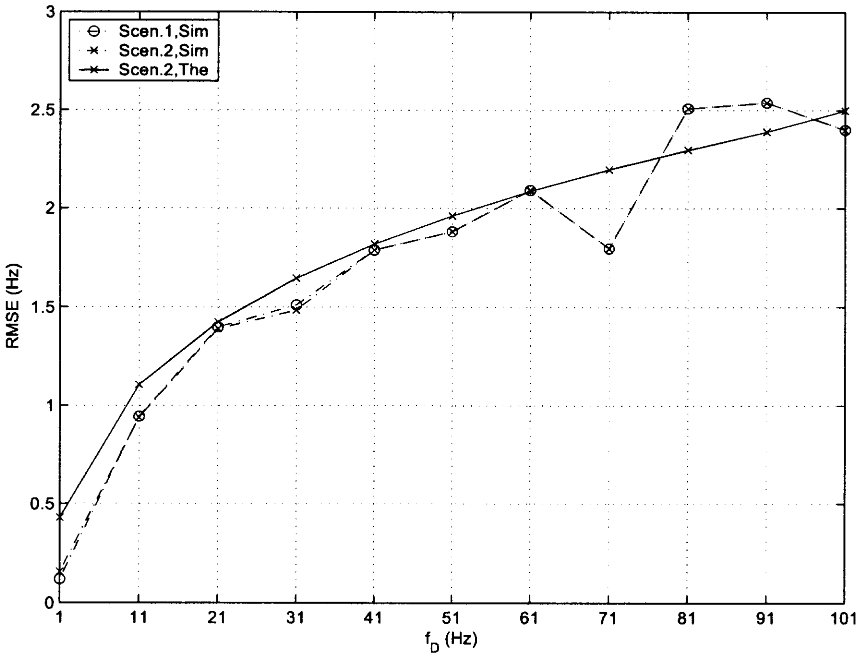

Figure 5.7 Performance of the speed estimator in wideband channels ($\eta = 1$, SNR = 10 dB).

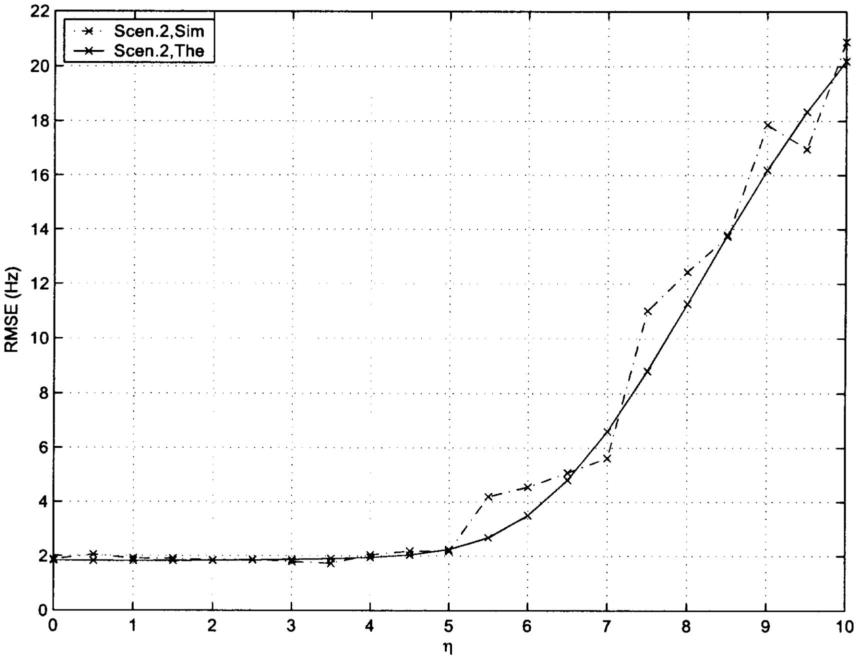

Figure 5.8 Effect of η (SNR=10 dB, $f_D = 41$ Hz).

of the space-time speed estimator in (5.14) versus the number of antenna elements L, in different propagation scenarios for $f_D = 41$ Hz. Clearly, the estimation error decreases significantly as L increases from one to two due to the spatial information used. However, further increase in L does not result in much performance gain, since the L estimates $\left\{\hat{f}^l_{D,\alpha}\right\}_{l=1}^{L}$ in (5.14) are highly correlated due to the small element spacing. This observation indicates that the space-time estimator is actually applicable to BS arrays with any shape or configuration, when using only two adjacent antennas. In the sequel, $L = 2$ is chosen as well.

Fig. 5.10 illustrates the RMSE versus f_D, for both Rayleigh and Rician channels with the scattering scenario $(\kappa = 100,\ \alpha = 60°, \alpha_0 = 60°)$. Clearly, the performance of the array-based estimator is much better for different Rice K factors. The effect of κ and α on the performance for $f_D = 41$ Hz, is shown in Fig. 5.11. Obviously, the array-based estimator provides a much smaller estimation error for different values of α. Finally, the effect of element spacing Δ is simulated in different scattering environments for $f_D = 41$ Hz. As shown in Fig. 5.12, the array-based estimator is fairly insensitive to the choice of Δ.

5.7 Application to Measured Data

This section compares the proposed PSD-based estimator in (5.5) (PSD) with seven other methods [5] [11]: five crossing-based methods consisting of the inphase zero crossing rate estimator (IZCR), the envelope level crossing rate estimator (ELCR), the inphase rate of maxima estimator (IROM), the envelope rate of maxima estimator (EROM), the instantaneous frequency zero crossing rate estimator (FZCR), and two covariance-based methods including the inphase integration estimator (IINT) and envelope integration estimator (EINT). These are all applied to the narrowband measured data collected at 910.25 MHz, in urban and suburban areas [16]. A vehicle moving with the constant speed of 15 mph, $f_D = 20$ Hz, collected sets of narrowband inphase and quadrature components at

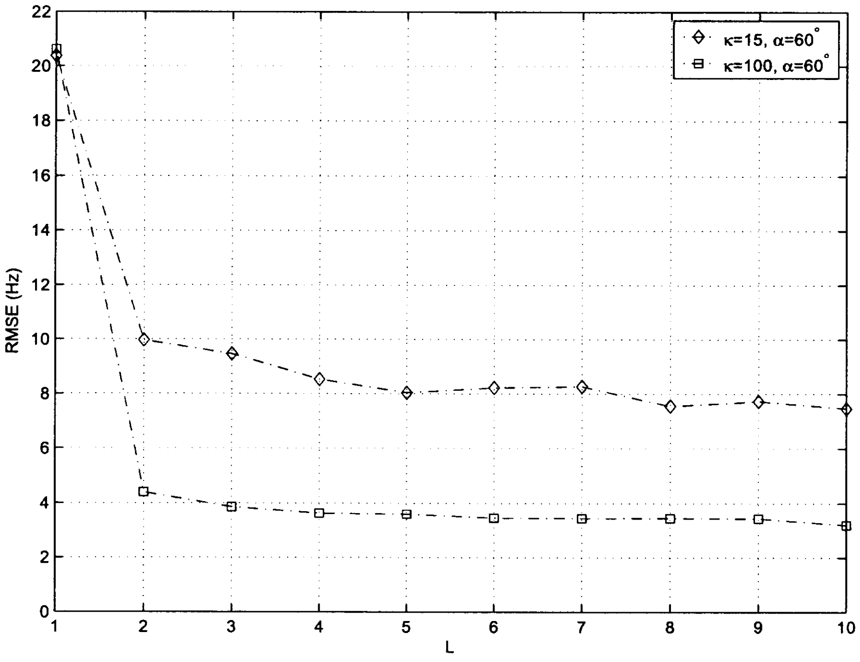

Figure 5.9 Effect of the number of antenna elements L on the space-time estimator in a noisy Rayleigh fading channel (SNR=10 dB, $f_D = 41$ Hz, $\Delta = 0.5$).

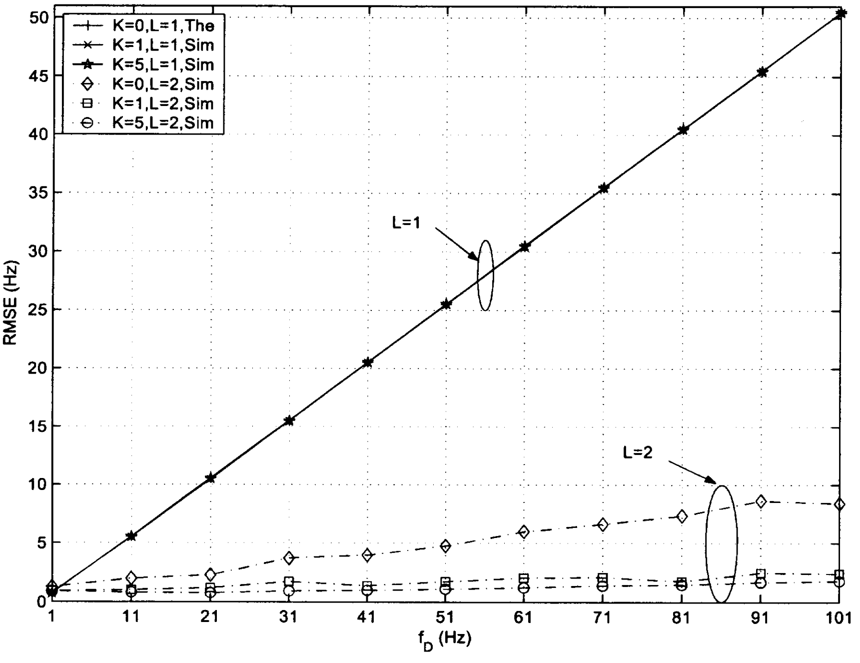

Figure 5.10 Performance of the space-time speed estimator (SNR=10 dB, $L = 2$, $\Delta = 0.5$): estimation error versus f_D for both Rayleigh and Rician multiple-antenna channels ($\kappa = 100$, $\alpha = 60°$, $\alpha_0 = 60°$).

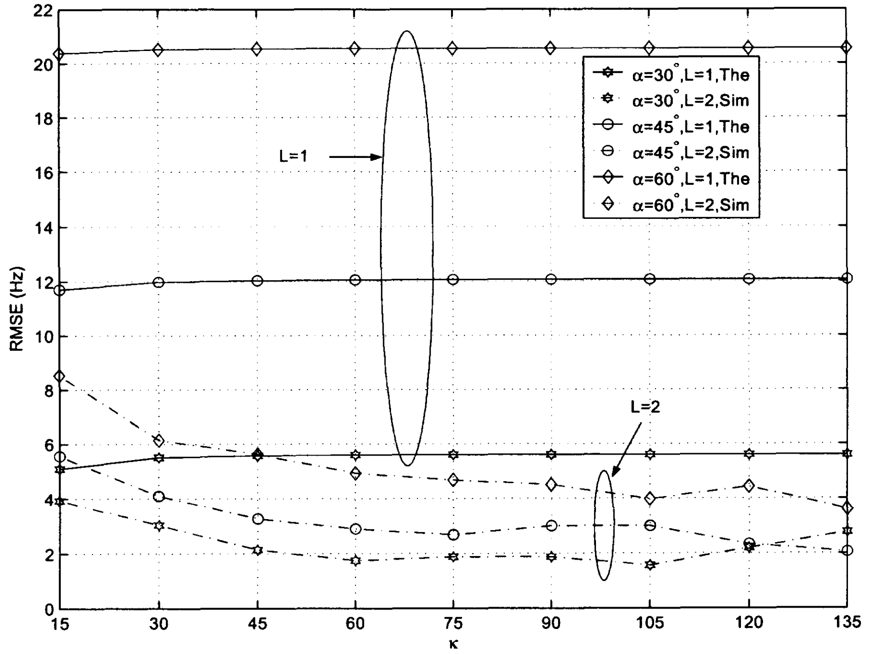

Figure 5.11 Performance of the space-time speed estimator (SNR=10 dB, $L = 2$, $\Delta = 0.5$): effect of κ and α in a Rayleigh multiple-antenna channel ($f_D = 41$ Hz).

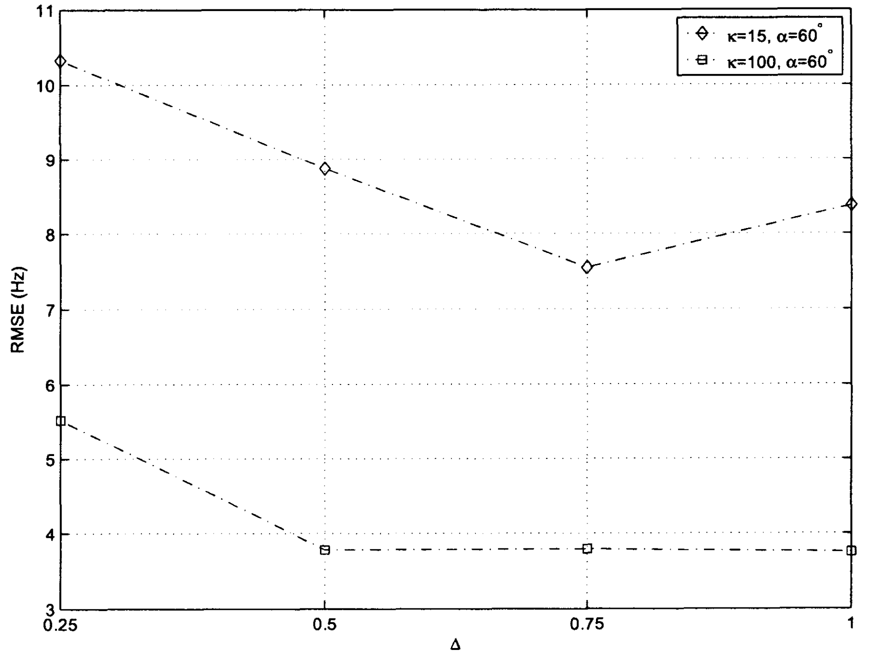

Figure 5.12 Effect of the element spacing Δ in a noisy Rayleigh multiple-antenna channel (SNR= 10 dB, $L = 2$, $f_D = 41$ Hz).

different locations, recorded as #0011, and so on. The signals were filtered by a 42-tap digital Kaiser filter. The bandwidth was set to 1 kHz in order to reject out-of-band noise, but large enough to pass through the signal Doppler spectrum unchanged. Each inphase (quadrature) component had approximately 250,000 samples, one sample per 28 ms. More information about the data can be found in [16].

Without any further preprocessing and for each record, IZCR, ELCR, IROM, EROM, FZCR, IINT, EINT, and the proposed nonparametric PSD estimator are used to estimate the maximum Doppler frequency from data segments of length 0.56 ms, 200 samples per segment. Each record includes nearly 1250 segments, and for a given method, 1250 estimates are obtained and combined by a simple averaging. Based on Fig. 5.13, PSD demonstrates the best performance and exhibits more reliable estimates for different records. To see the effect of the number of samples, larger data segments was chosen, 1.4 ms each with 500 samples, and the results are shown in Fig. 5.14. Note that the performance of FZCR degrades significantly while the RMSE of IZCR decreases. Overall, the proposed PSD-based speed estimator is able to provide significant performance improvement, when compared with traditional techniques.

5.8 Conclusion

In this Chapter, a robust speed technique has been proposed based on the unique spectral features of the mobile wireless fading channel. As a result, two temporal-only speed estimators applicable to narrowband and wideband channels, and one space-time speed estimator, based on an antenna array, were developed. The effects of noise, nonisotropic scattering with two and three dimensional propagation, and line-of-sight were extensively investigated through mathematical performance analysis and Monte Carlo simulations. Comparison with conventional speed estimation methods, using data collected in urban and suburban areas, demonstrated the utility of the new approach in real-world scenarios.

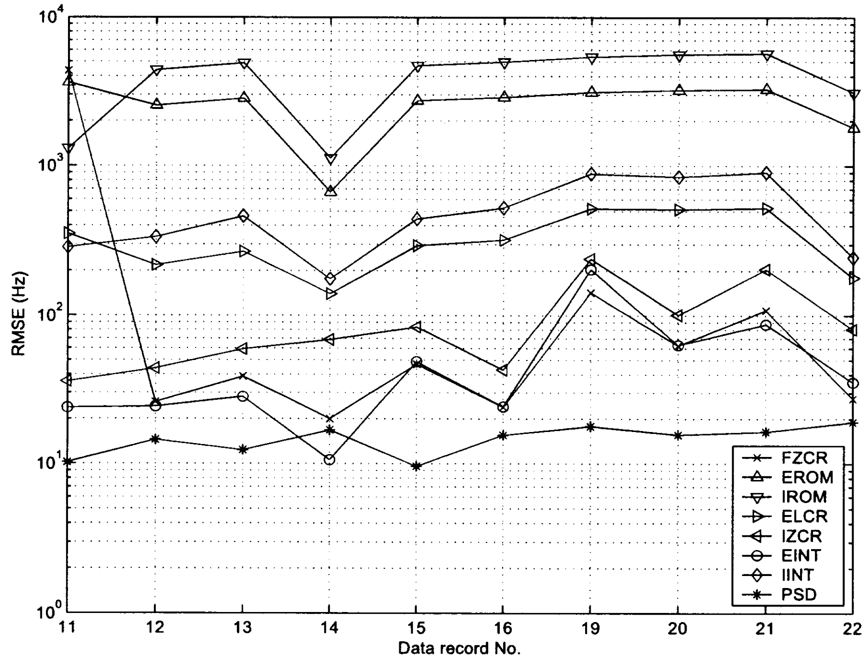

Figure 5.13 Performance comparison using measured data in a narrowband channel: 200 samples/segment.

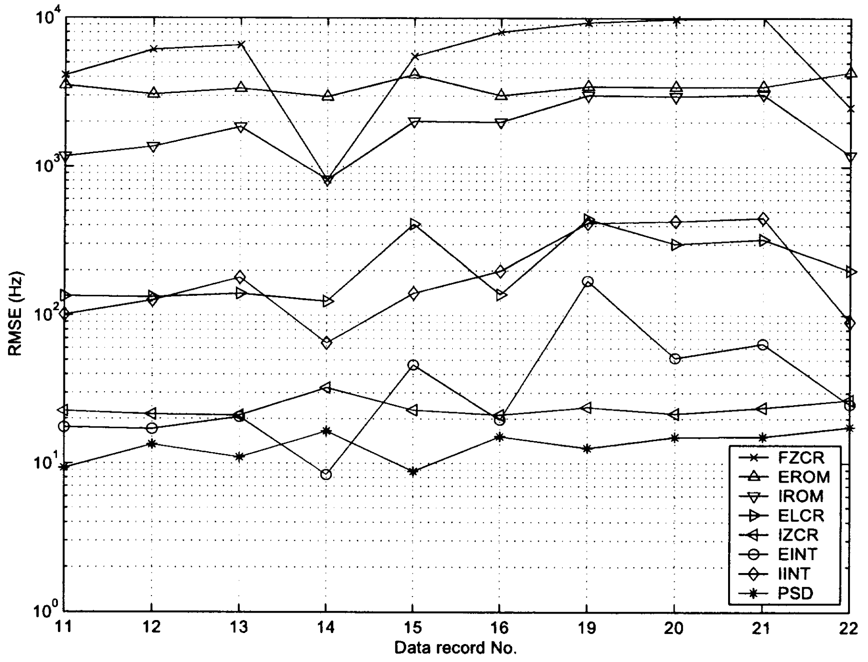

Figure 5.14 Performance comparison using measured data in a narrowband channel: 500 samples/segment.

CHAPTER 6

CYCLOSTATIONARITY-BASED DOPPLER SPREAD ESTIMATION

6.1 Introduction

All the existing speed estimation work including the studies in previous chapters of this dissertation are based on transmitted pilot tones. To the best of the author's knowledge, only one [55] has addressed blind speed estimation in a nonlinear modulation system with no analytical or simulation-based performance evaluation. In this Chapter, new speed estimators are developed by exploiting the cyclostationarity of linearly modulated signals. The new estimators can be applied blindly without using training symbols. This increases the data throughput. On the other hand, where pilot symbols are available, novel estimators are proposed which provide more accurate estimates compared to blind methods. Essentially, cyclostationarity-based estimators are not sensitive to additive stationary noise or interference of any color or distribution known to affect pilot-tone-based approaches. The robustness of the new estimators to nonisotropic scattering and variations of line-of-sight (LOS) is also investigated. Extensive Monte Carlo simulations are conducted to illustrate the performance of the new estimators.

The organization of this Chapter is as follows. The signal, channel, and noise models are discussed in Section 6.2. The cyclostationarity of linearly modulated waveforms is briefly reviewed in Section 6.3. The new single-antenna speed estimators are presented in Section 6.4. Extension to systems with multiple antennas is addressed in Section 6.5. Section 6.6 provides the numerical results, and Section 6.7 concludes the Chapter.

6.2 Signal, Channel, and Noise Models

The received lowpass complex envelope of a linearly modulated signal transmitted through a frequency-flat fading channel, can be expressed as [54]

$$z(t) = h(t)s(t) + v(t), \tag{6.1}$$

where $s(t) = \sum_m w(m)g(t - mT_s)$, and the following definitions are as follows:

$h(t)$:	fading channel,
$w(m)$:	stationary random sequence of transmitted symbols chosen from a finite-alphabet complex constellation,
$g(t)$:	convolution of the transmitter's signaling pulse and the receiver filter which, without loss of generality, is a raised cosine with rolloff factor $\beta \in [0, 1]$ [54],
$v(t)$:	a complex stationary process which represents the summation of noise and interference, independent of $h(t)$ and $w(m)$, and
T_s:	symbol period.

According to (2.3), the autocorrelation function of the unit-power ($\sigma_h^2 = 1$) fading process $h(t)$

$$\begin{aligned} r_h(\tau) =& \frac{K}{K+1}\exp(j2\pi f_D\tau\cos\alpha_0) + \frac{1}{K+1} \\ &\times \frac{I_0\left(\sqrt{\kappa^2 - 4\pi f_D^2\tau^2 + j4\pi\kappa f_D\tau\cos\alpha}\right)}{I_0(\kappa)}. \end{aligned} \tag{6.2}$$

6.3 Cyclostationarity of the Received Signal

The time-varying autocorrelation of the received signal $z(t)$, defined by $r_z(t;\tau) = r_z(t, u) = E[z(t)z^*(u)]$ with $u = t + \tau$, can be shown to be

$$r_z(t;\tau) = r_h(\tau)r_s(t;\tau) + r_v(\tau), \tag{6.3}$$

where

$$\begin{aligned} r_s(t;\tau) &= \sum_{m=-\infty}^{\infty} \sum_{n=-\infty}^{\infty} \tilde{r}_w(n-m) g(t-mT_s) g^*(t+\tau-nT_s) \\ &= \sum_{l=-\infty}^{\infty} \tilde{r}_w(l) \sum_{m=-\infty}^{\infty} g(t-mT_s) g^*(t+\tau-lT_s-mT_s), \end{aligned} \tag{6.4}$$

in which $\tilde{r}_w(l) = \tilde{r}_w(n-m) = E\{w(m)w^*(n)\}$. It is well known that $s(t)$ is a cyclostationary random process since $r_s(t;\tau)$ is periodic in t, with period T_s [56]. Consequently $r_z(t+kT_s;\tau) = r_z(t;\tau), \forall\ t,\tau$, indicating that $z(t)$ is cyclostationary as well, with the same period T_s.

The cyclic correlations which are the Fourier coefficients of $r_z(t;\tau)$ for cyclic frequencies $k/T_s = 0, \pm 1/T_s, \pm 2/T_s, \ldots$, are given by [56]

$$\begin{aligned} R_z(k;\tau) &= \frac{1}{T_s}\int_0^{T_s} r_z(t;\tau)\exp\{-j2\pi kt/T_s\}dt \\ &= r_h(\tau)R_s(k;\tau) + r_v(\tau)\delta_k, \end{aligned} \tag{6.5}$$

where δ_k is the Kronecker delta function, which is 1 when $k=0$ and 0 otherwise. Furthermore, $R_s(k;\tau)$ is the cyclic correlation of $s(t)$, which is the inverse Fourier transform of $s(t)$'s cyclic spectrum $\Omega_s(k;f)$, given by [56]

$$\Omega_s(k;f) = \frac{1}{T_s} G(f) G^*\left(f - \frac{k}{T_s}\right) \tilde{\Omega}_w(f), \tag{6.6}$$

where $G(f)$ is the Fourier transform of $g(t)$ and $\tilde{\Omega}_w(f)$ is the power spectrum of the sequence of transmitted symbols $\{w(m)\}$, which is also the Fourier transform of $\tilde{r}_w(l)$ and given by

$$\tilde{\Omega}_w(f) = \sum_{l=-\infty}^{\infty} \tilde{r}_w(l) e^{-j2\pi l T_s f}. \tag{6.7}$$

6.4 The Cyclostationarity-based Estimators

6.4.1 The Cyclic Correlation Approach

For an arbitrary proper complex process $z(t)$ [52], it is known that $r_{\dot{z}}(t;\tau) = r_{\dot{z}}(t,u) = \partial^2 r_z(t;u)/\partial t \partial u$, where dot denotes differentiation with respect to time t. According to (6.3),

$$r_{\dot{z}}(t;\tau) = r_{\dot{h}}(\tau) r_s(t;\tau) + r_{h\dot{h}}(\tau) r_{\dot{s}s}(t;\tau) + r_{\dot{h}h}(\tau) r_{s\dot{s}}(t;\tau) \\ + r_h(\tau) r_{\dot{s}}(t;\tau) + r_{\dot{v}}(\tau), \tag{6.8}$$

where $r_{h\dot{h}}(\tau) = E\{h(t)\dot{h}^*(t+\tau)\}$, $r_{\dot{h}h}(\tau) = E\{\dot{h}(t)h^*(t+\tau)\}$, $r_{s\dot{s}}(t;\tau) = E\{s(t)\dot{s}^*(t+\tau)\}$, $r_{\dot{s}s}(t;\tau) = E\{\dot{s}(t)s^*(t+\tau)\}$, and

$$r_{\dot{s}}(t,\tau) = \sum_{m=-\infty}^{\infty} \sum_{n=-\infty}^{\infty} \tilde{r}_w(n-m)\dot{g}(t-mT_s)\dot{g}^*(t+\tau-nT_s). \tag{6.9}$$

It is easy to show that $r_{s\dot{s}}(t;\tau)$, $r_{\dot{s}s}(t;\tau)$ and $r_{\dot{s}}(t,\tau)$ are periodic w.r.t. t with period T_s. Therefore, $\dot{z}(t)$ is cyclostationary as well, with the same period T_s. With the assumption of isotropic scattering and no LOS, i.e., $r_h(\tau) = J_0(2\pi f_D \tau)$ where $J_0(.)$ is the zero-order Bessel function of the first kind, obtain $r_{h\dot{h}}(0) = r_{\dot{h}h}(0) = 0$ and $r_{\dot{h}}(0) = -r_h''(\tau)|_{\tau=0} = 2\pi^2 f_D^2$, where prime denotes differentiation with respect to τ. Therefore, the cyclic correlation of $\dot{z}(t)$ at $\tau = 0$ can be obtained by calculating the k-th Fourier coefficients of (6.8) w.r.t. t

$$R_{\dot{z}}(k;0) = 2\pi^2 f_D R_s(k;0) + R_{\dot{s}}(k;0) + r_{\dot{v}}(0)\delta_k, \tag{6.10}$$

where $R_s(k;0)$ and $R_{\dot{s}}(k;0)$ are the k-th Fourier coefficients of (6.4) and (6.9), respectively.

To obtain a noise free estimator for f_D, choose $k \neq 0$ and divide $R_{\dot{z}}(k;0)$ in (6.10) by $R_z(k;0)$ in (6.5). After rearranging the terms, obtain

$$f_D^2 = \frac{1}{2\pi^2}\left(\frac{R_{\dot{z}}(k;0)}{R_z(k;0)} - \frac{R_{\dot{s}}(k;0)}{R_s(k;0)}\right), k \neq 0. \tag{6.11}$$

The cyclic correlations of $z(t)$ can be estimated from the discrete-time-version signal of $z(t)$, oversampled at a rate of P/T_s and represented by $\{z[n]\}_{n=0}^{N-1}$ [57]

$$\hat{R}_z(k; P\tau_d/T_s) = \frac{1}{\sqrt{N}} \sum_{n=0}^{N-\tau_d-1} z[n]z^*[n+\tau_d]e^{-j2\pi kn/P}, \tag{6.12}$$

where $\tau_d = 0, 1, 2, ..., N-1$. To estimate the cyclic correlations of $\dot{z}(t)$, first note that $\dot{z}(t)$ can be estimated from the oversampled version of $z(t)$ via a finite difference approximation, which yields $\{\dot{z}[n]\}_{n=0}^{N-1}$. Then, similarly to (6.12),

$$\hat{R}_{\dot{z}}(k; P\tau_d/T_s) = \frac{1}{\sqrt{N}} \sum_{n=0}^{N-\tau_d-1} \dot{z}[n]\dot{z}^*[n+\tau_d]e^{-j2\pi kn/P}. \tag{6.13}$$

Note that $R_s(k;0)$ and $R_{\dot{s}}(k;0)$ in (6.11) depend on the statistics of the symbols $\{w(m)\}$, as well as the pulse shape.

Blind Speed Estimator Assuming that the transmitted data symbol sequence $\{w(m)\}$ is white and zero-mean, eq. (6.6) simplifies to [56]

$$\Omega_s(k; f) = \frac{\sigma_w^2}{T_s} G(f)\, G^*\left(f - \frac{k}{T_s}\right), \tag{6.14}$$

where $\sigma_w^2 = E[|w(m)|^2]$ is the average power of the sequence. It is easily seen that $\Omega_s(k; f) = 0, \ \forall\ |k| \geq 2$ when $g(t)$ is a raised cosine. By taking the inverse Fourier transform of (6.14), it can be shown that

$$\begin{aligned} R_s(k;\tau) =& \frac{\sigma_w^2}{T_s} e^{j\pi k\tau/T_s} \int_{-\infty}^{\infty} G\left(f + \frac{k}{2T_s}\right) \\ &\times G^*\left(f - \frac{k}{2T_s}\right) e^{-j2\pi f\tau} df, \end{aligned} \tag{6.15}$$

which results in

$$\begin{aligned} R_s(1;\tau) &= \frac{\sigma_w^2 T_s}{4} e^{j\pi\tau/T_s} \int_{-\beta/(2T_s)}^{\beta/(2T_s)} \cos^2\left(\frac{\pi f T_s}{\beta}\right) e^{-j2\pi f\tau} df \\ &= \frac{\sigma_w^2 T_s^3 \sin\left(\pi\beta\tau/T_s\right)}{8\pi(T_s^2\tau - \beta^2\tau^3)} e^{j\pi\tau/T_s}. \end{aligned} \tag{6.16}$$

Based on (6.9) and (6.14), one has

$$\Omega_{\dot{s}}(k;f) = \sigma_w^2 T_s^{-1} \breve{G}(f)\, \breve{G}^*(f - k/T_s), \tag{6.17}$$

where

$$\breve{G}(f) = j2\pi f G(f). \tag{6.18}$$

Similarly to (6.15), obtain

$$\begin{aligned} R_{\dot{s}}(k;\tau) =& \frac{\sigma_w^2}{T_s} e^{j\pi k\tau/T_s} \int_{-\infty}^{\infty} \breve{G}\left(f + \frac{k}{2T_s}\right) \\ & \times \breve{G}^*\left(f - \frac{k}{2T_s}\right) e^{-j2\pi f\tau} df, \end{aligned} \tag{6.19}$$

which gives

$$\begin{aligned} R_{\dot{s}}(1;\tau) = & \int_{-\beta/(2T_s)}^{\beta/(2T_s)} \left(f^2 - \frac{1}{4T_s^2}\right) \cos^2\left(\frac{\pi f T_s}{\beta}\right) e^{-j2\pi f\tau} df \\ & \times \sigma_w^2 T_s \pi^2 e^{j\pi\tau/T_s}. \end{aligned} \tag{6.20}$$

By substituting (6.16) and (6.20) into (6.11), the blind speed estimator can be written as

$$\hat{f}_D = \frac{1}{\sqrt{2}\pi} \sqrt{\frac{\hat{R}_{\dot{z}}(1;0)}{\hat{R}_z(1;0)} - \frac{R_{\dot{s}}(1;0)}{R_s(1;0)}}, \tag{6.21}$$

where

$$\frac{R_{\dot{s}}(1;0)}{R_s(1;0)} = \frac{(\pi^2 - 6)\beta^2 - 3\pi^2}{3T_s^2}, \tag{6.22}$$

is obtained from (6.16) and (6.20).

Remark 1: Note that although, in theory, the fading channel $r_h(\tau)$ can be recovered by multiplying (6.5) with $R_s^{-1}(1;\tau)$, it is not easy to obtain a well-behaved one. This is due to the fact that there are many zero crossings in $R_s(1;\tau)$ which occur at $\tau = nT_s/\beta$, $n = 2, 3, \ldots$. This work deals with cyclic correlation (6.5) directly to develop the blind speed estimator (6.22).

Data-Aided Speed Estimator As previously noted, $R_s(k;\tau)$ and therefore $R_z(k;\tau)$, are dependent on the transmitted symbol sequence and on the rolloff factor of the pulse shaping filter. This indicates that there might be an optimal or a suboptimal training sequence for improving the performance of the cyclostationarity-based estimators. In general, the optimal solution is difficult to obtain due to the highly nonlinear form of the estimator (6.22). However, in order to completely recover $r_h(\tau)$ easily, it is possible to find a suboptimal sequence where $|R_s(1;\tau)|$ is constant for all τ. Note that this requirement for $R_s(1;\tau)$ means that $\Omega_s(1,f)$ must entail an impulse shape. If choosing the fixed training sequence $w(m) = (-1)^m \sigma_w$, in the Appendix G it has been shown that

$$R_s(1;\tau) = \frac{\sigma_w^2 T_s}{4} \exp\{j\pi\tau/T_s\}, \tag{6.23}$$

$$R_{\dot{s}}(1;\tau) = -\frac{\pi^2\sigma_w^2}{4T_s} \exp\{j\pi\tau/T_s\}. \tag{6.24}$$

Interestingly these do not depend on the rolloff factor β. Using the same approach that resulted in (6.21) and (6.22), the data-aided speed estimator can be derived as

$$\hat{f}_D = \frac{1}{\sqrt{2}\pi} \sqrt{\frac{\hat{R}_{\dot{z}}(1;0)}{\hat{R}_z(1;0)} + \frac{\pi^2}{T_s^2}}. \tag{6.25}$$

Remark 2: Clearly, the fading channel can be recovered by multiplying (6.6) with $R_s^{-1}(1;\tau)$ given in (6.23). Thus, to estimate the Doppler spread or mobile speed, use any methods which are developed directly based on $r_h(\tau)$, i.e., the correlation matching [5], polynomial solving [9] or other methods.

6.4.2 The Cyclic Spectrum Approach

By taking the Fourier transform of (6.5) w.r.t. τ, for $k \neq 0$, obtain

$$\Omega_z(k;f) = \Omega_h(f) \circledast \Omega_s(k;f), \; k \neq 0, \tag{6.26}$$

where $\circledast$ denotes convolution. Note that by choosing $k \neq 0$, the effect of noise disappears. Now, obtain f_D from the estimate of $\Omega_z(k; f)$. The consistent cyclic spectrum estimate can be obtained by windowing $\hat{R}_z(k; P\tau_d/T_s)$ in (6.12) with the window $W^{(2L_g+1)}(\tau_d)$, defined over $[-L_g, L_g]$ [57]

$$\begin{aligned}\hat{\Omega}_z(k; Pf_d/T_s) =& \frac{T_s}{P} \sum_{\tau_d=-L_g}^{L_g} W^{(2L_g+1)}(\tau_d)\hat{R}_z(k; P\tau_d/T_s) \\ & \times \exp\{-j2\pi f_d \tau_d\}. \end{aligned} \tag{6.27}$$

Data-Aided Speed Estimator Based on (6.23), $\Omega_s(1; f)$ is an impulse at $f = 1/(2T_s)$. Therefore, $\Omega_z(1; f)$ is simply the Doppler spectrum $\Omega_h(f)$ shifted from $f = 0$ to $f = 1/(2T_s)$. Hence, one can use the same technique as in [58] to estimate f_D, i.e.,

$$\hat{f}_D = \frac{P}{T_s}\left| -\frac{1}{2T_s} + \arg\max_f \left|\hat{\Omega}_z(1; f)\right|\right|. \tag{6.28}$$

Remark 3: This peak detection approach for the data-aided estimator can not, generally, be extended to the blind speed estimator. This is because the convolution in (6.26), in general, will not result in a power spectrum with a particular characteristic that helps speed estimation. However, in some extreme cases, i.e., $\beta = 0$, (6.28) is applicable to the blind method.

6.5 A Multi-Antenna Cyclostationarity-based Estimator

In this section, the proposed algorithm is extended to a system with multiple antennas in order to improve performance. Consider a uniform linear antenna array at an elevated base station (BS) of a marcocell, composed of L omnidirectional unit-gain elements, with element spacing d. The BS experiences no local scattering, whereas the single-antenna mobile station (MS) is surrounded by local scatters. Let the received signals at the l-th element be $z_l(t) = h_l(t)s(t) + v_l(t), l = 1, 2, ..., L$, which is similar to (6.1). Then the time-varying space-time crosscorrelation function between $z_a(t)$ and $z_b(t)$, $1 \leq a \leq b \leq L$, defined by $r_z((b-a)\Delta,(t;\tau)) = E[z_a(t)z_b^*(t+\tau)]$ such that $\Delta = d/\lambda$, is given by

$$r_z((b-a)\Delta,(t;\tau)) = r_h((b-a)\Delta,\tau)r_s(t;\tau) + r_v(\tau)\delta_{b-a}, \tag{6.29}$$

where the space-time channel crosscorrelation, defined by $r_h((b-a)\Delta,\tau) = E[h_a(t)h_b^*(t+\tau)]$, is given by (5.9) with $\sigma_h^2 = 1$

$$\begin{aligned} r_h((b-a)\Delta,\tau) = &\frac{K}{K+1}\exp\left(j(\zeta+\varrho)\cos\alpha_0\right) \\ &+ \frac{1}{K+1}\frac{I_0\left(\sqrt{\kappa^2-\zeta^2-\varrho^2-2\zeta\varrho+j2\kappa(\zeta+\varrho)\cos\alpha}\right)}{I_0(\kappa)}, \end{aligned} \tag{6.30}$$

where $\zeta = 2\pi f_D\tau$, and $\varrho = 2\pi(a-b)\Delta$. The same Rician factor K and unit channel power $E[|h_l(t)|^2] = \sigma_h^2 = 1$ at each element are assumed. Noise components are independent at different elements, with the same power σ_v^2. In Section 5.4 it has been shown that the angle spread at the BS is generally small for macrocells in urban, suburban, and rural areas, most often less than 30°; and the spatial channel cross-correlation function $r_h((b-a)\Delta,0) = E[h_a(t)h_b^*(t)]$, $1 \le a < b \le L$, can be accurately approximated by

$$r_h((b-a)\Delta,0) \approx \left\{\frac{\sigma_h^2}{K+1}\exp\left(-\frac{\varrho^2\sin^2\alpha}{2\kappa}\right) + \frac{K\sigma_h^2}{K+1}\right\}\exp\left\{j\varrho\cos\alpha\right\}. \tag{6.31}$$

Note that in (6.31), $\alpha_0 = \alpha$ is assumed due to the small angle spread at the BS.

With $\tau = 0$ and $a \neq b$ in (6.29), the time-varying spatial cross-correlation function in (6.29) can be written as

$$r_z((b-a)\Delta,(t;0)) = r_h((b-a)\Delta,0)r_s(t;0), \tag{6.32}$$

where $r_h((b-a)\Delta,0)$ for macrocells is given in (6.31) and $r_s(t;0)$ can be obtained from (6.4). Since noise components of different elements are independent, the effect of noise has not shown up in (6.32) as $a \neq b$. As will be shown in (6.33), $\cos\alpha$ can be estimated by looking at the phase of $r_z((b-a)\Delta,(t;0))$ in (6.32), due to the special form of $r_h((b-a)\Delta,0)$ in (6.31) and because $r_s(t;0)$ in (6.32) is real and positive.

When the BS experiences such heavy nonisotropic scattering (small angle spread), shown in Appendix E, there is a strong peak in the power spectrum of each branch $\Omega_{h_l}(f)$, at $f_D \cos\alpha$. On the other hand, based on (6.14), it can be shown that $\Omega_s(1; f)$, for a zero-mean i.i.d. sequence $\{w(m)\}$, is a uni-modal spectrum centered at $f = 1/(2T_s)$, with a bandwidth of β/T_s. In addition, for the training sequence $w(m) = (-1)^m \sigma_w$, note that from (6.23) $\Omega_{h_l}(f)$ is also an impulse at $f = 1/(2T_s)$. Therefore, according to (6.26) and due to the impulsive shape of $\Omega_{h_l}(f)$ when κ is large, it can be concluded that the peak of $\Omega_{z_l}(1; f)$ for each branch happens at $f = f_D \cos\alpha + 1/(2T_s)$. Relying now upon both cyclic spectrum and the spatial information provided by multiple antennas, the following space-time estimator is proposed.

Based on (6.32), estimate $\cos\alpha$ via

$$\widehat{\cos\alpha} \approx \frac{\measuredangle \hat{R}_z(\Delta, (0;0))}{(-2\pi\Delta)}, \tag{6.33}$$

where $\measuredangle$ denotes the phase of a complex number and $\hat{R}_z(\Delta, (0;0))$ is the estimate of $R_z(\Delta, (k;0)) = T_s^{-1} \int_0^{T_s} r_z(\Delta, (t;0)) \exp\{-j2\pi kt/T_s\} dt$ with $k = 0$ and $r_z(\Delta, (t;0)) = E[z_a(t) z_{a+1}^*(t)], \forall\, a \in [1, L-1]$. Note that $\hat{R}_z(\Delta, (0;0)) = (L-1)^{-1} \sum_{l=1}^{L-1} \hat{R}_z^l(\Delta, (0;0))$ where $\hat{R}_z^l(\Delta, (0;0)) = N^{-1/2} \sum_{n=0}^{N-1} z_l(n) z_{l+1}^*(n)$, $l \in [1, L-1]$, is the l-th adjacent-antenna-pair estimate of $R_z(\Delta, (0;0))$. It is worth emphasizing that if noise components $v_l(t), l = 1, 2, ..., L$ are spatially correlated, $\hat{R}_z(\Delta, (0;0))$ in (6.33) should be replaced with $\hat{R}_z(\Delta, (1;0))$ in order to have a noise-free estimate of $\widehat{\cos\alpha}$. Finally, f_D can be estimated via

$$\hat{f}_D = \frac{P}{\widehat{\cos\alpha} LT} \sum_{l=1}^{L} \left| -\frac{1}{2T_s} + \arg\max_f \left| \hat{\Omega}_{z_l}(1; f) \right| \right|, \tag{6.34}$$

where $\hat{\Omega}_{z_l}(1; f)$ can be obtained by (6.27). Note that the cyclic-spectrum-based estimator in (6.34) can be applied either blindly or with the aid of the training sequence $w(m) = (-1)^m \sigma_w$.

6.6 Simulation Results

In this section, first the performance of the proposed single antenna estimators is evaluated using Monte Carlo simulation; and next, the effect of noise, nonisotropic scattering, and LOS are investigated. The performance of the space-time estimator is then presented. The fading channel is generated using the spectral method [31]. The bandlimited Gaussian noise $v(t)$, with the autocorrelation $\sigma_v^2 g(\tau)$, is simulated by the same method. It is worth noting that the proposed algorithm does not put any constraint on the distribution of both the fading process and the noise, although for simulation purposes only, they are generated as complex Gaussian processes. The signal-to-noise ratio is defined as SNR $= \sigma_w^2/\sigma_v^2$. The performance of the estimator is measured by using the root mean squared error (RMSE) criterion $\{E[(\hat{f}_D - f_D)^2]\}^{1/2}$.

In all the simulations, the roll-off factor $\beta = 0.5$, oversampling rate $P = 8$, and the symbol duration $T_s = 0.001$ second. Each data-aided estimation uses $M = 256$ symbols and 200 Monte Carlo simulations, whereas blind algorithms use $M = 512$ 4-QAM i.i.d. symbols 400 Monte Carlo simulations. The abbreviations DA, NDA, CC, and CS in the figures refer to data aided, non-data aided (blind), cyclic correlation, and cyclic spectrum, respectively. For example, DA-CC in a legend box represents a data-aided cyclic correlation based speed estimator.

First, the performance of single antenna estimators is investigated, illustrated by Fig. 6.1 - Fig. 6.6. Fig. 6.1 shows the performance of three estimators DA-CC, NDA-CC, and DA-CS when the channel is isotropic, $\kappa = 0$, Rayleigh fading with SNR $= 10$ dB. Obviously, the DA-CS is the best, and DA-CC and NDA-CC have comparable estimation errors at small Dopplers, while DA-CC performs better than NDA-CC at large Dopplers. The robustness of these estimators against noise is shown in Fig. 6.2 in isotropic Rayleigh fading for a fixed $f_D T_s = 0.1$. Again, the DA-CS exhibits the best performance. Fig. 6.3 and Fig. 6.4 demonstrate the effect of nonisotropic scattering parameters κ and α. As seen, the CS-based method is less sensitive to κ than the CC-based techniques but more sensitive

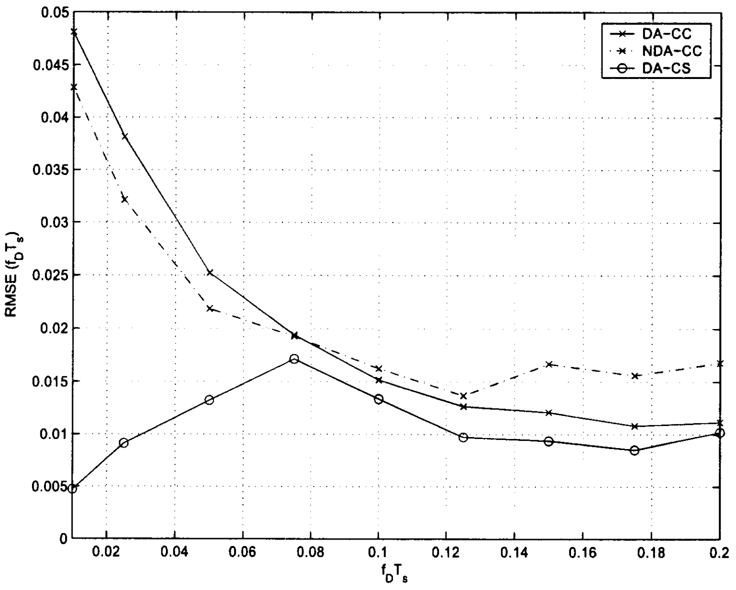

Figure 6.1 RMSE versus f_DT_s in isotropic Rayleigh fading, SNR = 10 dB.

to α. Based on Fig. 6.5 and Fig. 6.6, a similar observation can be made regarding the effect of the LOS parameters K and α_0. Note that for all the curves in Fig. 6.3 - Fig. 6.6, $f_DT_s = 0.1$ and SNR = 10 dB.

Now the performance of the space-time CS-based estimator in (6.34) is evaluated. In the simulation, $L = 4$ space-time correlated complex Gaussian processes for the macrocell scattering scenario of $\kappa = 100$ and $\alpha = 60°$ are generated, with $\Delta = 1/2$. For each branch, the noise power is the same as the single antenna case, with SNR = 10 dB per branch. Fig. 6.7 illustrates the estimation error for both DA and NDA approaches. Note that the DA-CS method provides excellent performance over a wide range of Dopplers. The curve for the DA-CS method for $L = 1$ is also illustrated in Fig. 6.7, which clearly shows the advantage of using more than one antenna. Apparently, the presence of LOS will further improve the performance.

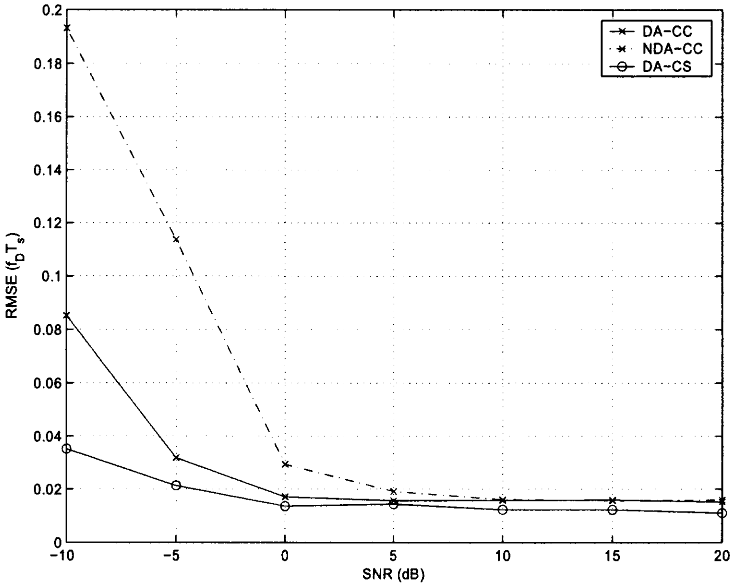

Figure 6.2 RMSE versus SNR in isotropic Rayleigh fading, $f_D T_s = 0.1$.

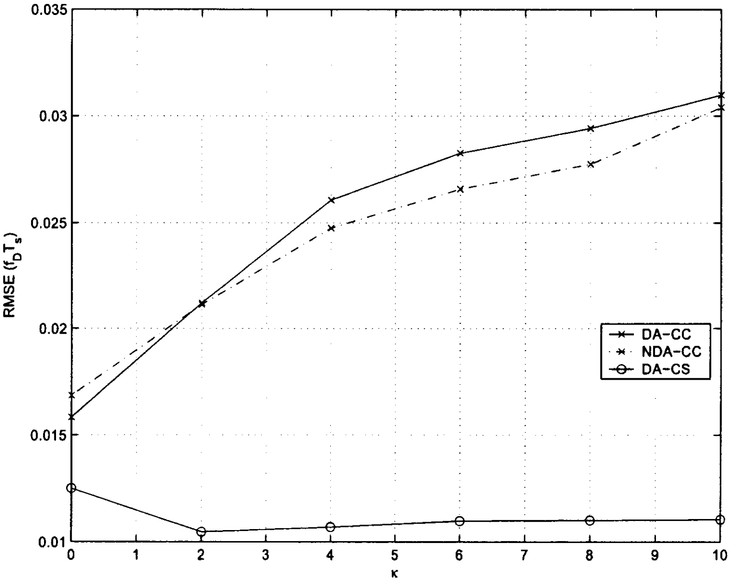

Figure 6.3 RMSE versus the nonisotropic scattering parameter κ in Rayleigh fading, SNR = 10 dB, $\alpha = 30°$, and $f_D T_s = 0.1$.

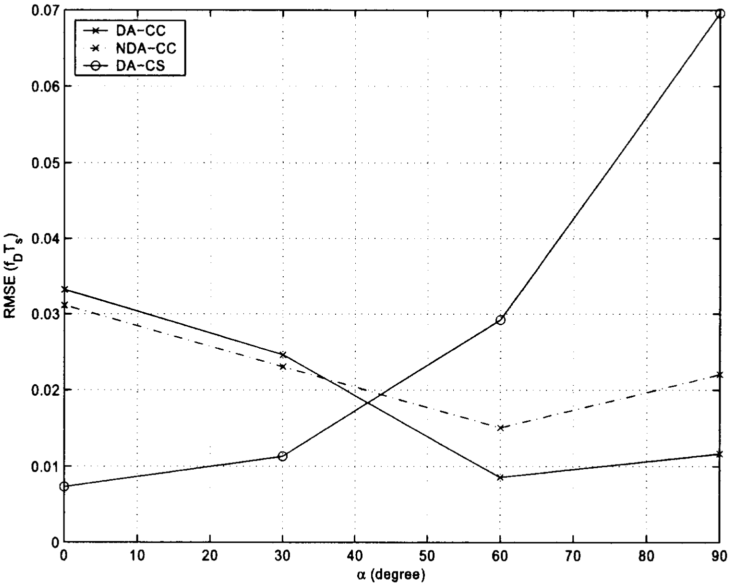

Figure 6.4 RMSE versus the mean AOA α in Rayleigh fading, SNR $= 10$ dB, $\kappa = 3.3$, and $f_DT_s = 0.1$.

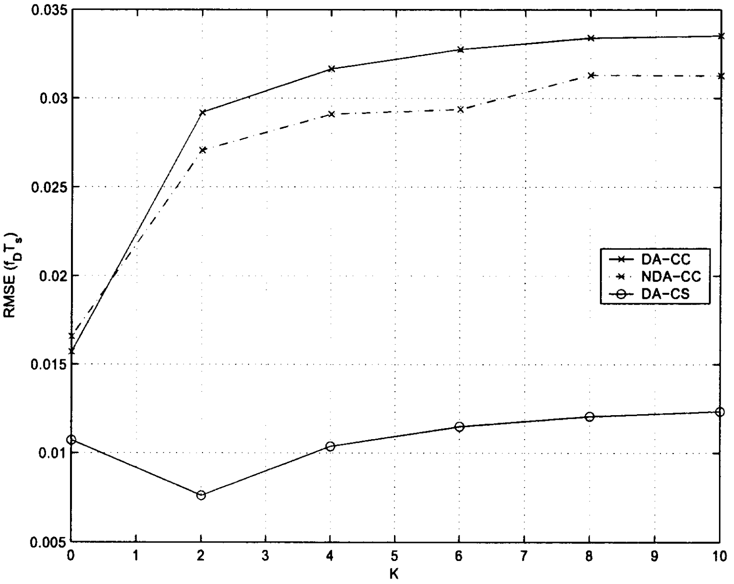

Figure 6.5 RMSE versus the Rician factor K in Rician isotropic fading, SNR $= 10$ dB, $\alpha_0 = 30°$, and $f_DT_s = 0.1$.

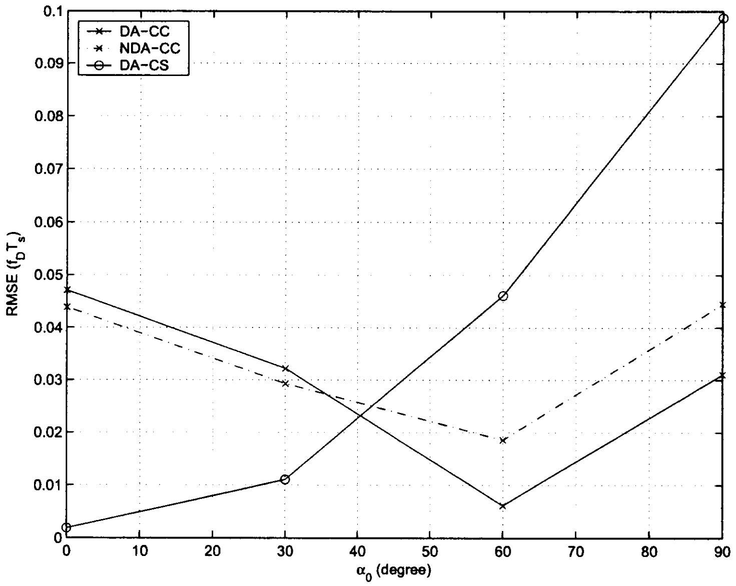

Figure 6.6 RMSE versus the LOS AOA α_0 in Rician isotropic fading, SNR = 10 dB, $K = 5$, and $f_DT_s = 0.1$.

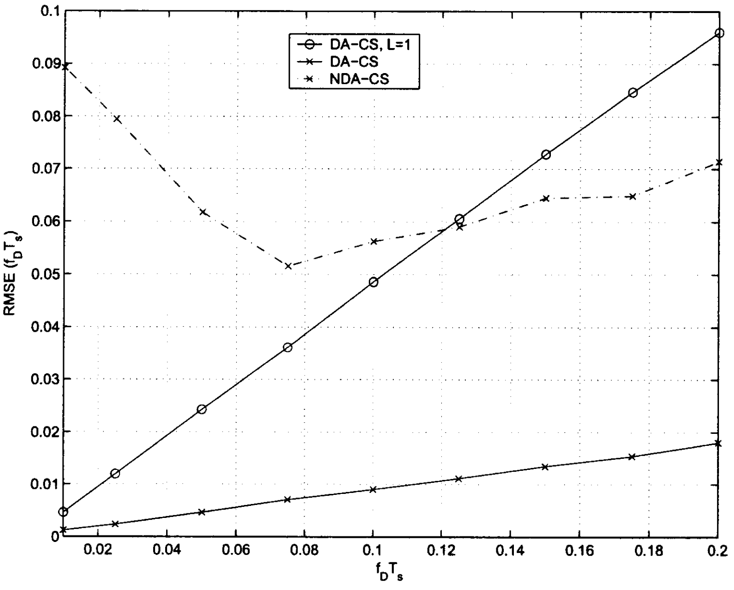

Figure 6.7 RMSE versus f_DT_s in Rayleigh fading, SNR = 10 dB, $\kappa = 100$, $\alpha = 60°$, $L = 4$, and $\Delta = 1/2$.

6.7 Conclusion

In this Chapter, methods have been proposed for estimating the mobile speed using a linearly modulated waveform transmitted in a fading channel. The new methods exploit the cyclostationarity of the received signal. Two classes of algorithms were developed based on the second order cyclic statistics, i.e., the cyclic correlation and cyclic spectrum. Compared with the conventional pilot-tone-based speed estimation techniques, the resulting estimators provide several benefits, including robustness to stationary noise and interference, as well as cyclostationary signals with different cyclic frequencies. These algorithms can also be implemented blindly thus increasing the data throughput.

CHAPTER 7

SUMMARY

The goal of this research has been to design robust speed estimators against noise and other channel uncertainties. Towards this end, the performance of conventional crossing and covariance based methods has been thoroughly studied both analytically and via simulation. Then the classic crossing based methods were extended to the output of diversity reception and the performance of the proposed six new diversity based estimators were investigated. Unlike traditional speed estimation algorithms, a more efficient but low complex solution was developed by exploring the feature of Doppler spectrum of mobile fading channels. The comparison of this new method (PSD) with existing ones is illustrated in Table 7.1. Its extension to multi-antenna systems was also proposed by taking advantage of the spatial information. Finally a new, but important category of speed estimation technique, which can be applied blindly, was proposed based on the inherent cyclostationarity of the modulated signal.

7.1 Contributions

The contributions of the work in this dissertation are summarized as follows:

Table 7.1 Comparison of speed estimation techniques

Estimation Technique	**Sensitivity to**			**Computational Complexity**
	Noise	*Nonisotropic*	*LOS*	
Crossing	High	Medium	High	Low
Covariance	High	Medium	High	Low
ML	Need to be estimated	Not studied	Not Studied	High
PSD	Low	Low	Low	Low

- In a unified framework, a variety of crossing-based and covariance-based speed estimation techniques were studied. Closed-form expressions for the bias and variance of the inphase-based estimators were presented and verified via simulation. It was demonstrated mathematically, that for large observation intervals, the performance of all these estimators is the same.

- Four new closed form expressions were derived for inphase zero crossing rate, inphase rate of maxima, phase zero crossing rate, and the instantaneous frequency zero crossing rate of the output of selection combining. Their application as speed estimators was investigated.

- A new speed estimation technique based on the PSD of fading channels was proposed. In comparison with the existing methods, it provides a significant performance gain in terms of robustness to noise, nonisotropic scattering, LOS, and different geometrical propagations. The analytic performance analysis was also presented and validated by Monte Carlo simulations.

- Relying upon the new PSD speed estimation algorithm, a space-time speed estimator which exploits the spatial information provided by multi-antenna system was developed. It shows excellent performance over a wide rage of mobile speeds and different propagation environments.

- By exploiting the cyclostationarity of the modulated waveform transmitted through fading channels, a new category of speed estimation technique was proposed. Two classes of algorithms based on the second order cyclic statistics were developed. Compared with the conventional pilot-tone-based speed estimation techniques, the resulting estimators provide several benefits, including robustness to stationary noise and interference, as well as cyclostationary signals with different cyclic frequencies. These algorithms can also be implemented blindly, thus can increase the data throughput.

7.2 Future Work

7.2.1 Performance Analysis of Cyclostationarity-based Estimators

It is interesting to establish and analyze the asymptotic (large sample) performance of the cyclostationarity-based based estimators as a function of the pulse shape bandwidth and the oversampling factor. For the cyclic correlation based estimators, the starting point could be the calculation of the asymptotic covariance matrices of the cyclic correlation estimates, which has been treated in several papers [59] [60]. On the other hand, for the cyclic-spectrum based estimators, [57] [61] could be good references to start with by looking at the properties of the cyclic spectrum estimates.

7.2.2 System Performance Evaluation

Previous work on system performance evaluation with application of mobile speed estimation were mainly focused on crossing- and covariance-based methods [12] [62] [63] [64] [65]. It would be another interesting future work to apply the proposed new speed estimators to current systems which typically include TDMA (GSM/EDGE), CDMA (3GPP WCDMA and CDMA2000) and OFDM(A) (WiMAX/802.16e). The impact of the accuracy of speed estimation on system performance in general comes from two aspects: adaptive receiver algorithm and handoff decision algorithm. However, in multicarrier system such as OFDM(A) and MC-CDMA, the effect of Doppler spread estimate on mitigation algorithm for intercarrier interference (ICI) is another problem worth investigating [66] [67] [68] [69] [70].

APPENDIX A

EXPECTED VALUES OF THE INPHASE-BASED ESTIMATORS IN NOISY RAYLEIGH CHANNELS WITH NONISOTROPIC SCATTERING

All the speed estimators discussed in Chapter 3 are unbiased or approximately unbiased. This holds only under the assumption of a noise-free isotropic Rayleigh fading channel, where $r_h(\tau) = J_0(\omega_D \tau)$. To evaluate the theoretical estimation errors of the inphase-based speed estimators in (3.8), (3.9), (3.18) and (3.26), in a noisy nonisotropic Rayleigh fading channel, use the following correlation function for the received signal $z(t)$, according to (3.1)

$$r_z(\tau) = r_h(\tau) + r_n(\tau). \tag{A.1}$$

For $r_h(\tau)$ in (A.1), (3.2) is used. The noise correlation function $r_n(\tau) = E[n(t)n^*(t+\tau)]$ is given by $\sigma_n^2 \text{sin}(2\pi B_{rx}\tau)/(2\pi B_{rx}\tau)$. This corresponds to a bandlimited flat-spectrum lowpass complex noise with the power σ_n^2 and the bandwidth B_{rx} in Hz. The SNR is defined as σ_h^2/σ_n^2; and $\sigma_h^2 = 1$ is assumed without loss of generality. As mentioned previously, $B_{rx} = 101$ Hz is used throughout the simulations. Note that the variance expressions in (3.28), (3.34) and (3.36) generally hold for (A.1). Closed-form formulas for the expected value of the four inphase-based estimators are given in the sequel. They also hold for (A.1).

Define $\beta(t) = \Re\{z(t)\}$, with $z(t)$ given in (3.1). For $r_\beta(\tau) = E[\beta(t)\beta^*(t+\tau)]$, $r_\beta(\tau) = (1/2)\Re\{r_z(\tau)\}$. It is well known that the zero crossing rate of a real Gaussian process can be calculated using its correlation function [2], which for $\beta(t)$ and using (A.1), can be written as

$$\begin{aligned} \frac{E[N_\beta(0,T)]}{T} &= \frac{1}{2\pi}\sqrt{\frac{-r_\beta''(0)}{r_\beta(0)}} \\ &= \frac{1}{2\pi}\sqrt{\frac{4\pi^2 B_{rx}^2 \sigma_n^2}{3(1+\sigma_n^2)} + \frac{\omega_D^2 (I_0(\kappa) + I_2(\kappa)\cos(2\alpha))}{2(1+\sigma_n^2) I_0(\kappa)}}. \end{aligned} \tag{A.2}$$

By replacing $N_\xi(0,T)$ in (3.8) with $N_\beta(0,T)$, the mean of the InphaseZCR estimator can be written as

$$E[\hat{\omega}_{D,1}] = \sqrt{\frac{8\pi^2 B_{rx}^2 \sigma_n^2}{3(1+\sigma_n^2)} + \frac{\omega_D^2 (I_0(\kappa) + I_2(\kappa)\cos(2\alpha))}{(1+\sigma_n^2) I_0(\kappa)}}. \tag{A.3}$$

For $\sigma_n^2 = \kappa = 0$, i.e., noise-free isotropic scattering, (A.3) reduces to $E[\hat{\omega}_{D,1}] = \omega_D$, as mentioned right after (3.11).

As mentioned earlier, the number of maxima of a process is the same as the number of upward or downward zero crossings of the derivative of the process. Therefore the rate of maxima of $\beta(t)$ can be calculated based on $\dot{\beta}(t)$ as

$$\frac{E[M_\beta(T)]}{T} = \frac{1}{2\pi}\sqrt{\frac{-r''_{\dot{\beta}}(0)}{r_{\dot{\beta}}(0)}} = \frac{1}{2\pi}\sqrt{\frac{r_\beta^{(4)}(0)}{-r''_\beta(0)}}. \tag{A.4}$$

where $r_\beta^{(4)}(\tau)$ is the fourth derivative with respect to τ. The lengthy closed form of (A.4) is not given to save space. By replacing $M_\xi(T)$ in (3.9) with $M_\beta(T)$, the mean of the InphaseROM estimator can be easily derived using (A.4). For isotropic Rayleigh fading without noise and $\sigma_h^2 = 1$, obtain $r_z(\tau) = J_0(\omega_D \tau)$ from (A.1). This makes it easy to verify that $E[\hat{\omega}_{D,2}] = \omega_D$, as mentioned right after (3.11).

To calculate the expected value of the InphaseCOV estimator in (3.18), one needs to use the approximation $E[\hat{\omega}_{D,5}] \approx \sqrt{E[\widehat{\omega^2_{D,5}}]}$ introduced previously. The term under the square root can be calculated from (3.20), where $c_y(\tau)$ is replaced by $c_\beta(\tau) = r_\beta(\tau) - \{E[\beta(t)]\}^2 = r_\beta(\tau) = (1/2)\Re\{r_z(\tau)\}$, $a = 1/2$ and $b = 1/8$. Note that $r_z(\tau)$ is given in (A.1). This gives the expected value of the inphaseCOV estimator as

$$E[\hat{\omega}_{D,5}] = \sqrt{\frac{20}{3T_0^2} - \frac{40}{T_0^5}\int_0^{T_0} \tau^2 r_\beta(\tau) d\tau}. \tag{A.5}$$

In order to obtain the expected value of the InphaseINT estimator in (3.26), it is necessary to use the approximation $E[\hat{\omega}_{D,6}] \approx \sqrt{E[\widehat{\omega^2_{D,6}}]}$. The term under the square root can be calculated from (3.25), with $d = 4$ and $y(t)$ replaced by $\beta(t)$. Since $E[\dot{\beta}^2(t)] =$

$r_{\dot\beta}(0) = -r''_\beta(0)$ and $r_\beta(\tau) = (1/2)\Re\{r_z(\tau)\}$, with $r_z(\tau)$ given in (A.1), it can be easily shown that

$$\begin{aligned} E[\hat\omega_{D,6}] &\approx \sqrt{-4r''_\beta(0)} \\ &= \sqrt{\frac{8\pi^2 B_{rx}^2\sigma_n^2}{3} + \frac{\omega_D^2(I_0(\kappa) + I_2(\kappa)\cos(2\alpha))}{I_0(\kappa)}}. \end{aligned} \tag{A.6}$$

For $\sigma_n^2 = \kappa = 0$, i.e., noise-free isotropic scattering, (A.6) simplifies to $E[\hat\omega_{D,6}] \approx \omega_D$, as given in (3.27).

APPENDIX B

THE ASYMPTOTIC VARIANCE OF THE INPHASE-BASED CROSSING ESTIMATORS

In this Appendix the asymptotic results given in (3.31) are proved. According to (3.10) in [20], that part of the integrand in (3.28) which is within the square brackets can be written as

$$\frac{\sigma_\zeta^2(\tau)}{\sqrt{1-r_\zeta^2(\tau)}}\left\{\sqrt{1-\rho_\zeta^2(\tau)}+\rho_\zeta(\tau)\cos^{-1}(-\rho_\zeta(\tau))\right\}-\gamma^2$$
$$=\frac{1}{2}\pi\left\{-r_\zeta''(\tau)+O\left[r_\zeta^2(\tau)+r_\zeta'^2(\tau)+r_\zeta''^2(\tau)\right]\right\},\ \text{as}\ \tau\to\infty. \tag{B.1}$$

To derive the asymptotic performance of $\hat{\omega}_{D,1}$ in (3.8), note that with $\zeta(t)=\sqrt{2}\xi(t)$ $r_\zeta(\tau)=2r_\xi(\tau)=\Re\{r_h(\tau)\}$ follows. Based on (3.30), it can be easily shown that

$$r_\xi(\tau)=\frac{\omega_D^{-1/2}\sqrt{2\pi}g}{2}\tau^{-1/2}\cos(\omega_D\tau-\pi/4)+O(\tau^{-1}),\ \text{as}\ \tau\to\infty, \tag{B.2}$$

where $g=p(0)+p(\pi)$. Also since $\tau^{-1}\cos^2(\omega_D\tau-\pi/4)=(\tau^{-1}/2)+(\tau^{-1}/2)\cos(2\omega_D\tau-\pi/2)=\tau^{-1}/2+O(\tau^{-1})$, as $\tau\to\infty$, obtain

$$r_\xi^2(\tau)=\frac{\omega_D^{-1}\pi g^2}{4}\tau^{-1}+O(\tau^{-1}),\ \text{as}\ \tau\to\infty. \tag{B.3}$$

By taking the derivative of (3.3) obtain

$$r_h'(\tau)=\int_{-\pi}^{\pi}-j\omega_D\cos(\phi)p(\phi)\exp[-j\omega_D\cos(\phi)\tau]d\phi. \tag{B.4}$$

Since the only difference between (B.4) and $r_h(\tau)$ in (3.3) is the extra term $-j\omega_D\cos(\phi)$, the following asymptotic form can be derived for $r_h'(\tau)$ by replacing $p(\phi)$ in (3.30) with

$-j\omega_D p(\phi)\cos\phi$

$$r'_h(\tau) = -j\omega_D \left(\frac{\omega_D\tau}{2\pi}\right)^{-1/2} \left[p(0)e^{j(\omega_D\tau-\pi/4)} - p(\pi)e^{-j(\omega_D\tau-\pi/4)}\right] + O(\tau^{-1}), \text{ as } \tau \to \infty. \tag{B.5}$$

Following the same procedure further results in

$$r''_h(\tau) = -\omega_D^2 \left(\frac{\omega_D\tau}{2\pi}\right)^{-1/2} \left[p(0)e^{j(\omega_D\tau-\pi/4)} + p(\pi)e^{-j(\omega_D\tau-\pi/4)}\right] + O(\tau^{-1}), \text{ as } \tau \to \infty. \tag{B.6}$$

Since $r_\xi(\tau) = (1/2)\Re\{r_h(\tau)\}$, by taking the real parts of (B.5) and (B.6), easily obtain

$$r'_\xi(\tau) = \frac{\sqrt{2\pi\omega_D g}}{2}\tau^{-1/2}\sin(\omega_D\tau - \pi/4) + O(\tau^{-1}), \text{ as } \tau \to \infty, \tag{B.7}$$

$$r''_\xi(\tau) = -\frac{\omega_D^{3/2}\sqrt{2\pi g}}{2}\tau^{-1/2}\cos(\omega_D\tau - \pi/4) + O(\tau^{-1}), \text{ as } \tau \to \infty. \tag{B.8}$$

Also, since the asymptotic form for both $\tau^{-1}\sin^2(\omega_D\tau - \pi/4)$ and $\tau^{-1}\cos^2(\omega_D\tau - \pi/4)$ is $\tau^{-1}/2 + O(\tau^{-1})$, further obtain

$$r'^2_\xi(\tau) = \frac{\pi g^2\omega_D}{4}\tau^{-1} + O(\tau^{-1}), \text{ as } \tau \to \infty, \tag{B.9}$$

$$r''^2_\xi(\tau) = \frac{\pi g^2\omega_D^3}{4}\tau^{-1} + O(\tau^{-1}), \text{ as } \tau \to \infty. \tag{B.10}$$

Based on $r_\zeta(\tau) = 2r_\xi(\tau)$, and after replacing $r^2_\zeta(\tau)$, $r'^2_\zeta(\tau)$, and $r''^2_\zeta(\tau)$ in (B.1) with (B.3), (B.9) and (B.10), respectively, the right-hand side of (B.1) simplifies to

$$-\pi r''_\xi(\tau) + O(\tau^{-1}), \text{ as } \tau \to \infty. \tag{B.11}$$

As soon becomes clear, the following two results are needed to calculate the asymptotic variance of $\hat{\omega}_{D,1}$

$$\begin{aligned}\int_0^T r_\xi''(\tau)d\tau = r_\xi'(T) - r_\xi'(0) &= \frac{\sqrt{2\pi\omega_D}g}{2}T^{-1/2}\sin(\omega_D T - \pi/4) + O(T^{-1})\\ &= O(T^{-1/2}),\ \text{as } T \rightarrow \infty, \qquad \text{(B.12)}\end{aligned}$$

$$\begin{aligned}\int_0^T \tau r_\xi''(\tau)d\tau = Tr_\xi'(T) - r_\xi(T) + r_\xi(0) &= \frac{\sqrt{2\pi\omega_D}g}{2}T^{1/2}\sin(\omega_D T - \pi/4) + O(1)\\ &+ \frac{\sqrt{2\pi}\omega_D^{-1/2}g}{2}T^{-1/2}\cos(\omega_D T - \pi/4) + O(T^{-1})\\ &= O(T^{1/2}),\ \text{as } T \rightarrow \infty. \qquad \text{(B.13)}\end{aligned}$$

Note that $r_\xi'(T)$ and $r_\xi(T)$ for large T are obtained from (B.7) and (B.2), respectively.

There are two integrals on the right-hand side of (3.28). By replacing the square brackets in (3.28) with (B.11), the first integral can be shown to be $O(T^{-1/2}) + O(\ln T)$, as $T \rightarrow \infty$. The former term comes from (B.12), whereas the latter is the integral of τ^{-1}. Furthermore, by replacing the square brackets in (3.28) with (B.11), the second integral can be reduced to $O(T^{1/2}) + O(T)$, as $T \rightarrow \infty$. The former is taken from (B.13), and the latter is the integral of 1. Therefore, the whole integral on the right-hand side of (3.28) can be written as $O(T^{-1/2}) + O(\ln T) + T^{-1}[O(T^{1/2}) + O(T)] = O(\ln T)$, as $T \rightarrow \infty$. This completes the proof of (3.31) for the asymptotic variance of $\hat{\omega}_{D,1}$.

To prove the asymptotic performance of the estimator in (3.9), first note that now $\zeta(t) = (2/\omega_D)\dot{\xi}(t)$. Therefore $r_\zeta(\tau)$ in (B.1) is given by

$$r_\zeta(\tau) = (4/\omega_D^2)r_{\dot{\xi}}(\tau) = -(4/\omega_D^2)r_\xi''(\tau) = -(2/\omega_D^2)\Re\{r_h''(\tau)\}, \qquad \text{(B.14)}$$

where $r''_h(\tau)$ is given by (B.6). Obviously, $r'_\zeta(\tau) = -(2/\omega_D^2)\Re\{r_h^{(3)}(\tau)\}$ and $r''_\zeta(\tau) = -(2/\omega_D^2)\Re\{r_h^{(4)}(\tau)\}$, where $r_h^{(3)}(\tau)$ and $r_h^{(4)}(\tau)$ asymptotically behave as follows

$$r_h^{(3)}(\tau) = j\omega_D^3 \left(\frac{\omega_D \tau}{2\pi}\right)^{-1/2} \left[p(0)e^{j(\omega_D\tau - \pi/4)} - p(\pi)e^{-j(\omega_D\tau-\pi/4)}\right] + O(\tau^{-1}), \text{ as } \tau \to \infty, \tag{B.15}$$

and

$$r_h^{(4)}(\tau) = \omega_D^4 \left(\frac{\omega_D \tau}{2\pi}\right)^{-1/2} \left[p(0)e^{j(\omega_D\tau - \pi/4)} + p(\pi)e^{-j(\omega_D\tau-\pi/4)}\right] + O(\tau^{-1}), \text{ as } \tau \to \infty. \tag{B.16}$$

These two are obtained following the same technique used to derive (B.5). When comparing the asymptotics of $r''_h(\tau)$ in (B.6) with $r_h(\tau)$ in (3.30), $r_h^{(3)}(\tau)$ in (B.15) with $r'_h(\tau)$ in (B.5), and $r_h^{(4)}(\tau)$ in (B.16) with $r''_h(\tau)$ in (B.6), observe that each pair takes the same form, if these constants outside the square brackets are ignored (which will not affect the conclusion). This means that the right-hand side of (B.2) and then the right-hand side of (3.28), are asymptotically the same as those previously derived for $\hat{\omega}_{D,1}$. Therefore, the asymptotic variance of $\hat{\omega}_{D,2}$ is the same as $\hat{\omega}_{D,1}$, given in (3.31).

APPENDIX C

DERIVATION OF THE JOINT PDF OF THE COMBINER OUTPUT AND ITS DERIVATIVE

According to (4.7), the SC diversity system produces the signal $\gamma(t)$ and its derivative $\dot{\gamma}(t)$ such that

$$\gamma(t) = \gamma_i(t) \text{ and } \dot{\gamma}(t) = \dot{\gamma}_i(t) \text{ if } \rho_i(t) = \max(\{\rho_k(t)\}_{k=1}^{L}), \tag{C.1}$$

which means the output at time instant t is coming from the branch with the largest instantaneous envelope. Of course, i may change as t changes.

Define the event $\mathscr{E}_i = \{\Psi : \rho_i(t) = \max(\{\rho_k(t)\}_{k=1}^{L})\}$, $i = 1, 2, ..., L$, with the probability $P(\mathscr{E}_i)$, where Ψ represents a point of the sample space. Based on the total probability theorem [29], the joint distribution function of $\gamma(t)$ and $\dot{\gamma}(t)$ can be written as

$$F(\gamma, \dot{\gamma}) = \sum_{i=1}^{L} F(\gamma, \dot{\gamma} | e_i) P(\mathscr{E}_i), \tag{C.2}$$

where $F(\gamma, \dot{\gamma} | \mathscr{E}_i) = P(\gamma_i \leq \gamma, \dot{\gamma}_i \leq \dot{\gamma} | \mathscr{E}_i)$. This results in

$$F(\gamma, \dot{\gamma}) = \sum_{i=1}^{L} P(\gamma_i \leq \gamma, \dot{\gamma}_i \leq \dot{\gamma}, \mathscr{E}_i). \tag{C.3}$$

With i.i.d. branches, (C.3) simplifies to

$$\begin{aligned} F(\gamma, \dot{\gamma}) &= L P(\gamma_1 \leq \gamma, \dot{\gamma}_1 \leq \dot{\gamma}, \mathscr{E}_1) \\ &= L P(\gamma_1 \leq \gamma, \dot{\gamma}_1 \leq \dot{\gamma}, \rho_2 < \rho_1, \rho_3 < \rho_1, ..., \rho_L < \rho_1) \\ &= L \int_0^\infty P(\gamma_1 \leq \gamma, \dot{\gamma}_1 \leq \dot{\gamma}, \rho_2 < \rho_1, \rho_3 < \rho_1, ..., \rho_L < \rho_1 | \rho_1) f_{\rho_1}(\rho_1) d\rho_1 \\ &= L \int_0^\infty P(\gamma_1 \leq \gamma, \dot{\gamma}_1 \leq \dot{\gamma} | \rho_1) P^{L-1}(\rho_2 < \rho_1 | \rho_1) f_{\rho_1}(\rho_1) d\rho_1. \end{aligned} \tag{C.4}$$

Since the envelope of each branch is Rayleigh distributed, obtain

$$P(\rho_2 < \rho_1|\rho_1) = \int_0^{\rho_1} \frac{\rho_2}{b_0} \exp\left(-\frac{\rho_2^2}{2b_0}\right) d\rho_2 = 1 - \exp\left(-\frac{\rho_1^2}{2b_0}\right), \tag{C.5}$$

which after substitution in (C.4) and using the binomial expansion, simplifies (C.4) to

$$F(\gamma, \dot{\gamma}) = L \sum_{k=0}^{L-1} \binom{L-1}{k} (-1)^k \int_0^\infty \exp\left(-\frac{k}{2b_0}\rho_1^2\right) P(\gamma_1 \le \gamma, \dot{\gamma}_1 \le \dot{\gamma}|\rho_1) f_{\rho_1}(\rho_1) d\rho_1. \tag{C.6}$$

By taking the derivative of (C.6) with respect to γ and $\dot{\gamma}$ one obtains the joint PDF of $\gamma(t)$ and $\dot{\gamma}(t)$

$$f_{\gamma\dot{\gamma}}(\gamma, \dot{\gamma}) = L \sum_{k=0}^{L-1} \binom{L-1}{k} (-1)^k \int_0^\infty \exp\left(-\frac{k}{2b_0}\rho_1^2\right) f_{\gamma_1\dot{\gamma}_1}(\gamma, \dot{\gamma}|\rho_1) f_{\rho_1}(\rho_1) d\rho_1, \tag{C.7}$$

where $f_{\gamma_1\dot{\gamma}_1}(.,.|\rho_1)$ is the joint PDF of $\gamma(t)$ and $\dot{\gamma}(t)$, conditioned on $\rho_1(t)$. Equation (C.7) can be written in the following more compact form

$$f_{\gamma\dot{\gamma}}(\gamma, \dot{\gamma}) = L \sum_{k=0}^{L-1} \binom{L-1}{k} (-1)^k \int_0^\infty f_{\rho_1\gamma_1\dot{\gamma}_1}(\rho_1, \gamma, \dot{\gamma}) \exp\left(-\frac{k}{2b_0}\rho_1^2\right) d\rho_1, \tag{C.8}$$

where $f_{\rho_1\gamma_1\dot{\gamma}_1}(.,.,.)$ is the joint PDF of $\rho_1(t)$, $\gamma_1(t)$, and $\dot{\gamma}_1(t)$.

APPENDIX D

DERIVATION OF SC INPHASE RATE OF MAXIMA

To derive the inphase rate of maxima, substituting (4.24) into (4.10) with $\dot{x} = 0$ leads to

$$\begin{aligned}\frac{E[M_x(T)]}{T} &= \int_0^\infty \ddot{x} p_{\dot{x}\ddot{x}}(0, \ddot{x}) d\ddot{x} \\ &= \frac{L}{2\pi^2\sqrt{b_0 b_2 B}} \sum_{k=0}^{L-1} \binom{L-1}{k} (-1)^k \Theta(k),\end{aligned} \tag{D.1}$$

where

$$\begin{aligned}\Theta(k) = &\int_{\ddot{x}=0}^{\infty} \int_{\varphi_1=0}^{2\pi} \int_{\rho_1=0}^{\infty} \ddot{x} \exp\left(-\frac{b_0}{2B}\ddot{x}^2\right) \\ &\times \exp\left\{-\frac{b_2 \ddot{x} \cos\varphi_1}{B}\rho_1 - \left(\frac{k+1}{2b_0} + \frac{b_2^2 \cos^2\varphi_1}{2b_0 B}\right)\rho_1^2\right\} \rho_1 d\ddot{x} d\varphi_1 d\rho_1.\end{aligned} \tag{D.2}$$

Using (3.462.5) in [36] to (D.2), one has

$$\Theta(k) = \Theta_1(k) + \Theta_2(k) \tag{D.3}$$

with

$$\begin{aligned}\Theta_1(k) &= \int_{\varphi_1=0}^{2\pi} \int_{\rho_1=0}^{\infty} \frac{B}{b_0}\rho_1 \exp\left\{-\left(\frac{k+1}{2b_0} + \frac{b_2^2\cos^2\varphi_1}{2b_0 B}\right)\rho_1^2\right\} d\varphi_1 d\rho_1 \\ &= \frac{2\pi B}{\sqrt{(k+1)^2 B + (k+1) b_2^2}},\end{aligned} \tag{D.4}$$

and

$$\begin{aligned}\Theta_2(k) &= -\int_{\varphi_1=0}^{2\pi} \int_{\rho_1=0}^{\infty} \frac{(2\pi B)^{1/2} b_2 \rho_1^2 \cos\varphi_1}{2b_0^{3/2}} \exp\left\{-\frac{k+1}{2b_0}\rho_1^2\right\} \\ &\quad\times \left(1 - \Phi\left(\frac{b_2 \rho_1 \cos\varphi_1}{\sqrt{2b_0 B}}\right)\right) d\varphi_1 d\rho_1 \\ &= 2\int_{\alpha=-\pi/2}^{\pi/2} \int_{\rho_1=0}^{\infty} \frac{(2\pi B)^{1/2} b_2 \rho_1^2 \cos\alpha}{2b_0^{3/2}} \exp\left\{-\frac{k+1}{2b_0}\rho_1^2\right\} \\ &\quad\times \Phi\left(\frac{b_2\rho_1\cos\alpha}{\sqrt{2b_0 B}}\right) d\alpha d\rho_1,\end{aligned} \tag{D.5}$$

where $\Phi(x) = 2\pi^{-1/2}\int_0^x e^{-t^2}dt$ is the error function and $\Phi(-x) = -\Phi(x)$ is used. By using (6.286.1) in [36] for (D.5), it can be shown that

$$\Theta_2(k) = \frac{2\pi B^{1/2} b_2}{(k+1)^{3/2}} - \frac{8B^2}{3b_2^2}\int_0^{\frac{\pi}{2}} \frac{{}_2F_1\left(\frac{3}{2}, 2; \frac{5}{2}; -\frac{(k+1)B}{b_2^2\cos^2\alpha}\right)}{\cos^2\alpha} d\alpha, \qquad \text{(D.6)}$$

where ${}_2F_1(.,.;.;.)$ is the hypergeometric function [36]. By substituting (D.6), (D.4), and (D.3) into (D.1), finally obtain

$$\begin{aligned}\frac{E[M_x(T)]}{T} =& \frac{L}{2\pi}\sum_{k=0}^{L-1}\binom{L-1}{k}(-1)^k\left\{\frac{B}{\sqrt{(k+1)^2 b_0 b_2 B + (k+1) b_0 b_2^3}}\right.\\ &\left.+\frac{b_2^{1/2}}{b_0^{1/2}(k+1)^{3/2}} - \frac{4B^{3/2}}{3\pi b_0^{1/2} b_2^{5/2}}\int_0^{\frac{\pi}{2}} \frac{{}_2F_1\left(\frac{3}{2}, 2; \frac{5}{2}; -\frac{(k+1)B}{b_2^2\cos^2\alpha}\right)}{\cos^2\alpha} d\alpha\right\}.\end{aligned}$$

(D.7)

APPENDIX E

THE PEAK IN THE POWER SPECTRUM

The power spectral density (PSD) of unit-power $h(t)$ for an arbitrary AOA distribution $p(\theta)$, in the two-dimensional plane, with a unit-gain isotropic receive antenna can be expressed as [2]

$$\Omega_h(f) = \frac{1}{\sqrt{f_D^2 - f^2}} \left(p(\theta) + p(-\theta) \right), \tag{E.1}$$

where $\theta = \cos^{-1}(f/f_D)$. In a heavily nonisotropic scattering, i.e., $\kappa > 10$, $p(\theta)$ is approximately Gaussian with mean α and variance $1/\kappa$, and observe that $p(\theta)/\, p(-\theta) = \exp(2\kappa\theta\alpha)$. Clearly, as $\kappa \to \infty$ and for a given f, $\Omega_h(f) \approx p(\theta)/\sqrt{f_D^2 - f^2}$ when α and θ have the same sign, and $\Omega_h(f) \approx p(-\theta)/\sqrt{f_D^2 - f^2}$, when α and θ have opposite signs. Without loss of generality, choose positive α and θ, which yield

$$\Omega_h(f) \approx \frac{p(\theta)}{\sqrt{f_D^2 - f^2}} = \sqrt{\frac{\kappa}{2\pi(f_D^2 - f^2)}} \exp\left\{ -\frac{\kappa \left(\cos^{-1}(f/f_D) - \alpha\right)^2}{2} \right\}. \tag{E.2}$$

By taking the derivative of (E.2) with respect to f and setting it to zero, assuming $f \neq \pm f_D$ and some simplifications, obtain

$$\frac{1}{\kappa} + \left(\left(\frac{f_D}{f} \right)^2 - 1 \right)^{\frac{1}{2}} \left(\cos^{-1}\left(\frac{f}{f_D} \right) - \alpha \right) = 0. \tag{E.3}$$

When $\kappa \gg 1$, $f = f_D \cos\alpha$ is the root of eq. (E.3). To verify that $f = f_D \cos\alpha$ corresponds to the maximum of $\Omega_h(f)$ in (E.2), it is necessary to look at the second derivative of (E.2) with respect to f at $f = f_D \cos\alpha$

$$-\frac{\sqrt{\kappa}(\kappa - 4 - (\kappa + 2)\cos(2\alpha))}{2\sqrt{2\pi} f_D^3 \sin^5\alpha}, \tag{E.4}$$

which is negative for $\alpha > 0$, when $\kappa \gg 1$.

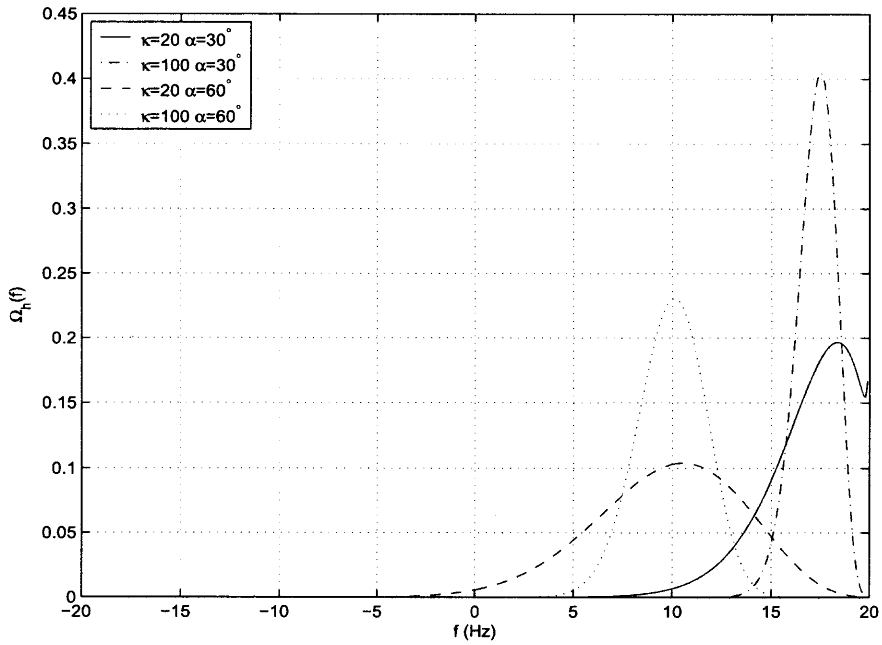

Figure E.1 The power spectral density $\Omega_h(f)$.

To show that the peak at $f = f_D \cos\alpha$ includes most of the signal power as $\kappa \rightarrow \infty$, use the method of Laplace [71] to obtain the power centered around $f = f_D \cos\alpha$, over a sufficiently small bandwidth ε

$$P_{f_D \cos\alpha} = \int_{f_D \cos\alpha - \varepsilon/2}^{f_D \cos\alpha + \varepsilon/2} \Omega_h(f) df \approx \Phi(U\sqrt{\kappa/2}), \tag{E.5}$$

where $\Phi(x) = 2\pi^{-\frac{1}{2}} \int_0^x e^{-t^2} dt$ is the error function, and $U = \left|\cos^{-1}(\cos\alpha + f_D^{-1}\varepsilon/2) - \alpha\right|$. Since U is a finite positive number, $P_{f_D \cos\alpha} \approx 1$ as $\kappa \rightarrow \infty$. Therefore, for large κ, the power is mostly concentrated at $f = f_D \cos\alpha$. To further validate this observation, PSD's $\Omega_h(f)$ in (E.1) have been plotted for different κ and α, as shown in Fig. E.1, with $f_D = 20$ Hz. As κ increases, the sharp peak at $f_D \cos\alpha$ becomes more visible.

APPENDIX F

PROOF OF PROPOSITION 1

At N discrete frequencies $\{\mu_k\}_{k=1-N/2}^{N/2}$, with N even, the discrete Fourier transform (DFT) of an N-element vector $\mathbf{z}$ is the vector $\mathbf{Z}$ defined by

$$
\begin{aligned}
\mathbf{Z} &= \boldsymbol{\Upsilon}^{\dagger}\mathbf{z}, \\
\boldsymbol{\Upsilon} &= [\mathrm{e}(\mu_{1-N/2})\ \mathrm{e}(\mu_{2-N/2})\ \ldots\ \mathrm{e}(\mu_{N/2})], \\
\mathrm{e}(\mu_k) &= \frac{[1\ e^{j2\pi\mu_k} \ldots\ e^{j2\pi\mu_k(N-1)}]^{\mathsf{T}}}{\sqrt{N}}, \\
\mathbf{z} &= [z[0]\ z[1]\ \ldots\ z[N-1]]^{\mathsf{T}}, \\
\mathbf{Z} &= [Z[\mu_{1-N/2}]\ Z[\mu_{2-N/2}]\ \ldots\ Z[\mu_{N/2}]]^{\mathsf{T}},
\end{aligned}
\tag{F.1}
$$

where $(.)^{\mathsf{T}}$ and $(.)^{\dagger}$ stand for transpose and transpose conjugate, respectively. According to (5.4), clearly, $\hat{S}_z(\mu_k) = |Z[\mu_k]|^2$. If $\mathbf{z}$ is a zero-mean proper complex Gaussian random vector, the complex random vector $\mathbf{Z}$, resulting from a linear transformation of $\mathbf{z}$, is proper and Gaussian with zero mean [52]. It is also well known that the real and imaginary part of each component of a proper random vector are uncorrelated [52]. Consequently, $\mathrm{Re}(Z[\mu_k])$ and $\mathrm{Im}(Z[\mu_k])$ for any k, are independent real Gaussian random variables with the same variance, given by $E[|Z[\mu_k]|^2]/2$, where $E[|Z[\mu_k]|^2] = \mathbf{e}^{\dagger}(\mu_k)\mathbf{R}\mathbf{e}(\mu_k)$, in which $\mathbf{R} = \mathbb{E}[\mathbf{z}\mathbf{z}^{\dagger}]$ with each element being $r_{il} = r_z\left((i-l)/f_s\right)$. Now it is easy to verify that $\hat{S}_z(\mu_k)$ has an exponential PDF

$$
p_{\hat{S}_z(\mu_k)}(s) = \frac{1}{\bar{S}_z(\mu_k)} \exp\left(-\frac{s}{\bar{S}_z(\mu_k)}\right),\ s > 0,
\tag{F.2}
$$

where, by definition,

$$
\bar{S}_z(\mu_k) = E[\hat{S}_z(\mu_k)] = E[|Z[\mu_k]|^2] = \mathbf{e}^{\dagger}(\mu_k)\mathbf{R}\mathbf{e}(\mu_k).
\tag{F.3}
$$

That a Toeplitz matrix can be diagonalized by the DFT matrix $\mathbf{\Upsilon}$ asymptotically [72] is well known. Therefore, for large N, diagonalization of $\mathbf{R}$ yields the following result of the correlation matrix of $\mathbf{Z}$

$$\mathbb{E}[\mathbf{Z}\mathbf{Z}^{\dagger}] = \mathbf{\Upsilon}^{\dagger}\mathbf{R}\mathbf{\Upsilon} \approx \Lambda, \tag{F.4}$$

where Λ is a diagonal matrix consisting of the eigenvalues of $\mathbf{R}$. Eq. (F.4) indicates that the elements of the Gaussian random vector $\mathbf{Z}$ are asymptotically independent. Therefore, it can be concluded that as $N \longrightarrow \infty$, the random variables $\{\hat{S}_z(\mu_k)\}_{k=1-N/2}^{N/2}$ are independent for different k.

APPENDIX G

DERIVATION OF (6.23) AND (6.24)

For a given training sequence $w(m) = (-1)^m \sigma_w$ which is deterministic, one needs to rewrite (6.4) as

$$\begin{aligned} r_s(t;\tau) &= \sum_m \sum_n w(m) w^*(n) g(t - mT_s) g^*(t + \tau - nT_s) \\ &= \sigma_w^2 \sum_m \sum_n (-1)^{(m+n)} g(t - mT_s) g^*(t + \tau - nT_s) \\ &= \sigma_w^2 \sum_l (-1)^l \sum_m g(t - mT_s) g^*(t + \tau - mT_s - lT_s) \\ &= \sum_l \tilde{r}_{ts}(l) \sum_m g(t - mT_s) g^*(t + \tau - mT_s - lT_s). \end{aligned} \tag{G.1}$$

In the derivation $m = n + l$ is used and $\tilde{r}_{ts}(l) = (-1)^l \sigma_w^2$. By comparing (G.1) with (6.4) and then using (6.6), when such a training sequence is transmitted, obtain the cyclic spectrum of $s(t)$ as

$$\Omega_s(k; f) = \frac{1}{T_s} G(f)\, G^*\left(f - \frac{k}{T_s}\right) \tilde{\Omega}_{ts}(f), \tag{G.2}$$

where

$$\begin{aligned} \tilde{\Omega}_{ts}(f) &= \sum_{l=-\infty}^{\infty} \tilde{r}_s(l) e^{-j2\pi l T_s f} = \sigma_w^2 \sum_{l=-\infty}^{\infty} (-l)^l e^{-j2\pi l T_s f} \\ &= \sigma_w^2 \sum_{l=-\infty}^{\infty} e^{jl\pi} e^{-j2\pi l T_s f} = \sigma_w^2 \sum_{l=-\infty}^{\infty} e^{j\pi(1-2T_s f)l} \\ &= \sigma_w^2 \sum_{m=-\infty}^{\infty} \delta\left(f - \frac{m}{2T_s}\right), m \text{ is odd.} \end{aligned} \tag{G.3}$$

The Poisson's sum formula [73, p. 786] is used in the last step of derivation of (G.3). Note that for raised cosine pulse $g(t)$, it is already known that $\Omega_G(f) \triangleq G(f)\, G^*\left(f - \frac{k}{T_s}\right) =$

$0, \forall |k| \geq 2$ and is bandlimited within $[(1-\beta)/(2T_s), (1+\beta)/(2T_s)]$ for $k = 1$. Also, $\Omega_G((1-\beta)/(2T_s)) = \Omega_G((1+\beta)/(2T_s)) = 0$. Therefore,

$$\begin{aligned} \Omega_s(1; f) &= \frac{\sigma_w^2}{T_s} \Omega_G \left(\frac{1}{2T_s} \right) \delta \left(f - \frac{1}{2T_s} \right) \\ &= \frac{\sigma_w^2 T_s}{4} \delta \left(f - \frac{1}{2T_s} \right). \end{aligned} \tag{G.4}$$

Clearly, taking the Fourier transform of (G.4) w.r.t. f leads to (6.23).

Following the same procedure, it is easily shown that the cyclic spectrum of $\dot{s}(t)$

$$\begin{aligned} \Omega_{\dot{s}}(k; f) &= \frac{1}{T_s} \breve{G}(f) \breve{G}^* \left(f - \frac{k}{T_s} \right) \tilde{\Omega}_{ts}(f) \\ &= -\frac{4\pi^2 f^2}{T_s} G(f) G^* \left(f - \frac{k}{T_s} \right) \tilde{\Omega}_{ts}(f) \\ &= -\frac{\pi^2 \sigma_w^2}{4T_s} \delta \left(f - \frac{1}{2T_s} \right), \end{aligned} \tag{G.5}$$

where $\breve{G}(f)$ is given in (6.18). Apparently, (6.24) is reached after taking the Fourier transform of (G.5).

REFERENCES

[1] M. J. Chu and W. E. Stark, "Effect of mobile velocity on communications in fading channels," *IEEE Trans. Veh. Technol.*, vol. 49, pp. 202–210, 2000.

[2] G. L. Stüber, *Principles of Mobile Communication*, 2nd ed. Boston, MA: Kluwer, 2001.

[3] K. Baddour and N. Beaulieu, "Nonparametric Doppler spread estimation for flat fading channels," in *IEEE Wireless Commun. and Networking Conf.*, New Orleans, LA, 2003, pp. 953–958.

[4] S. Mohanty, "VEPSD: A novel velocity estimation algorithm for next-generation wireless systems," *IEEE Trans. Wireless Commun.*, vol. 4, pp. 2655–2660, 2005.

[5] A. Abdi, H. Zhang, and C. Tepedelenlioglu, "Speed estimation techniques in cellular systems: Unified performance analysis," in *Proc. IEEE Veh. Technol. Conf.*, Orlando, FL, 2003, pp. 1522–1526.

[6] J. Holtzman and A. Sampath, "Adaptive averaging methodology for handoffs in cellular systems," *IEEE Trans. Veh. Technol.*, vol. 44, pp. 59–66, 1995.

[7] K. Anim-Appiah, "On generalized covariance-based velocity estimation," *IEEE Trans. Veh. Technol.*, vol. 48, pp. 1546–1557, 1999.

[8] C. Tepedelenlioglu and G. Giannakis, "On velocity estimation and correlation properties of narrow-band mobile communication channels," *IEEE Trans. Veh. Technol.*, vol. 50, pp. 1039–1052, 2001.

[9] J. Lin and J. G. Proakis, "A parametric method for Doppler spectrum estimation in mobile radio channels," in *Proc. Conf. Inf. Sciences and Systems*, Baltimore, MD, 1993, pp. 875–880.

[10] K. E. Baddour and N. C. Beaulieu, "Robust Doppler spread estimation in nonisotropic fading channels," *IEEE Trans. Wireless Commun.*, vol. 4, pp. 2677–2682, 2005.

[11] H. Zhang and A. Abdi, "Mobile speed estimation using diversity combining in fading channels," in *Proc. IEEE Global Telecommun. Conf.*, Dallas, TX, 2004, pp. 3685–3689.

[12] L. Krasny, H. Arslan, D. Koilpillai, and S. Chennakeshu, "Doppler spread estimation in mobile radio systems," *IEEE Commun. Lett.*, vol. 5, pp. 197–199, 2001.

[13] A. Dogandzic and B. Zhang, "Estimating Jakes' Doppler power spectrum parameters using the Whittle approximation," *IEEE Trans. Signal Processing*, vol. 53, pp. 987–1005, 2005.

[14] R. Narasimhan and D. C. Cox, "Speed estimation in wireless systems using wavelets," *IEEE Trans. Commun.*, vol. 47, pp. 1357–1364, 1999.

[15] L. Wang, M. Silventoinen, and Z. Honkasalo, "A new algorithm for estimating mobile speed at the TDMA-based cellular system," in *Proc. IEEE Veh. Technol. Conf.*, Atlanta, GA, 1996, pp. 1145–1149.

[16] A. Abdi, J. A. Barger, and M. Kaveh, "A parametric model for the distribution of the angle of arrival and the associated correlation function and power spectrum at the mobile station," *IEEE Trans. Veh. Technol.*, vol. 51, pp. 425–434, 2002.

[17] R. Janaswamy, *Radiowave Propagation and Smart Antennas for Wireless Communications*. Boston, MA: Kluwer, 2001.

[18] T. Aulin, "A modified model for the fading signal at a mobile radio channel," *IEEE Trans. Veh. Technol.*, vol. 28, pp. 182–203, 1979.

[19] A. Abdi and M. Kaveh, "Parametric modeling and estimation of the spatial characteristics of a source with local scattering," in *Proc. IEEE Int. Conf. Acoust., Speech, Signal Processing*, Orlando, FL, 2002, pp. 2821–2824.

[20] G. Lindgren, "Spectral moment estimation by means of level crossings," *Biometrika*, vol. 61, pp. 401–418, 1974.

[21] A. Abdi and S. Nader-Esfahani, "Expected number of maxima in the envelope of a spherically invariant random process," *IEEE Trans. Inform. Theory*, vol. 49, pp. 1369–1375, 2003.

[22] C. Tepedelenlioglu, A. Abdi, G. B. Giannakis, and M. Kaveh, "Estimation of Doppler spread and signal strength in mobile communications with applications to handoff and adaptive transmission," *Wirel. Commun. Mob. Comput.*, vol. 1, pp. 221–242, 2001.

[23] K. S. Miller and M. M. Rochwarger, "A covariance approach to spectral moment estimation," *IEEE Trans. Inform. Theory*, vol. 18, pp. 588–596, 1972.

[24] ——, "Some remarks on spectral moment estimation," *IEEE Trans. Commun.*, vol. 20, pp. 260–262, 1972.

[25] K. S. Miller, *Complex Stochastic Processes: An Introduction to Theory and Application*. Reading, MA: Addison-Wesley, 1974.

[26] P. A. Bello, "Some techniques for the instantaneous real-time measurement of multipath and Doppler spread," *IEEE Trans. Commun. Technol.*, vol. 13, pp. 285–292, 1965.

[27] J. M. Perl and D. Kagan, "Real-time HF channel parameter estimation," *IEEE Trans. Commun.*, vol. 34, pp. 54–58, 1986.

[28] C. Tepedelenlioglu, "Performance analysis of velocity (Doppler) estimators in mobile communications," in *Proc. IEEE Int. Conf. Acoust., Speech, Signal Processing*, Orlando, FL, 2002, pp. 2201–2204.

[29] A. Papoulis, *Probability, Random Variables, and Stochastic Processes*, 3rd ed. Singapore: McGraw-Hill, 1991.

[30] J. S. Bendat and A. G. Piersol, *Measurement and Analysis of Random Data.* New York: Wiley, 1966.

[31] K. Acolatse and A. Abdi, "Efficient simulation of space-time correlated MIMO mobile fading channels," in *Proc. IEEE Veh. Technol. Conf.*, Orlando, FL, 2003, pp. 652–656.

[32] A. Abdi, "On the second derivative of a Gaussian process envelope," *IEEE Trans. Inform. Theory*, vol. 48, pp. 1226–1231, 2002.

[33] A. Abdi and M. Kaveh, "Level crossing rate in terms of the characteristic function: A new approach for calculating the fading rate in diversity systems," *IEEE Trans. Commun.*, vol. 50, 2002.

[34] X. Dong and N. C. Beaulieu, "Average level crossing rate and average fade duration of selection diversity," *IEEE Commun. Lett.*, vol. 5, pp. 396–398, 2001.

[35] Y. C. Ko, A. Abdi, M. S. Alouini, and M. Kaveh, "A general framework for the calculation of the average outage duration of diversity systems over generalized fading channels," *IEEE Trans. Veh. Technol.*, vol. 51, pp. 1672–1680, 2002.

[36] I. S. Gradshteyn and I. M. Ryzhik, *Table of Integrals, Series, and Products*, A. Jeffery, Ed. Academic, 1994.

[37] S. O. Rice, "Statistical properties of a sine wave plus noise," *Bell Syst. Tech. J.*, vol. 27, pp. 109–157, 1948.

[38] B. R. Davis, "Random FM in mobile radio with diversity," *IEEE Trans. Commun.*, vol. 19, pp. 1259–1267, 1971.

[39] G. Azemi, B. Senadji, and B. Boashash, "Mobile unit velocity estimation in micro-cellular systems using the ZCR of the instantaneous frequency of the received signal," in *Proc. IEEE Int. Symp. Signal Processing Applications*, Paris, France, 2003, pp. 289–292.

[40] J. D. Parsons, *The Mobile Radio Propagation Channel*, 2nd ed. Chichester, England: Wiley, 2000.

[41] A. D. Spaulding and D. Middleton, "Optimum reception in an impulsive interference environment - part I: Coherent detection," *IEEE Trans. Commun.*, vol. 25, pp. 910–923, 1977.

[42] J. Haring and A. J. H. Vinck, "Performance bounds for optimum and suboptimum reception under class-A impulsive noise," *IEEE Trans. Commun.*, vol. 50, pp. 1130–1136, 2002.

[43] P. Stoica and R. L. Moses, *Introduction to Spectral Analysis.* Upper Saddle River, New Jersey: Prentice Hall, 1997.

[44] X. Zhao, J. Kivinen, P. Vainikainen, and K. Skog, "Characterization of Doppler spectra for mobile communications at 5.3 GHz," *IEEE Trans. Veh. Technol.*, vol. 52, pp. 14–23, 2003.

[45] W. C. Jakes, *Microwave Mobile Communications.* New York: Wiley, 1974, ch. Multipath interference, pp. 11–78.

[46] W. C. Y. Lee, "Effects on correlation between two mobile radio basestation antennas," *IEEE Trans. Commun.*, vol. 21, pp. 1214–1224, 1973.

[47] K. I. Pedersen, P. E. Mogensen, and B. H. Fleury, "A stochastic model of the temporal and azimuthal dispersion seen at the base station in outdoor propagation environments," *IEEE Trans. Veh. Technol.*, vol. 49, pp. 437–447, 2000.

[48] P. Pajusco, "Experimental characterization of D.O.A at the base station in rural and urban area," in *Proc. IEEE Veh. Technol. Conf.*, Ottawa, ON, Canada, 1998, pp. 993–997.

[49] A. Abdi and M. Kaveh, "A versatile spatio-temporal correlation function for mobile fading channels with non-isotropic scattering," in *Proc. IEEE Workshop Statistical Signal Array Processing*, Pocono Manor, PA, 2000, pp. 58–62.

[50] O. Besson and P. Stoica, "Decoupled estimation of DOA and angular spread for a spatially distributed source," *IEEE Trans. Signal Processing*, vol. 48, pp. 1872–1882, 2000.

[51] M. Ghogho, A. Swami, and T. S. Durrani, "Frequency estimation in the presence of Doppler spread: Performance analysis," *IEEE Trans. Signal Processing*, vol. 49, pp. 777–789, 2001.

[52] F. D. Neeser and J. L. Massey, "Proper complex random processes with applications to information theory," *IEEE Trans. Inform. Theory*, vol. 39, pp. 1293–1302, 1993.

[53] S. Miyamoto, M. Katayama, and N. Morinaga, "Performance analysis of QAM systems under class A impulsive noise environment," *IEEE Trans. Electromagn. Compat.*, vol. 37, pp. 260–267, 1995.

[54] J. G. Proakis, *Digital Communications*, 4th ed. New York: McGraw-Hill, 2001.

[55] M. Ghogho, A. Swami, and T. Durrani, "Blind synchronization and Doppler spread estimation for MSK signals in time-selective fading channels," in *Proc. IEEE Int. Conf. Acoust., Speech, Signal Processing*, Istanbul, Turkey, 2000, pp. 2665–2668.

[56] W. A. Gardner, *Introduction to Random Processes: With Applications to Signals and Systems*, 2nd ed. New York: McGraw-Hill, 1990.

[57] A. V. Dandawate and G. B. Giannakis, "Nonparametric polyspectral estimators for *k*th-order (almost) cyclostationary processes," *IEEE Trans. Inform. Theory*, vol. 40, pp. 67–84, 1994.

[58] H. Zhang and A. Abdi, "A robust mobile speed estimator in fading channels: Performance analysis and experimental results," in *Proc. IEEE Global Telecommun. Conf.*, St. Louis, MO, 2005, pp. 2569–2573.

[59] P. Ciblat, P.Loubaton, E. Serpedin, and G. B. Giannakis, "Asymptotic analysis of blind cyclic correlation based symbol-rate estimators," *IEEE Trans. Inform. Theory*, vol. 48, pp. 1922–1934, 2002.

[60] Y. Wang, P. Ciblat, E. Serpedin, and P. Loubaton, "Performance analysis of a class of nondata-aided frequency offset and symbol timing estimators for flat-fading channels," *IEEE Trans. Signal Processing*, vol. 50, pp. 2295–2305, 2002.

[61] G. B. Giannakis, *Digital Signal Processing Handbook*, V. K. Madisetti and D. Williams, Eds. CRC, 1998.

[62] C. Xiao, K. D. Mann, and J. C. Olivier, "Mobile speed estimation for TDMA-based hierarchical cellular systems," *IEEE Trans. Veh. Technol.*, vol. 50, pp. 981–991, 2001.

[63] M. Kirsch and F. Berens, "Mobile speed estimation for 3G mobile radio systems using the normalized autocovariance function," in *Proc. IEEE Int. Zurich Seminar on Broadband Communications. Access, Transmission, Networking*, Zurich, Switzerland, 2002, pp. 48–1–48–4.

[64] H. Schober and F. Jondral, "Velocity estimation for OFDM based communication systems," in *Proc. IEEE Veh. Technol. Conf.*, Vancouver, BC, Canada, 2002, pp. 715–718.

[65] T. Yucek, R. Tannious, and H. Arslan, "Doppler spread estimation for wireless OFDM systems," in *Proc. IEEE/Sarnoff Symposium on Advances in Wired and Wireless Communication*, Princeton, NJ, 2005, pp. 233–236.

[66] T. Wang, J. G. Proakis, E. Masry, and J. R. Zeidler, "Performance degradation of OFDM systems due to Doppler spreading," *IEEE Trans. Wireless Commun.*, vol. 5, pp. 1422–1432, 2005.

[67] Y. Mostofi and D. C. Cox, "ICI mitigation for pilot-aided OFDM mobile systems," *IEEE Trans. Wireless Commun.*, vol. 4, pp. 765–774, 2005.

[68] A. N. Lozhkin, "Improving mobility in wireless MAN," in *PIMRC*, Berlin, Germany, 2005, pp. 1601–1605.

[69] M. Russell and G. L. Stüber, "Interchannel interference analysis of OFDM in a mobile environment," in *Proc. IEEE Veh. Technol. Conf.*, Chicago, IL, 1995, pp. 820–824.

[70] P. Robertson and S. Kaiser, "The effects of Doppler spreads in OFDM(A) mobile radio systems," in *Proc. IEEE Veh. Technol. Conf.*, Houston, TX, 1999, pp. 319–333.

[71] E. T. Copson, *Asymptotic Expansions*. Cambridge, U.K.: Cambridge Univ. Press, 1965.

[72] R. M. Gray, "On the asymptotic eigenvalue distribution of toeplitz matrices," *IEEE Trans. Inform. Theory*, vol. 18, pp. 725–730, 1972.

[73] P. B. C. A. Bruce Carlson and J. C. Rutledge, *Communication Systems: An Introduction to Signals and Noise in Electrical Communication*. McGraw-Hill, 2002.